CHEMICAL ENGINEERING SCIENCE
GENIE CHIMIQUE

VOL. 9 1959 No. 4

Some remarks on chemical equilibrium and kinetics in the nitrogen oxides–water system

J. J. CARBERRY

Engineering Research Laboratory, E. I. du Pont de Nemours & Co., Inc., Wilmington, Delaware

(*Received* 1 *January* 1958; *in revised form* 1 *April* 1958)

Abstract—A consideration of a substantial body of kinetic evidence which specifies N_2O_4 as the chief reactant species in the $NO_2 - N_2O_4 - H_2O - HNO_3$ system suggested that the equilibrium data for this system would be more logically expressed in terms of N_2O_4. Apparent temperature independence is achieved by this manner of correlation. Literature data proving the ionization of N_2O_4 in solutions are in accord with the kinetic and equilibrium data. The ionic nature of the reaction would seem to preclude the existence of a purely gas-phase reaction between these nitrogen oxides and water.

Résumé—Une étude des nombreux résultats cinétiques indiquant que N_2O_4 est le réactif principal dans le système $NO_2 - N_2O_4 - H_2O - HNO_3$, a suggéré l'utilisation logique de N_2O_4 pour exprimer les données de l'équilibre. Cette méthode de corrélation permet d'obtenir une indépendance apparente de la température. Les résultats de la littérature, prouvant l'ionisation de N_2O_4 ne solution, sont en accord avec les données cinétiques et de l'équilibre. Le caractère ionique de la réaction semblerait exclure l'existence d'une réaction purement en phase gazeuse entre ces oxydes de l'azote et l'eau.

Zusammenfassung—Aus einer kinetischen Betrachtung, welche N_2O_4 als den mass gebenden Reaktanten im System $NO_2 - N_2O_4 - H_2O - HNO_3$ kennzeichnet, folgt auch, dass die Gleichgewichtsdaten dieses Systems mit mehr Berechtigung in Ausdrücken von N_2O_4 anzugeben sind. Man erhält bei dieser Zuordnung eine scheinbare Temperaturunabhängigkeit. Literaturwerte über die Ionisation von N_2O_4 in Lösungen sind mit den kinetischen und Gleichgewichtswerten in Übereinstimmung. Der Ionen-Charakter der Reaktion scheint die Annahme einer reinen Gasphasenreaktion zwischen diesen Stickoxyden und Wasser auszuschliessen.

IT would be difficult to cite a process so common to the industrial chemical scene and yet posing so severe a challenge to our comprehension of its fundamental mechanisms as that of the absorption of nitrogen oxides in water to produce nitric acid. The reactions involved are recognized to be the vapour-phase oxidation of nitric oxide by oxygen followed by absorption and reaction of the nitrogen dioxide in the aqueous phase to produce nitric acid and gaseous nitric oxide. The nitric oxide oxidation

$$2\,NO + O_2 \longrightarrow 2\,NO_2 \qquad (1)$$

has been the subject of rigorous study for many decades. BODENSTEIN [3] initiated this work, revealing the third-order kinetics and the well-known negative temperature coefficient of this reaction. Thirty years later, TREACY and DANIELS [19] postulated that the mechanism of Reaction (1) is

$$NO + O_2 \rightleftharpoons NO_3 \qquad (2)$$

$$NO_3 + NO \longrightarrow 2\,NO_2 \qquad (3)$$

where Reaction (3) is rate-controlling. Thus, the negative temperature dependency and over-all third-order kinetics of the reaction are apparently rationalized.

With respect to the reaction of nitrogen dioxide with water and aqueous solutions of nitric acid, there has been evidenced an equally intense interest. Chemical equilibrium has been determined by ABEL *et al.* [2], BURDICK and FREED [4], CHAMBERS and SHERWOOD [7], DENBIGH and PRINCE [9], and EPSHTEIN [10]. The reaction has usually been written as

$$2\,NO_2 + H_2O \rightleftharpoons HNO_3 + HNO_2 \qquad (4)$$

and

$$3\,HNO_2 \rightleftharpoons HNO_3 + H_2O + 2\,NO \qquad (5)$$

The over-all reaction becomes

$$3\,NO_2 + H_2O \rightleftharpoons 2\,HNO_3 + NO \qquad (6)$$

At equilibrium, therefore

$$K_e' = \frac{p_{NO}}{p^3_{NO_2}} \cdot \frac{a^2_{HNO_3}}{a_{H_2O}} = K_1 K_2 \qquad (7)$$

where K_e' is the thermodynamic equilibrium constant which is conveniently expressed as the product of $K_1 = p_{NO}/p^3_{NO_2}$ and $K_2 = a^2_{HNO_3}/a_{H_2O}$. In the absence of reliable activity measurements, the above equilibrium is commonly expressed as

$$\log_{10} \frac{p_{NO}}{p^3_{NO_2}} = \log_{10} K_1 \text{ vs. weight per cent. } HNO_3.$$

The data of numerous workers are shown in this form in Fig. 1.

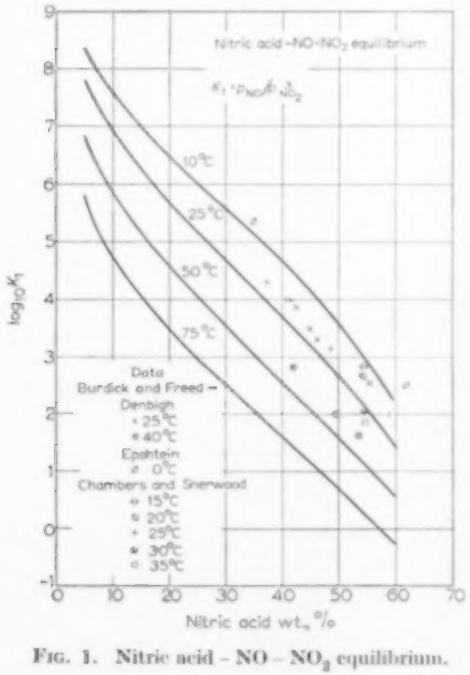

FIG. 1. Nitric acid – NO – NO_2 equilibrium.

ABSORPTION KINETICS

The kinetics of absorption have been subjected to investigation principally by CHAMBERS and SHERWOOD [7], DENBIGH and PRINCE [9], CAUDLE and DENBIGH [6], PETERS [16], and more recently by WENDEL and PIGFORD [20]. Interpretations have failed to come into agreement in two respects. First, while the work of Chambers and Sherwood supports a gas-film diffusion step as rate-controlling, DENBIGH and PRINCE believed that chemical reaction in the liquid phase controls the over-all absorption. The more recent work of CAUDLE and DENBIGH appears to reconcile the issue in that it was shown that the gas rate did affect the absorption insofar as local eddying and mixing in the reactant liquid phase is a function of gas rate.

The second point of disagreement pertains to the existence of a gas-phase reaction between water vapour and nitrogen dioxide. There are compelling arguments both for and against the gas-phase production of nitric acid. CHAMBERS and SHERWOOD [7], PETERS [16] and MCHANEY [15] submit evidence in favour of a gas-phase reaction occurring simultaneously with the liquid-phase process. WENDEL [21] has discussed the issue at some length and concludes that the data supporting the gas-phase reaction are indirect and that inferences drawn from the existence of nitric acid mists, gas-phase exotherms, and the generation of NO in an alkali system are tentative since other mechanisms can be postulated to account for these observations.

On the other hand, SIMON [18], KUZ'MINYKH [13], and the author [5] found that no reaction occurs between NO_2 (N_2O_4) and water vapour *in experiments conducted in the absence of a liquid phase.* It may be significant that support

of a gas-phase reaction is found in studies where a condensed phase exists, while data taken in completely gaseous systems do not indicate reactivity of NO_2 and water.

Not unrelated to this issue is the problem of specifying which one or more of the nitrogen oxides (NO_2, N_2O_4, N_2O_3) are the reactant species in the absorption process. On the basis of the general equilibrium correlation (equation 7) one would infer that NO_2 is the reactant in the absorption step. However, a vast body of chemical kinetic evidence dictates otherwise. DENBIGH [9] found a negative temperature dependence of rate constants evaluated in terms of NO_2. However, positive temperature dependency was displayed when N_2O_4 was considered as the reacting agent. CAUDLE and DENBIGH [6] and WENDEL [21] have shown that the rate of nitrogen oxides absorption in water increases linearly with the partial pressure of N_2O_4 in the gas. Since

$$2\,NO_2 = N_2O_4 \tag{8}$$

DENBIGH [9] concluded that two elementary reactions are involved in the absorption process:

$$N_2O_4 + H_2O \rightleftharpoons HNO_3 + HNO_2 \tag{9}$$

$$2\,HNO_2 \rightleftharpoons NO + NO_2 + H_2O \tag{10}$$

The rate data were correlated by DENBIGH with the equation

$$\frac{d\,(N_2O_4)}{dt} = k\left[(N_2O_4) - C\,(N_2O_4)^{1/4}\,(NO)^{1/2}\right] \tag{11}$$

while the experimental equilibrium data were expressed in terms of NO_2 as shown in Fig. 1. These kinetic data certainly suggest that N_2O_4 is the key reactant in the $NO_2 - H_2O$ system.

The reactive nature of N_2O_4 relative to its monomer NO_2 is indicated in systems other than those involving water. In a study of the kinetics of the reactions of nitrogen dioxide with various alcohols, FAIRLIE *et al.* [11] found that third-order kinetics and a negative temperature coefficient characterized the initial reaction rate. When, however, their rate equation was written in terms of N_2O_4, second-order kinetics and a normal temperature dependency resulted. They concluded that N_2O_4, not NO_2, is the reactant species with alcohols. Subsequent work [8] on the same system demonstrated that this reaction is heterogeneous in nature involving the reaction of N_2O_4 and adsorbed alcohol on polar surfaces.

With this imposing body of evidence favouring N_2O_4 as the chief reactant candidate in various systems, it appears that equilibrium data for the nitrogen oxides – water system would be more logically expressed in terms of N_2O_4 rather than NO_2. Given the dimerization equilibrium constant for Reaction (8)

$$K_3 = \frac{p_{N_2O_4}}{p^2_{NO_2}} \tag{12}$$

then the nitrogen oxides – acid equilibrium expressed in terms of N_2O_4, NO, H_2O, and HNO_3 is

$$K_e = \frac{p_{NO}}{p^{1.5}_{N_2O_4}} \cdot \frac{a^2_{HNO_3}}{a_{H_2O}}$$

$$= \frac{p_{NO}}{K_3^{1.5}\,p^3_{NO_2}} \cdot K_2 = \frac{K_1}{K_3^{1.5}} \cdot K_2$$

$$K_e = K_4 K_2$$

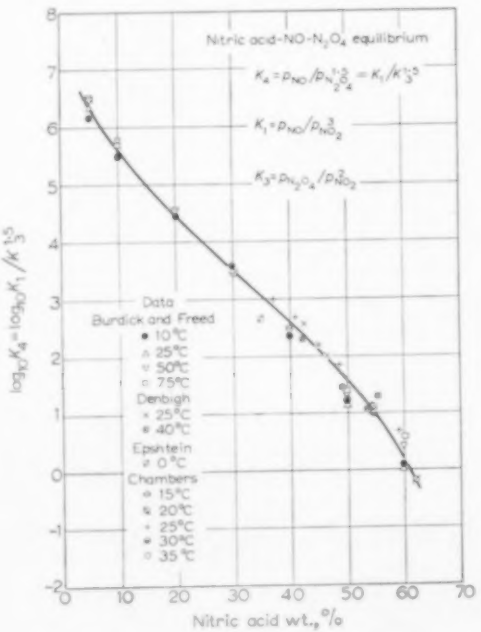

FIG. 2 Nitric acid –NO – N_2O_4 equilibrium.

where

$$K_4 = K_1/K_3^{1.5} \tag{13}$$

and

$$K_1 = p_{NO}/p^3_{NO_2}$$

Therefore, the equilibrium data of Fig. 1 may be stated in terms of N_2O_4 by simply dividing the published values of K_1 by $K_3^{1.5}$. BODENSTEIN [3] measured K_3 for Reaction (8) over a temperature range of 9–113°C. Employing BODENSTEIN's data, all the data in Fig. 1 have been translated accordingly and the resulting correlation appears in Fig. 2.

Evidently, within the limits of the experimental errors involved in the original equilibrium data, the new correlation reveals apparent temperature independence in the range of 10–55 per cent by wt. HNO_3. The spread of the data in the dilute (< 10 per cent) and concentrated (> 55 per cent) regions of acid strength is beyond comment since the original data in those regions are not experimental but extrapolated values*.

The correlation presented in Fig. 2 would suggest that one of the chief factors contributing to the reduction in equilibrium concentration of HNO_3 with increasing temperature is indeed the paucity of N_2O_4 in equilibrium with NO_2 at the higher temperature levels. Certainly a dynamic equilibrium model stated in terms of N_2O_4 is in accord with the kinetic evidence cited above.

Given the BODENSTEIN NO_2–N_2O_4 equilibrium constant as a function of temperature, it follows that the correlation in Fig. 2 may be utilized to predict acid equilibrium in temperature regions presently devoid of experimental data.

REACTION MECHANISM

While the kinetic studies and implications of the correlation in Fig. 2 signify the key role of N_2O_4 in the reaction under discussion, further evidence of even greater import is to be found in studies devoted to N_2O_4 behaviour in solutions. GRAY and YOFFE [12], in their review of 1955 on the reactivity and structure of nitrogen dioxide, cite and discuss a wealth of evidence for the ionization of N_2O_4 according to the reaction

$$N_2O_4 = NO^+ + NO_3^- \tag{14}$$

This ionization occurs even in pure liquid N_2O_4, and solvents of high dielectric constant (e.g., water) obviously enhance Reaction (14). ROBERTSON *et al.* [17] attribute the conductance values of the HNO_3–H_2O–NO_2 (N_2O_4) system to the presence of NO^+ and NO_3^-. Very recently, MILLER and WATSON [14] found that "in concentrations up to one molal N_2O_4, the concentration of undissociated N_2O_4 is small." Further, the concentration of NO_2 does not exceed 0·02 molal in concentrated solutions of N_2O_4 and nitric acid [14]. The reaction sequence involved in the absorption and reaction of NO_2 with water may be writen as

$$2\,(NO_2)_{gas} = (N_2O_4)_{gas} \tag{15a}$$

$$\left.\begin{aligned}(N_2O_4)_{gas} = (N_2O_4)_{solution} &= NO^+ + NO_3^-\\ N_2O_4 + H_2O &= H^+ + NO_3^- + HNO_2\end{aligned}\right\} \tag{15b}$$

$$2\,HNO_2 = H_2O + NO + NO_2 \tag{15c}$$

Following GRAY and YOFFE [12], the rate of reaction of N_2O_4 with water can be written

$$\frac{-d\,(N_2O_4)}{dt} = 3/4\,[k_f\,(N_2O_4)\,(H_2O) - k_r\,(H^+)\,(NO_3^-)\,(HNO_2)] \tag{16}$$

Since

$$(HNO_2) = \alpha\,(N_2O_4)^{1/4}\,(NO)^{1/2}\,(H_2O)^{1/2} \tag{17}$$

then

$$\frac{-d\,(N_2O_4)}{dt} = 3/4\,k_f\,(H_2O)\left[(N_2O_4) - \alpha\frac{k_r}{k_f}\frac{(HNO_3)}{(H_2O)^{1/2}}\,(N_2O_4)^{1/4}\,(NO)^{1/2}\right] \tag{18}$$

$$= k\,[(N_2O_4) - C\,(N_2O_4)^{1/4}\,(NO)^{1/2}] \tag{19}$$

The above expression is identical with that found experimentally by DENBIGH (equation 11).

*Subsequent to the initial preparation of this paper, it has been brought to the author's attention that R. L. MENEGUS in an unpublished report, in 1943, employed an N_2O_4 correlation of acid equilibrium as a basis for extrapolating values into the range of acid concentrations greater than 60 per cent by wt.

DENBIGH and PRINCE [9] first demonstrated accord between their experimental correlation (equation 11) and the theoretical rate expression derived from Reactions (9) and (10). Equation (19) obviously results from a consideration of only Reactions (9) and (10), i.e., evidence of ionization does not alter the final form of the theoretical rate expression. It was the identity of the experimental and theoretical expressions which led DENBIGH and PRINCE [9] to the firm conclusion that chemical reaction, rather than gas-film diffusion, controlled the absorption of nitrogen dioxide into water and nitric acid.

It is of interest to note that although DENBIGH and PRINCE [9] correlated their equilibrium data in terms of NO_2, as shown in Fig. 1, an examination of the constant C in their rate expression (equation 11) reveals that

$$(RT)^{1/4}\, C = 1/\sqrt{K_4}$$

In other words, the virtual temperature independence of the present equilibrium correlation (Fig. 2) was implied in DENBIGH's experimental rate expression.

A possible explanation for the unusual equilibrium correlation is suggested by examination of equation (18) in the light of the ionic mechanism. At equilibrium expressed in terms of partial pressure of the N_2O_4 and NO, it is evident that the "equilibrium constant," K_4, contains solubility equilibrium constants for the gases as well as an ionization constant and the appropriate activity coefficients. Thus, compensating temperature dependencies of the various physical and chemical equilibria would seem to account for insignificant temperature effect upon over-all equilibrium expressed in terms of N_2O_4.

Clearly Fig. 2, *per se*, does not prove N_2O_4 to be the chief reactant. Primarily, the kinetic and ionization data provide the chief support for the reactant candidacy of N_2O_4. It should be noted, however, that while the kinetic data cited specify N_2O_4 rather than NO_2 as reactant, in the absence of knowledge of the N_2O_4 ionization, the locale (gas and/or liquid phase) of the reaction remains open to debate.

As the ionic nature of the N_2O_4 water reaction is evident, one is compelled to make the inevitable suggestion that since gas-phase ionic reactions are quite unlikely, a purely gas-phase reaction between NO_2 (N_2O_4) and water is implausible. This contention does not preclude reaction between gaseous NO_2 (N_2O_4) and water droplets or a water fog. Such an event would be truly heterogeneous and in accord with the above mechanistic picture. It cannot be overemphasized that, with the exception of MCHANEY's work [15], the reliable data of those who infer the existence of a vapour-phase reaction were obtained in systems containing a condensed aqueous phase, while experimenters who have worked with gaseous systems find no evidence of a gas-phase generation of acid from NO_2 (N_2O_4) and water. KUZ'MINYKH [14] performed his experiments under both conditions and his results verify this generalization. Obviously, only a few droplets of water need exist in the gas phase to constitute acid and NO generation with the possible consequent formation of a fog or mist.

The role of NO in absorption kinetics requires comment at this point. That its presence in a nitrogen oxides gas enhances the rate of absorption in water, acid, and alkali has been attributed to the reaction

$$NO + NO_2 = N_2O_3 \qquad (20)$$

The species N_2O_3 is the anhydride of nitrous acid as N_2O_5 is the anhydride of nitric acid. While thermodynamics indicates that only small amounts of N_2O_3 exist in equilibrium with NO and NO_2 at process temperatures, the rate of attainment of equilibrium is quite rapid. Reaction of N_2O_3 with alkali yields primarily the nitrite salt, while in the absence of NO the alkali system produces nearly equimolar quantities of nitrite and nitrate salts. The reaction in alkali is expressed by the reactions

$$N_2O_3 + H_2O \longrightarrow 2\,HNO_2 \qquad (21)$$

$$2\,HNO_2 + 2\,OH^- \longrightarrow 2\,H_2O + 2\,NO_2^- \qquad (22)$$

The formation of nitrous acid from its anhydride, N_2O_3, by Reaction (21) is known to occur quite rapidly in the gas as well as liquid phase [12]. Ionization in the case of the N_2O_3–H_2O system is apparently the consequence of OH^- ion attack upon the HNO_2 formed via the hydration reaction.

The direct evidence for the rapid gas-phase formation of nitrous acid by Reaction [21] would suggest that perhaps the mist or fog encountered in some nitrogen peroxide absorption studies is nitrous rather than nitric acid.

Conclusions

The results of numeorus kinetic studies of the nitrogen oxides–water system clearly indicate that N_2O_4 is the chief reactant species in this system. This suggestion prompted a correlation of the nitrogen oxides – aqueous acid equilibrium data in terms of N_2O_4, rather than NO_2, with the result that apparent temperature independence of the equilibrium data is realized. Physical measurements revealing the ionization of dissolved N_2O_4 into NO^+ and NO_3^- ions in aqueous media not only support the kinetic and chemical equilibrium data but provide potent support to the argument that a purely gas-phase reaction between N_2O_4 and water vapour is an unlikely event.

Acknowledgement—The author is indebted to Dr. T. H. Chilton for his most valuable advice during the preparation of this manuscript.

Notation

a_{HNO_3} = activity of nitric acid in solution
a_{H_2O} = activity of water in solution
C = constant in equations (11) and (19)
k = rate constant in equations (11) and (19)
K_e = equilibrium constant for Reactions (9) and (10)
K_e' = equilibrium constant for reaction (6)
$K_1 = p_{NO}/p^3_{NO_2}$
$K_2 = a^2_{HNO_3}/a_{H_2O}$
K_3 = equilibrium constant for Reaction (8)
$K_4 = \dfrac{K_1}{K_3^{1.5}}$
p_{NO_2} = partial pressure of NO_2
$p_{N_2O_4}$ = partial pressure of N_2O_4
p_{NO} = partial pressure of NO
R = gas law constant
T = absolute temperature
( ) = denotes concentration of enclosed species
x = constant in equation (17)

References

[1] Abel E. *Z. Phys. Chem.* 1930 **148** 337.
[2] Abel E., Schmid H. and Stein M. *Z. Elektrochem.* 1930 **36** 692.
[3] Bodenstein M. *Z. Elektrochem.* 1916 **22** 327 ; *Z. Phys. Chem.* 1922 **100** 68.
[4] Burdick C. L. and Freed E. S. *J. Amer. Chem. Soc.* 1921 **43** 518.
[5] Carberry J. J. Unpublished Data. University of Notre Dame, 1951.
[6] Caudle P. G. and Denbigh K. G. *Trans. Faraday Soc.* 1953 **49** 39.
[7] Chambers F. S. and Sherwood T. K. *Ind. Engng. Chem.* 1931 **29** 1415 ; *J. Amer. Chem. Soc.* 1937 **59** 316.
[8] Collins T. G. and Kaemmerer J. F. MS Thesis. University of Notre Dame, 1954.
[9] Denbigh K. G. and Prince A. J. *J. Chem. Soc.* 1947 790.
[10] Epshtein D. A. *J. Gen. Chem.* U.S.S.R. 1939 **9** 792.
[11] Fairlie A. M., Carberry J. J. and Treacy J. C. *J. Amer. Chem. Soc.* 1953 **75** 3786.
[12] Gray P. and Yoffe A. D. *Chem. Rev.* 1955 **55** 1069.
[13] Kuz'minykh I. and Udintseva Y. *Khimstroy* 1934 **6** 523.
[14] Miller D. J. and Watson D. *J. Chem. Soc.* 1957 1369.
[15] McHaney L. MS Thesis. University of Illinois 195.
[16] Peters M. S., Ross C. P. and Klein J. E. *Amer. Inst. Chem. Engrs. J.* 1955 **1** 105.
[17] Robertson G. D., Mason D. M. and Sage B. H. *Ind. Engng. Chem.* 1952 **44** 2928.
[18] Simon R. H. M. B.S. Thesis. University of Delaware 1948.
[19] Treacy J. C. and Daniels F. *J. Amer. Chem. Soc.* 1955 **77** 2033.
[20] Wendel M. M. and Pigford R. L. *Amer. Inst. Chem. Engrs. J.* 1958, **4**, 249.
[21] Wendel M. M. Ph.D. Thesis. University of Delaware 1956.

Chemical Engineering Science, 1959, Vol. 9, pp. 195 to 204. Pergamon Press Ltd. London. Printed in Great Britain

Design of cooler condensers for gas–vapour mixtures

T. MIZUSHINA, N. HASHIMOTO* and M. NAKAJIMA†

Department of Chemical Engineering, Kyoto University, Kyoto, Japan

(*Received* 25 *February* 1958)

Abstract—Graphical method for design of cooler condensers by MIZUSHINA and KOTOO [9] is extended to general gas–vapour systems including air–water having high vapour concentrations. Moreover this is applicable regardless of whether the mixture continues saturated or superheated, and also simpler than other methods developed previously though it may be less rigorous.

Two examples of air–water system and one example of air–benzene system are solved by this method. It is shown that there are good agreement between the results of this method and those of more rigorous ones, i.e. COLBURN and HOUGEN [6] method or BRAS [1] modification.

Résumé—Les auteurs étendent au système général gaz-vapeur comprenant air-eau, à forte concentration en vapeur, la méthode graphique de MIZUSHINA et KOTOO (9) pour le calcul d'un condenseur. Cette méthode est applicable indifféremment si le mélange se maintient saturé ou surchauffé, et elle est plus simple que d'autres méthodes décrites précédemment bien qu'elle soit moins rigoureuse.

Deux exemples du système air-eau, et un exemple du système air-benzène, sont résolus par cette méthode. Les auteurs montrent qu'il y a concordance entre les résultats de cette méthode et ceux de méthodes plus rigoureuses par exemple la méthode de COLBURN et HOUGEN [6] ou la modification de BRAS [1].

Zusammenfassung—Die graphische Methode für den Entwurf von Kühler-Kondensatoren nach MIZUSHINA und KOTOO [9] wird auf allgemeine Gas-Dampf-Systeme einschliesslich Luft-Wasser mit hohen Dampfkonzentrationen ausgedehnt. Ferner ist diese Methode sowohl für gesättigte wie überhitzte Systeme anwendbar und ist auch einfacher als früher entwickelte Verfahren, wenn sie auch weniger exakt ist.

Zwei Beispiele des Luft-Wasser-Systems und ein Beispiel des Luft-Benzol-Systems werden nach dieser Methode behandelt. Es ergibt sich eine gute Übereinstimmung mit den Ergebnissen exakter Methoden, z.B. nach COLBURN and HOUGEN [6] oder auch nach der modifizierten Methode von BRAS [1].

INTRODUCTION

IN a cooler condenser, vapour condenses at the cooling surface and the temperature of gas–vapour mixture decreases. The simultaneous transfer of heat and mass makes the design problem complicated. Since COLBURN and HOUGEN [6] published their paper on this subject first, various methods were proposed. Colburn and Hougen's stepwise calculation is the most rigorous but limited to saturated gas–vapour mixtures. Though this disadvantage was removed by BRAS [1] who proposed a new general method suitable even in case of superheating, the tediousness of the stepwise method is still its disadvantage. COLBURN [5] in a recent paper emphasized the necessity of a simplified method of the calculation and proposed a method based on the terminal conditions only. Its result is, however, sometimes far from the rigorous value as shown by CAIRNS [4].

For simpler calculation which can be applied regardless of whether the mixture is saturated or not, graphical methods may be most hopeful, and have been developed by several authors.

* Present address: Hitachi Ltd., Kudamatsu, Japan.
† Present address: Himeji Institute of Technology.

Mickley's method [8] can be applied only to the case of air–water vapour mixture having low vapour content.

Just before Mickley's paper was published, Mizushina and Kotoo [9] proposed a graphical method which is useful for general systems of gas–vapour mixture but with low vapour concentrations.

Cribb and Nelson [7] developed a graphical calculation method which operates successfully for a gaseous mixture even with high vapour concentration. However, it is tedious to construct and use two charts, i.e. temperature–enthalpy and temperature–humidity charts. They assumed that the ratio of heat transfer coefficient to mass transfer coefficient is constant because the heat capacity of the gas mixture is constant over the whole range of humidity. This assumption is valid for the particular system used by these authors but may not for others. Moreover, their assumption on mass transfer coefficient being constant over the whole cooling surface is quite doubtful when the mass velocity of gas mixture in the apparatus changes considerably in consequence of vapour condensation.

Recently, Bras [2, 3] developed graphical procedures for the determination of the liquid gas interface conditions, by which trial and error computations were eliminated. However it is still tedious that values of properties should be obtained by point to point calculations.

The graphical method which will be developed in this paper is simpler and applicable to any system of gas–vapour mixture having any vapour concentration though it may be less rigorous. Moreover, this method can handle the situation even when the mixture is not saturated. Essentially this is an extension of Mizushina and Kotoo's graphical method [9] which is limited to the case of low vapour concentration, to that of high vapour concentration.

The Development of a Graphical Method for Air–Water System

Basic equations

In a counter current cooler condenser, the ratio of heat transfer coefficient to mass transfer coefficient is

$$\frac{h_g}{k_g} = c_g M_g p_{BM} \left(\frac{Sc}{Pr}\right)^{\frac{1}{3}} \qquad (1)^*$$

The relation between k_g and k_g' is

$$k_g (p_g - p_i)\, dA = \frac{k_g'}{M_v} (H_g - H_i)\, dA$$

Substituting $H = [p/(P-p)]\,(M_v/M_B)$ into the above equation gives

$$k_g = \frac{k_g'}{M_v}\frac{M_v}{M_B}\left(\frac{p_g}{P-p_g} - \frac{p_i}{P-p_i}\right)\frac{1}{p_g - p_i}$$

$$= \frac{k_g'}{M_B}\left\{\frac{P}{(P-p_g)(P-p_i)}\right\} \qquad (2)$$

From equations (1) and (2) one obtains

$$\frac{h_g}{k_g'} = \frac{c_g M_g p_{BM}}{M_B}\left\{\frac{P}{(P-p_g)(P-p_i)}\right\}\left(\frac{Sc}{Pr}\right)^{\frac{1}{3}} = \alpha c_s \qquad (3)$$

where

$$\alpha = \frac{c_g M_g p_{BM}}{c_s M_B}\left\{\frac{P}{(P-p_g)(P-p_i)}\right\}\left(\frac{Sc}{Pr}\right)^{\frac{1}{3}}$$

Since $\qquad c_g M_g P = c_s M_B (P - p_g)$

$$\alpha = \frac{p_{BM}}{P-p_i}\left(\frac{Sc}{Pr}\right)^{\frac{1}{3}} \qquad (4)$$

Even in the case of high vapour content, the value of $p_{BM}/(P-p_i)$ is ordinarily $0{\cdot}8 \sim 1$, and the value of $(Sc/Pr)^{\frac{1}{3}}$ may be taken as 0·9 for air–water system. Therefore, the value of α approximates to unity for air–water system. This approximation is conservative.

Hence, regardless of vapour concentration,

$$\frac{h_g}{k_g'} = c_s \qquad (5)$$

This is an extension of Lewis' relation.

Therefore, the following conventional enthalpy equation is applicable to a cooler condenser of the humid air containing any amount of water-vapour.

$$-G_B\, di_g = \frac{h_g}{c_s}(i_g - i_i)\, dA \qquad (6)$$

where, the enthalphy of humid air is defined as

$$i_g = c_s t_g + \lambda_0 H_g \qquad (7)$$

*In the case of gas system [10], the power to Schmidt and Prandtl modulus is $\frac{1}{2}$ rather than $\frac{1}{3}$.

The surface area is obtained by

$$A = G_B \int_{i_{g2}}^{i_{g1}} \frac{c_s \, di_g}{h_g (i_g - i_i)} \tag{8}$$

Heat balance gives the inclination of operating line.

$$\frac{di_g}{dt_i} = \frac{L \, c_l}{G_B} \tag{9}$$

The inclination of path line of air condition is

$$\frac{di_g}{dt_g} = \frac{i_g - i_i}{t_g - t_i} \tag{10}$$

And the inclination of tie line is

$$\frac{i_g - i_i}{t_l - t_i} = -\frac{h_0 \, c_s}{h_g} \tag{11}$$

Consideration of the change of values of h_g and c_s in the condenser.

If there is a large amount of the change of the values of h_g and c_s from the inlet to the outlet of a condenser owing to the condensation of the vapour, it is desirable to take them into account.

For gas systems, heat transfer coefficient may be expressed as follows.

$$h_g = j \, c_g \, G' / (Pr)^{\frac{1}{3}} \tag{12}*$$

where

$$j = C \left(\frac{dG'}{\mu} \right)^{-n} \tag{13}$$

The relations between the quantities on dry basis and those on total basis are

$$G' = G_B' (1 + H_g) \tag{14}$$

$$c_g = c_s / (1 + H_g) \tag{15}$$

Introducing equations (14) and (15) into equations (12) and (13), one obtains

$$h_g = C \left(\frac{dG_B'}{\mu} \right)^{-n} c_s \, G_B' \, (1 + H_g)^{-n} / (Pr)^{\frac{1}{3}} \tag{16}$$

Defining h_B as fictitious heat transfer coefficient for the flow of stagnant gas only gives

$$h_B = j_B \, c_B \, G_B' / (Pr)^{\frac{1}{3}} \tag{17}$$

*Refer to the footnote on page 196.

where

$$j_B = C \left(\frac{dG_B'}{\mu} \right)^{-n} \tag{18}$$

Assuming the values of viscosity and Prandtl number of the stagnant gas as same as those of the mixture respectively, and comparing equations (16), (17) and (18), the following equations are obtained.

$$\frac{h_g}{c_s} = \frac{h_B}{\beta \, c_B} \tag{19}$$

where

$$\beta = (1 + H_g)^n \tag{20}$$

Substituting equations (19) into equations (8) and (11), the following equations are obtained.

$$A = G_B \int_{i_{g2}}^{i_{g1}} \frac{c_B \beta}{h_B} \frac{di_g}{i_g - i_i}$$

$$= \frac{c_B \, G_B}{h_B} \int_{i_{g2}}^{i_{g1}} \frac{\beta \, di_g}{(i_g - i_i)} \tag{21}$$

$$\frac{i_g - i_i}{t_i - t_i} = -\frac{\beta \, h_0 \, c_B}{h_B} \tag{22}$$

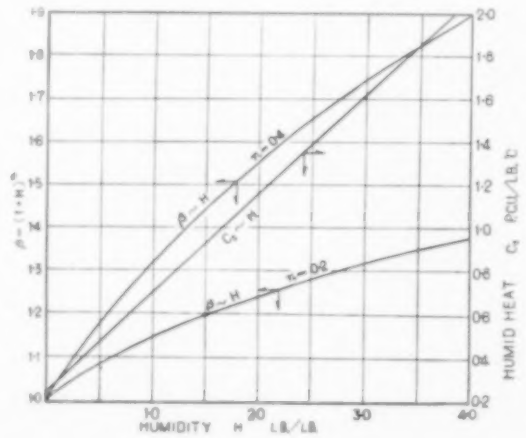

FIG. 1. Relations between β and humidity and humid heat and humidity.

Design procedure

The values of β are plotted against the humidity H_g on Fig. 1, $n = 0{\cdot}4$ is for the flow across tube banks and $n = 0{\cdot}2$ is for the flow inside tubes. c_s vs. H_g are also plotted on Fig. 1.

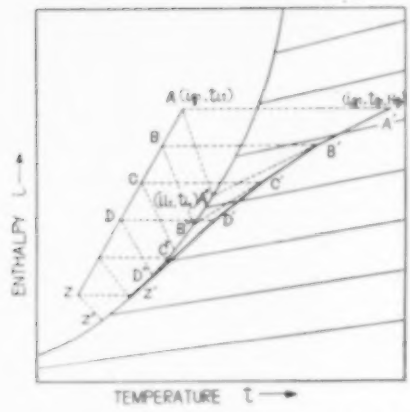

Fig. 2. Enthalpy–temperature chart.

Fig. 2 is the enthalpy–temperature chart with a group of constant humidity lines.

If it is assumed that the condition of inlet gas, the enthalpy of outlet gas, the temperature of water available and the water and gas flow rates are known, the procedure for the graphical method is as follows.

(1) Calculate the heat transfer coefficient of gas film h_g defined by equation (12) at the gas inlet. Knowing the values of c_s and β at the inlet gas condition from Fig. 1, calculate c_B/h_B by equation (19).

Also, calculate the combined conductance, h_0, made up of the conductances of the condensate film, metal pipe, scale and the cooling water film. In most practical cases of air–water vapour mixture, h_0 can be taken as constant.

(2) Plot the operating line AZ on the enthalpy-temperature chart.

(3) Subdivide the operating line into several equal increments (A . B . C . . . Z).

(4) Plot point A' (t_{g1}, i_{g1}, H_{g1}).

(5) Construct a tie line of slope $-\beta h_0 c_B/h_B$ through the point A (t_{l1}, i_{g1}) and locate A'' (t_{i1}, i_{i1}) on the saturation curve. The value of β can be obtained from Fig. 1 for the humidity H_{g1}.

(6) Join point A' (t_{g1}, i_{g1}) with point A'' (t_{i1}, i_{i1}) and intersect a line through point B parallel to the abscissa at point B'. B' represents the condition (t_g, i_g, H_g) of the second point.

(7) Repeat steps (5) and (6) for the remaining increments. β should be obtained for the humidity of each point. A' B' C' . . . . Z' is the path line of the gas condition.

(8) If the gas becomes saturated at any point, the gas condition changes hereafter following the saturation curve.

(9) Plot $\beta/(i_g - i_i)$ vs. i_g, and obtain $\int_{i_{g2}}^{i_{g1}} \beta\, di_g/(i_g - i_i)$ graphically.

(10) Calculate the value of A by equation (21).

The calculation results and the comparison of them with the results of the other methods

(*a*) *Example of* Colburn *and* Hougen [6] (*saturated mixture*). Using the procedure mentioned above, the example in Colburn and Hougen's paper was solved.

$$c_g = 0{\cdot}41 \text{ P.c.u./lb } ^\circ\text{C}$$
$$G' = 10{,}800 \text{ lb/hr ft}^2$$
$$Pr = 0{\cdot}76$$
$$Re = 19{,}600$$
$$j = 0{\cdot}0063$$

All of these values are taken from Colburn and Hougen's paper.

Substituting these values into equation (12), the heat transfer coefficients of gas film, h_g is calculated.

$$h_g = (0{\cdot}0063)\,(0{\cdot}41)\,(10{,}800)/(0{\cdot}76)^{\frac{1}{3}}$$
$$= 31{\cdot}9 \text{ P.c.u./ft}^2 \text{ hr } ^\circ\text{C}$$

Humidity H_g is calculated from vapour pressure.

$$H_g = \frac{(0{\cdot}835)\,(18)}{(0{\cdot}165)\,(29)} = 3{\cdot}14 \text{ lb/lb}$$

Hence, the value of c_s is obtained by Fig. 1 as

$$c_s = 1{\cdot}69 \text{ P.c.u./lb } ^\circ\text{C}$$

Since the gas flows across tube banks, the value of β is obtained by $n = 0{\cdot}4$ curve in Fig. 1.

$$\beta = 1{\cdot}765$$

From equation (19)

$$\frac{c_B}{h_B} = \frac{c_s}{\beta\, h_g} = \frac{1{\cdot}69}{(1{\cdot}765)\,(31{\cdot}9)} = 0{\cdot}03$$

Colburn and Hougen gave the value of the combined conductance as

$$h_0 = 310 \text{ P.c.u./hr ft}^2\ ^\circ\text{C}$$

Since the gas condition at the inlet is $t_{g1} = 95^\circ$C and $H_{g1} = 3{\cdot}14$, the enthalpy of the gas mixture at this point is calculated as follows.

$$\begin{aligned} i_{g1} &= c_{s1}\, t_{g1} + \lambda_0\, H_{g1} \\ &= (1{\cdot}69)\,(95) + (595)\,(3{\cdot}14) \\ &= 2{,}030 \text{ P.c.u./lb} \end{aligned}$$

Since the mixture at the outlet is saturated at $t_{g2} = 40\ ^\circ$C,

$$\begin{aligned} H_{g2} &= 0{\cdot}049 \text{ lb/lb} \\ c_{s2} &= 0{\cdot}262 \text{ P.c.u./lb } ^\circ\text{C} \\ i_{g2} &= 40 \text{ P.c.u./lb} \end{aligned}$$

The cooling water temperatures are shown in Colburn and Hougen's paper as follows.
At the gas inlet

$$t_{l1} = 60^\circ\text{C}$$

At the gas outlet

$$t_{l2} = 25^\circ\text{C}$$

Thus, the operating line can be plotted on the enthalpy–temperature chart.

Since the gas is saturated with vapour from the beginning in this example, the path line of the gas condition coincide with the saturation curve.

Following the procedure mentioned above, the results tabulated in Table 1 are obtained. And the surface area of the condenser is calculated by equation (21)

$$A = \frac{G_B\, c_B}{h_B} \int_{i_{g2}}^{i_{g1}} \frac{\beta\, di_g}{i_g - i_i}$$

$$G_B = 2{\cdot}800 \text{ lb/hr}$$

$$\frac{c_B}{h_B} = 0{\cdot}03$$

$$\int_{i_{g2}}^{i_{g1}} \frac{\beta\, di}{i_g - i_i} = 8{\cdot}295$$

$$A = (2{\cdot}800)\,(0{\cdot}03)\,(8{\cdot}295) = 696 \text{ ft}^2.$$

The Colburn and Hougen's result is 695 ft². The good agreement between both results is apparent.

In Fig. 3, the temperatures of gas, condensate surface and water are plotted against the surface area of the condenser. The solid lines are for Colburn and Hougen results, and the broken lines are for the results of this method. This again shows the comparatively good agreement between both methods. Enthalpy difference between the two points at higher temperature is larger than the amount of heat transferred where the condensate is assumed to be at the same temperature as the gas mixture owing to the fact that the enthalpy is based upon 0°C

Table 1. *Factors determined from the graphical method on* Colburn and Hougen *example*

Point (No.)	t_g (°C)	H_g (lb/lb)	i_g (P.c.u./lb)	t_l (°C)	β	$\frac{h_0\,\beta\,c_B}{h_B}$	t_i (°C)	i_i (P.c.u./lb)	$i_g - i_i$ (P.c.u./lb)	$10^3\ \beta/(i_g - i_i)$	A (ft²)
1	95·0	3·14	2030	60·0	1·765	16·45	93·4	1480	550	3·21	696
2	93·2	2·20	1421	49·2	1·593	14·83	89·3	832	589	2·70	550
3	90·0	1·40	912	40·3	1·419	13·21	80·5	380	532	2·67	436
4	84·7	0·80	528	33·6	1·265	11·79	65·6	148	380	3·33	346
5	75·8	0·40	270	29·1	1·144	10·65	48·7	61	209	5·48	254
6	71·7	0·30	206	28·0	1·111	10·35	43·3	47	159	6·98	220
7	64·7	0·20	140	26·8	1·076	10·02	37·3	35	105	10·25	175
8	51·0	0·10	75	25·6	1·039	9·68	30·8	25	50	20·80	97
9	46·5	0·07	55	25·3	1·027	9·56	28·6	22·5	32·5	31·60	53
10	40·0	0·049	40	25·0	1·019	9·49	27·0	20·5	19·5	52·30	0

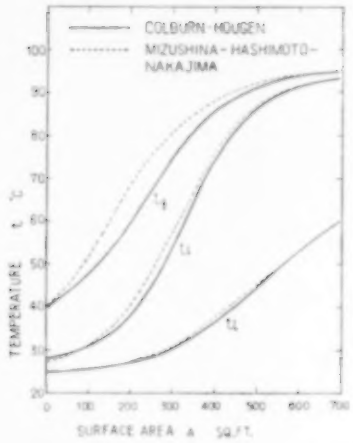

Fig. 3. Gas temperature, t_g, interface temperature, t_i, and cooling water temperature, t_l vs. surface area of a condenser.

water. Therefore, the temperature decreasing rate at higher temperature of this calculation is lower than that of Colburn and Hougen.

However, water temperature distribution lines of both methods coincide each other closely. This means that the calculated amount of heat transferred across a certain range of the surface area is the same for both methods.

(*b*) *Example of* Bras [1] (*unsaturated mixture*). At the gas inlet.

$$c_g = 0{\cdot}245 \text{ P.c.u./lb } ^\circ\text{C}$$
$$G' = 11{,}200 \text{ lb/hr ft}^2$$
$$Pr = 0{\cdot}76$$
$$Re = 14{,}600$$
$$j = 0{\cdot}0035$$
$$h_g = 11{\cdot}0 \text{ P.c.u./hr ft}^2 \,^\circ\text{C}$$
$$H_g = 0{\cdot}11 \text{ lb/lb}$$
$$c_c = 0{\cdot}272 \text{ P.c.u./lb } ^\circ\text{C}$$

In this case the gas flows in tubes, therefore $n = 0{\cdot}2$.

$$\beta = 1{\cdot}021$$
$$\frac{c_B}{h_B} = 0{\cdot}0242$$
$$h_0 = 113 \text{ P.c.u./hr ft}^2 \,^\circ\text{C}$$
$$i_{g1} = 105{\cdot}5 \text{ P.c.u./lb}$$
$$t_{l1} = 23^\circ\text{C}$$

At the gas outlet

$$i_{g2} = 22{\cdot}8 \text{ P.c.u./lb}$$
$$t_{l2} = 19{\cdot}5^\circ\text{C}$$

The calculation results are shown in Table 2. The value of integration is 3·31, and

$$G_B = 7{,}050 \text{ lb/hr}$$

The surface area is, therefore

$$A = (7{,}050)\,(0{\cdot}0242)\,(3{\cdot}31) = 565 \text{ ft}^2$$

The result of Bras is 561 ft². The difference is only + 0·7 per cent.

A Graphical Method for Vapour-Gas Mixture Other than Air–Water System

Basic equations

Equations (3) and (4) can be applied to this case too. However, $(Sc/Pr)^{0{\cdot}5}$ is not equal to unity in this case. However, it may be assumed

Table 2. Factors determined from the graphical method on Bras *example*

Point (No.)	t_g (°C)	H_g (lb/lb)	i_g (P.c.u./lb)	t_l (°C)	β	$\frac{h_0 \beta c_B}{h_B}$	t_i (°C)	i_i (P.c.u./lb)	$i_g - i_i$ (P.c.u./lb)	$10^2 \beta/(i_g - i_i)$
1	136·5	0·110	105·5	23·0	1·025	2·78	43·8	48·0	57·5	1·78
2	117·7	0·100	93·5	22·5	1·024	2·77	41·1	42·0	51·5	1·99
3	93·0	0·085	77·0	21·8	1·020	2·77	37·1	34·5	42·5	2·40
4	73·0	0·070	62·0	21·1	1·017	2·76	33·3	29·0	33·0	3·09
5	62·3	0·060	53·0	20·8	1·014	2·75	30·9	25·0	28·0	3·62
6	52·0	0·050	44·0	20·4	1·012	2·75	28·5	22·5	21·5	4·71
7	42·8	0·040	35·0	20·0	1·010	2·74	25·7	19·0	16·0	6·32
8	34·2	0·030	27·0	19·7	1·007	2·74	23·5	17·0	10·0	10·07
9	29·4	0·025	22·8	19·5	1·006	2·73	22·2	16·0	6·8	14·78

that α is constant in a condenser. Therefore, equation (5) should be written as

$$h_g/k_g' = \alpha\, c_s \tag{5'}$$

Hence,

$$-G_B\, di_g = \frac{h_g}{\alpha\, c_s}(i_g' - i_i')\, dA \tag{6'}$$

where i' is " modified enthalpy " (9) and defined as

$$i_g' = \alpha\, c_s t_g + \lambda_0 H_g \tag{7'}$$

Therefore,

$$A = \alpha\, G_B \int_{i_{g2}}^{i_{g1}} \frac{c_s}{h_g} \frac{di_g}{(i_g' - i_i')} \tag{8'}$$

The inclination of operating line is given by equation (9).
And the inclination of path line of gas condition is

$$\frac{di_g}{dt_g} = \frac{1}{\alpha} \frac{(i_g' - i_i')}{(t_g - t_i)} \tag{10'}$$

And the inclination of tie line is

$$\frac{i_g' - i_i'}{t_i - t_i} = -\frac{h_0\, \alpha\, c_s}{h_g} \tag{11'}$$

The difference between i_g and i_g' is given from equations (7) and (7').

$$i_g' - i_g = (\alpha - 1)\, c_s t = (\alpha - 1)(c_B + c_v H)\, t \tag{23}$$

And this value is a function of t and H.

Consideration of the change of values of h_g and c_s in the condenser

Equations (12)–(20) can be applied to this case too.
Hence,

$$A = \alpha\, G_B \int_{i_{g2}}^{i_{g1}} \frac{\beta\, c_B}{h_B} \frac{di}{(i_g' - i_i')}$$

$$= \frac{\alpha\, c_B\, G_B}{h_B} \int_{i_{g2}}^{i_{g1}} \frac{\beta\, di_g}{(i_g' - i_i')} \tag{21'}$$

$$\frac{i_g' - i_i'}{t_i - t_i} = -\frac{\alpha\, \beta\, h_0\, c_B}{h_B} \tag{22'}$$

Design procedure

Fig. 4 is an enthalpy-temperature chart of a vapour-gas mixture other than air–water system with the saturation curve for modified enthalpy.

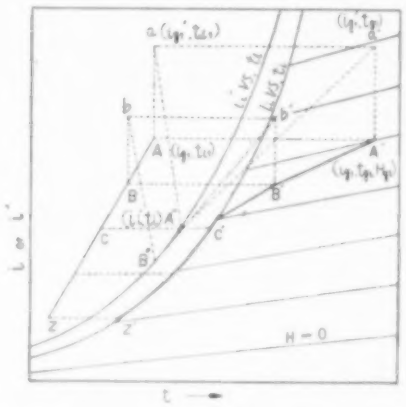

Fig. 4. Enthalpy and modified enthalpy–temperature chart.

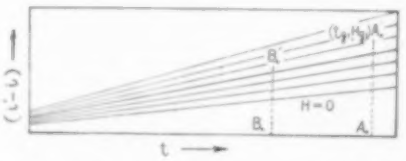

Fig. 5. Difference between modified enthalpy and enthalpy.

Fig. 5 is a diagram of the relation between enthalpy and modified enthalpy. A group of inclined straight lines of parameter H is plotted by equation (23) and shows the relation between $(i_g' - i_g)$ and t at constant H. It is convenient to take the ordinates and abscissae of Figs. 4 and 5 of the same scales.

It is assumed that the condition of inlet gas, the enthalpy of outlet gas, the temperature of cooling water available and the water and gas flow rates are known as in the above section.

Then, the operating line AZ and the point representing the condition of inlet gas, $A'(t_{g1}, H_{g1}, i_{g1})$ can be plotted on Fig. 4.

Plotting point $A_0'(t_{g1}, H_{g1})$ on Fig. 5, one can obtain $(i_{g1}' - i_{g1})$ from the length of the vertical line, $A_0' A_0$. Plot points a and a' on Fig. 4 so

that $A\,a = A'\,a' = A_0'\,A_0$. The points a and a' represent (i_{g1}', t_{l1}) and (i_{g1}', t_{g1}) respectively.

The values of c_B/h_B, β and h_0 can be obtained just like the preceding section. In the case of a gas–organic vapour mixture, however, the thermal resistance of the condensate film predominates in h_0 and varies considerably in a condenser. Therefore, the value of h_0 should be calculated at each point. And also the value of α can be calculated by equation (4) assuming $p_{BM}/(P - p_i) = 1$, and using average values of Pr and Sc. Thus, one calculates the inclination of the tie line $-\alpha\,\beta\,h_0\,c_B/h_B$, and constructs the tie line from a, and locates $A''\,(i_i', t_i)$ on the saturation curve for i_i' vs. t_i.

Join point a' with A''. Since the inclination of $a'\,A''$ is $(i_{g1}' - i_{i1}')/(t_{g1} - t_{i1})$, equation (10′) indicates that the inclination of the path line at point A' is equal to $(1/\alpha)$ times the value of that of $a'\,A''$. Now, one can construct the path line of gas condition from A' through B'. B' corresponds to the next point B on the operating line.

The steps mentioned above should be repeated until one reaches the final point Z.

Then, plot $\beta/(i_g' - i_i')$ vs. i_g and calculate the value of the integral in equation (21′). Finally, one can calculate the surface area A by equation (21′).

The comparison of results of calculation and experiment

The procedure mentioned above is applied to Run No. 14 D of Smith and Robson's experiment [11] with air–benzene system.

At the gas inlet

$$Pr = 0{\cdot}698$$
$$Sc = 0{\cdot}341$$

At the gas outlet

$$Pr = 0{\cdot}761$$
$$Sc = 0{\cdot}584$$

In average

$$Pr = 0{\cdot}730$$
$$Sc = 0{\cdot}463$$

Hence

$$\alpha = \left(\frac{0{\cdot}463}{0{\cdot}730}\right)^{\frac{1}{3}} = 0{\cdot}80$$

Table 3. Factors determined from the graphical method on Smith and Robson *example*

Point (No.)	t_g (°C)	H_g (lb/lb)	i_g (P.c.u./lb)	i_g' (P.c.u./lb)	t_l (°C)	β	h_0 (P.c.u./ft² hr °C)	$\alpha\,\beta\,h_0 c_B/h_B$	t_i (°C)	i_i' (P.c.u./lb)	$i_g' - i_i'$ (P.c.u./lb)	$10^4\,\beta/(i_g' - i_i')$
1	90·0	20·40	2754	2639	32·80	1·845	241	225·58	43·6	131	2508	7·36
2	86·8	18·90	2536	2434	32·58	1·818	180	94·01	55·7	266	2168	8·39
3	84·3	17·38	2318	2226	32·26	1·789	164	79·98	56·6	283	1943	9·21
4	81·9	15·83	2106	2018	31·94	1·758	150	71·79	56·4	278	1740	10·10
5	79·4	14·25	1882	1811	31·62	1·723	140	65·76	55·4	263	1548	11·13
6	76·7	12·67	1664	1600	31·30	1·686	133	60·99	53·8	237	1363	12·37
7	73·8	11·04	1446	1394	30·98	1·644	127	56·78	51·9	212	1182	13·91
8	71·3	9·42	1228	1183	30·66	1·599	122	53·14	49·5	183	1000	15·99
9	70·0	7·76	1010	974	30·34	1·543	118	49·47	46·7	157	817	18·88
10	68·0	6·09	792	765	30·02	1·479	114	45·96	43·7	133	630	23·46
11	65·9	4·43	574	553	29·70	1·403	111	42·07	40·3	109	444	31·60

Now, one can make an enthaply and modified enthalpy–temperature chart and a diagram of the relation between enthalpy and modified enthalpy.

The condition at the gas inlet and outlet are

$$i_{g1} = 2{,}754 \text{ P.c.u./lb}$$
$$t_{l1} = 32{\cdot}9\,^{\circ}\text{C}$$
$$t_{l2} = 29{\cdot}7\,^{\circ}\text{C}$$

The inclination of operating line is

$$\frac{L\,C_l}{G_B} = \frac{2760}{0{\cdot}14 \times 29} = 680$$

Now, the operating line can be fixed on enthalpy–temperature chart.

At the gas inlet, the heat transfer coefficient

$$h_g = 10{\cdot}1 \text{ P.c.u./ft}^2 \text{ hr } ^{\circ}\text{C}$$

And

$$H_g = 20{\cdot}4 \text{ lb/lb}$$
$$\beta = (1 + 20{\cdot}4)^{0{\cdot}2} = 1{\cdot}845$$
$$c_s = 0{\cdot}24 + (20{\cdot}4)\,(0{\cdot}3)$$
$$= 6{\cdot}36 \text{ P.c.u./lb } ^{\circ}\text{C}$$

Therefore

$$\frac{c_B}{h_B} = \frac{6{\cdot}36}{(10{\cdot}1)\,(1{\cdot}845)} = 0{\cdot}342$$

The value of h_0 is obtained at each point using a conventional Nusselt equation for condensate film conductance.

Point to point calculation results are shown in Table 3.

The values of integration in equation (21′) is 3·08, and

$$\frac{\alpha\, c_B\, G_B}{h_B} = (0{\cdot}80)\,(0{\cdot}342)\,(0{\cdot}14 \times 29) = 1{\cdot}11$$

The surface area is, therefore

$$A = (1{\cdot}11)\,(3{\cdot}08) = 3{\cdot}42 \text{ ft}^2$$

Compared to 3·09 ft² as calculated by the rigorous method of COLBURN and HOUGEN, and 3·3 ft² as found experimentally by ROBERTSON and SMITH, the agreement is good.

Acknowledgements—The Authors wish to acknowledge their indebtedness to the late Dr. A. P. COLBURN and Dr. R. L. PIGFORD of University of Delaware for encouraging the first of the authors to work on the subject.

NOTATION

A = area of transfer surface, ft²

C = constant in equations (13) and (18)

c = specific heat, P.c.u./lb °C

c_s = humid heat, P.c.u./lb of dry gas °C

d = diameter of tube, ft

G_B = flow rate of stagnant gas, lb/hr

G' = mass velocity of gas vapour mixture, lb/hr ft²

G_B' = mass velocity of stagnant gas, lb/hr ft²

H = humidity, lb/lb of dry gas

h = coefficient of heat transfer, P.c.u./ft² hr °C

h_B = fictitious coefficient of heat transfer when only stagnant gas flows, P.c.u./ft² hr °C

h_0 = combined conductances other than the gas film P.c.u./ft² hr °C

i = enthalpy of gas vapour mixture, P.c.u./lb of dry gas

i' = modified enthalpy of gas vapour mixture, P.c.u./lb of dry gas

k_g = mass transfer coefficient, lb mole/ft² hr atm

k_g' = mass transfer coefficient, lb/ft² hr (lb/lb of dry gas)

L = flow rate of cooling water, lb/hr

M = molecular weight, lb/mole

n = number of power

P = total pressure in condenser, atm

p = partial vapour pressure, atm

p_{BM} = average partial pressure of stagnant gas in gas film, atm

t = temperature, °C

α = constant defined by equation (4)

β = variable defined by equation (20)

λ_0 = latent heat of vaporization at 0°C, P.c.u./lb

μ = viscosity, lb/hr ft

Pr = Prandtl number

Sc = Schmidt number

Re = Reynolds number

Subscripts:

B = stagnant gas

g = gas–vapour mixture or gas film

i = interface

l = cooling water

v = vapour

References

[1] Bras G. H. P. *Chem. Engng.* 1953 223, 238.

[2] Bras G. H. P. *Petrol. Refiner* 1956 **35** 177; 1957 **36** 149.

[3] Bras G. H. P. *Chem. Engng. Sci.* 1957 **6** 277.

[4] Cairns R. C. *Chem. Engng. Sci.* 1953 **2** 127.

[5] Colburn A. P. *Proc. Gen. Disc. on Heat Transfer*, p. 1. Institute of Mechanical Engineering, London 1951.

[6] Colburn A. P. and Hougen O. A. *Ind. Engng. Chem.* 1934 **26** 1178.

[7] Cribb G. S. and Nelson E. T. *Chem. Engng. Sci.* 1956 **5** 20.

[8] Mickley H. S. *Chem. Engng. Prog.* 1949 **45** 739.

[9] Mizushina T. and Kotoo T., *Chem. Engng.* (*Japan*) 1949 **13** 75.

[10] Mizushina T. and Nakajima M. *Chem. Engng.* (*Japan*) 1951 **15** 30.

[11] Smith J. C. and Robson H. T. *Proc. Gen. Disc. on Heat Transfer* p. 38. Institute Mechanical Engineers, London 1951.

Chemical Engineering Science, 1959, Vol. 9, pp. 205 to 217. Pergamon Press Ltd. London. Printed in Great Britain

Gas–liquid flow in horizontal pipes

C. J. HOOGENDOORN

Koninklijke/Shell-Laboratorium, Amsterdam. (N. V. De Bataafsche Petroleum Maatschappij, The Hague)

(*Received* 24 *December* 1957)

Abstract—To obtain information on gas–liquid flow under operational processing conditions, an investigation was made of the flow of air–water and air–oil mixtures in horizontal smooth pipes with inner diameters ranging from 24 mm to 140 mm, and rough pipes with an inner diameter of 50 mm.

As a result of this, diagrams can be given from which the flow patterns for these mixtures can be predicted with reasonable accuracy for all pipe diameters within the range investigated.

For the pressure drop the Lockhart-Martinelli correlation appeared to be valid for plug, slug and froth flow at atmospheric pressure only; for wave and mist–annular flow it was inadequate under any conditions. Separate new correlations are given for these cases; those for plug, slug and froth flow include the influence of gas density.

The results of holdup measurements have been correlated empirically with the slip velocity between the phases. A special holdup meter has been developed enabling accurate measurements to be made.

Résumé—On a étudié l'écoulement de mélanges à deux phases (air–eau et air–huile) en tubes lisses horizontaux d'un diamètre intérieur de 24 à 140 mm, et en tubes rugueux d'un diamètre intérieur de 50 mm, pour mieux comprendre le comportement des courants à deux phases dans les conditions de pratique.

Les résultats ont été utilisés pour tracer des diagrammes permettant d'établir avec une précision raisonnable les configurations de l'écoulement de ces mélanges dans des tubes d'un diamètre intérieur quelconque, compris dans les limites de nos mesures.

Les valeurs de Lockhart-Martinelli pour la perte de charge ont paru être valables pour les zones de circulation sous forme de tampons, de bouchons et de mousse à pression atmosphérique seulement ; pour les zones de circulation ondulatoire et annulaire avec pulvérisation, elles n'étaient applicable sous aucune condition. Pour ces cas de nouvelles valeurs sont données ; celles qui se rapportent aux zones de circulation sous forme de tampons, de bouchons et de mousse, tiennent compte de l'influence de la densité du gaz.

Une relation entre les résultats des mesures du hold-up et la vitesse de glissement entre les phases a été établie d'une façon empirique. On a mis au point un jauge spécial qui permet de mesurer le hold-up avec précision.

Zusammenfassung—Um Kenntnis über die Zweiphasenströmung unter Betriebsbedingungen zu erhalten, wurde die Strömung von Luft-Wasser- und Luft-öl-Mischungen in waagerechten, glatten Rohren mit lichten Durchmessern zwischen 24 und 140 mm und rauhen Rohren mit lichten Durchmessern von 50 mm untersucht.

Als ein Ergebnis dieser Arbeit werden Diagramme angegeben, aus denen sich die Strömungsform für diese Mischungen aussagen lässt und zwar mit hinreichender Genauigkeit für alle Rohrdurchmesser im untersuchten Bereich.

Für den Druckabfall scheint die Beziehung von Lockhart – Martinelli für Kolben-, Tropf- und Schaumströmung nur bei atmosphärischem Druck gültig zu sein. Für Wellen- und Tröpfchen-Ring-Strömung war sie in allen Fällen nicht brauchbar. Für diese Strömungsarten werden neue Beziehungen mitgeteilt, Die Gleichungen für Kolben-, Tropf- und Schaumströmung enthalten den Einfluss der Gasdichte.

Die Ergebnisse von Messungen des Flüssigkeitsgehaltes konnten empirisch mit der Schlupfgeschwindigkeit zwischen den Phasen in Beziehung gesetzt werden. Ein besonderes Messgerät für den Flüssigkeitsgehalt wurde entwickelt und ergab ausreichende Messgenauigkeiten.

1. INTRODUCTION

A NUMBER of authors have studied gas–liquid flow in pipes of diameters small in comparison with the diameters used in technology. Quite recently some experimental data were given by REID *et al.* [16] for air–water flow in 4 in. and 6 in. pipes, but only for a narrow range of air and water velocities. BAKER [3] gives some field results for 4 in. to 10 in. pipes, the validity of which is restricted to the special cases he studied.

An investigation of gas–liquid flow through horizontal large-diameter pipes was therefore made, to extend the region of pipe diameters covered.

The influence of the following parameters was established:

1. Pipe diameter. Smooth pipes of inner diameter $D = 24$, 50, 91 and 140 mm were used. The smaller pipe diameters were included not only for check measurements, but also for a series of measurements covering a wider range of gas and liquid mass velocities than reported in literature.
2. Liquid properties. Water, spindle oil, and gas oil were used as liquids.
3. Gas density over a narrow range. Air pressure ranged between 1 and 3 atm.
4. Pipe roughness. Various degrees of roughness were investigated in pipes of $D = 50$ mm.

The flow pattern, the pressure drop, and the liquid holdup were studied.

2. EXPERIMENTAL SETUP AND MEASURING PROCEDURE

Figure 1 gives a flow scheme of the experimental setup. The 25 m horizontal test section was of transparent perspex pipes.

The pressure drop was measured only at locations beyond an inflow length of 60 D. For the 24 and 50 mm pipes 3 successive measuring sections each 4 m in length were used, and for the 91 and 140 mm pipes one measuring section of 8 m. The measurements in rough pipes were made in 3 sections of 2 m each, preceded by 17 m of smooth perspex pipes of the same diameter. Pressure taps were located in special flanges and the pressure was transmitted from the underside of these flanges to normal U-tube manometers through liquid-filled lines. Care was taken to keep air out of these lines.

Different entrance devices for the air and liquid were tested; the influence of change in inlet

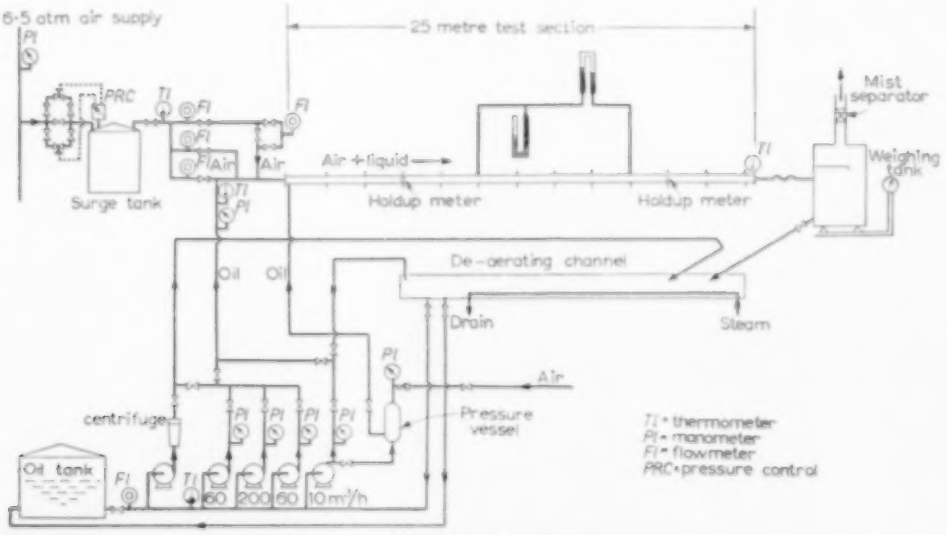

FIG. 1. Flow scheme of 25 m test setup.

device was found to be negligible beyond 60 D, except in one case mentioned below.

Four centrifugal pumps and a pressure vessel made a wide range of liquid flow rates possible (0·02 to 320 m³/h). High flow rates were measured with an orifice meter, the low rates by weighing. The liquid used was recirculated after de-aeration in a channel 25 m long.

Compressed air was used from a 6·5 atm. supply with a maximum capacity of 1800 kg/hr. The air flow rate was measured with orifice meters of different sizes.

Liquid and air temperatures were measured in the separate supply lines and at the end of the test section. The oil temperature was regulated with a steam coil in the de-aeration channel.

Properties of the circulating liquid (see Table 1) such as density, viscosity, and surface tension were regularly checked. For the properties of the air the data for dry air could be taken since its moisture content was negligibly low.

For measuring the liquid holdup a capacitive method was developed. Three stainless steel discs (spacing 9 mm) were mounted in the pipe parallel to the direction of flow (see Fig. 2). They form the electrodes of a capacitor, the capacitance of which depends on the liquid holdup in the pipe. The discs (same diameter as the pipe) are circular in shape except at the point where they are mounted in the pipe wall. A linear relationship between holdup and capacitance is thus obtained. This makes the method almost independent of the configuration of the gas–liquid mixture and makes it possible to determine mean values for the holdup in a fluctuating flow. Such holdup meters were used in the perspex pipes of D = 50, 91 and 140 mm.

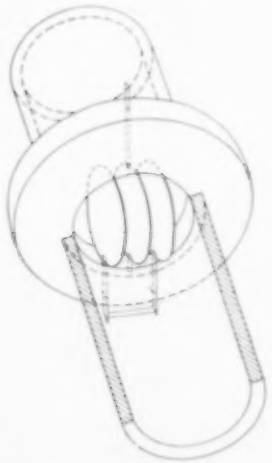

Fig. 2. Holdup meter.

The holdup meter was calibrated under different conditions:

1. By filling a closed horizontal section of 4 m length to a known liquid level, the holdup meter being fixed at its mid-point. This represents the case of stratified and wave flow (flow patterns as described below). A linear relationship between capacitance and holdup was found.
2. By placing a 3 m section in a vertical position, again with the holdup meter at its mid-point. Gas–liquid flow through this pipe may show different dispersions representing either plug, slug or froth flow. In a vertical arrangement the holdup can easily be determined by suddenly closing the air and oil supply. (Only in the case of a fine dispersion did the calibration curve differ somewhat from that found by method 1).

The capacitive method was checked by means of a series of experiments in the 50 mm I.D. pipe with a radio-active tracer. For this purpose an oil-soluble radio-active tracer was homogeneously mixed with the oil. In this case the radiation intensity of a part of the pipe depends linearly on the liquid holdup. The results showed that the differences in holdup between both methods were random, giving a standard deviation of 0·03. Only for froth flow was a significant difference found and this was probably due to a finer dispersion than obtained in the vertical calibration. The capacitive method was corrected accordingly in that region.

For each combination of pipe diameter and liquid a series of about 12 runs was done, each run being performed under eight or more different measuring conditions. The ranges of the superficial mass velocities of liquid and air are given in Table 2. Each series started with a run of one-

phase liquid flow in order to check the measuring procedure. The friction factors thus obtained were in agreement within ± 5 per cent with the factors for smooth pipes given by MOODY [14]. For the rough pipes the roughness was found from the one-phase liquid friction factors by comparing them with the factors given by MOODY [14]. The roughness values thus obtained for the different cases were $\frac{\epsilon}{D} = 0{\cdot}030$; 0·019; 0·0030 and 0·0012.

All the pressure drop data were corrected for a compressibility effect. When the pressure drop becomes appreciable the gas expansion accelerates both the gas and liquid phase. An approximate impulse correction ΔP_c based on mean velocities was used to obtain the friction pressure drop between sections 1 and 2 from the measured pressure drop. It was found from:

$$\Delta P_c = \frac{m_l^2}{\rho_l}\left[\frac{1}{R_{l_2}} - \frac{1}{R_{l_1}}\right] + m_g^2\left[\frac{1}{\rho_{g_2}(1 - R_{l_2})} - \frac{1}{\rho_{g_1}(1 - R_{l_1})}\right]. \quad (1)$$

The correction was small for the tests in the 91 and 140 mm pipes, but for the 24 and 50 mm pipes it amounted to 15 per cent of the total pressure drop in cases of high velocity.

Table 1. *Liquid properties at operating temperature of* 28°C

	Viscosity ν_l (m^2/s)	*Density* ρ_l (kg/m^3)	*Surface tension* σ (N/m)
Gas oil	$2{\cdot}9 \times 10^{-6}$	815	27×10^{-3}
Spindle oil	23×10^{-6}	905	30×10^{-3}

Table 2. *Range of superficial mass velocities*

Pipe dia. D (m)	m_g (kg/m^2 s)	m_l (kg/m^2 s)
0·024	0·4–220	30–4500
0·050	0·05–165	1·5–6000
0·091	0·5–80	20–5500
0·140	0·2–55	5–5000

3. DISCUSSION OF RESULTS

3.1 *Flow patterns*

Visual observation shows that different flow patterns may occur with gas–liquid flow in horizontal pipes. In accordance with results obtained with small diameter pipes (BERGELIN and GAZLEY [4], ALVES [1], KOSTERIN [9]) we observed the following flow patterns*) in our tests:

a. Stratified flow. The liquid flows in the lower part of the pipe and the air over it with a smooth interface between the two phases.

b. Wave flow. Similar to stratified flow, except for a wavy interface, due to a velocity difference between the two phases. In wave + mist flow the difference in velocity is so great, that a certain amount of atomization takes place.

c. Plug flow. The gas moves in bubbles or plugs along the upperside of the pipe.

d. Slug flow. Splashes or slugs of liquid occasionally pass through the pipe with a higher velocity than the bulk of the liquid. Pressure fluctuations are typical for this type of flow.

e. Mist–annular flow. The liquid is partly atomized in the gas phase and partly flowing in an annular film along the pipe wall.

f. Froth flow. The gas is dispersed in fine bubbles through the liquid phase.

Charts have been proposed (ISBIN *et al.* [7], KOSTERIN [9] and WHITE and HUNTINGTON [18]) to show the ranges of flow variables for the different flow patterns. They all use the gas and liquid velocities or combinations of these as variables and the different charts can be transformed into each other. The chart proposed by KOSTERIN [9] is used for representing our results (see Fig. 3).

*A film entitled "Simultaneous flow of gas and liquid" and showing these flow patterns for air–gas-oil flow in 91 mm I.D. pipes is in preparation and will be obtainable on loan from the local Shell organization.

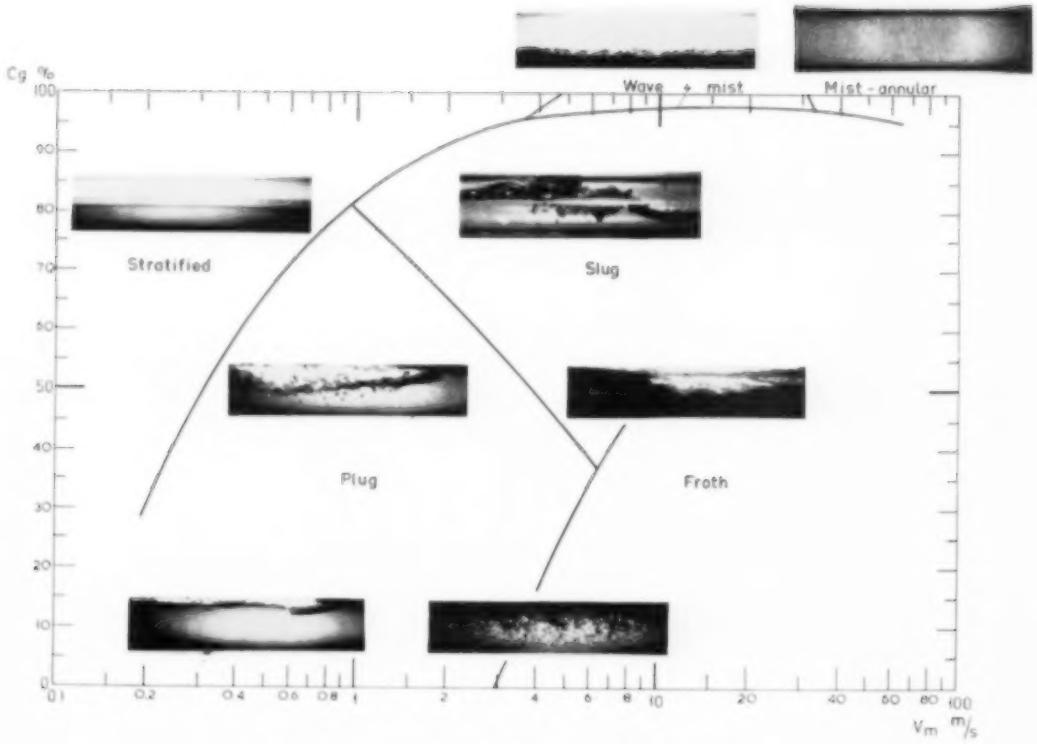

Fig. 3. General diagram for flow regions with gas-oil flow.

Here the relevant variables are the mixture velocity v_m and the gas percentage c_g, with:

$$v_m = \frac{Q_g + Q_l}{\frac{\pi}{4} D^2} \text{ and } c_g = \frac{Q_g}{Q_g + Q_l} \times 100\%.$$

Q_g = gas flow rate by volume,

Q_l = liquid flow rate by volume.

Our results with air–spindle-oil and air–gas-oil flow in pipes of different diameters showed that the influence of liquid viscosity and pipe diameter on the location of the lines of transition between the various flow pattern regions is small. These transition lines are in fact transition zones with a breadth comparable to the shift of the transition lines due to change in pipe diameter or oil. Thus one chart (Fig. 3) can be given presenting all our results for air–oil flow. Deviations from this generalized chart may occur in cases where the gas density is different from that used in our experiments (1·2 — 3 kg/m³) especially near the transition lines. The same holds for cases of high liquid viscosities (> 50 cS).

Our results for air–water flow showed nearly the same transition lines (see Fig. 4(a)) except for wave flow, which occupies a much larger region.

Although the influences of pipe diameter and liquid properties on the various transition lines are small and have been neglected for the general diagram of Fig. 3 they can be discussed by a more detailed study of our results. Figures 4(a), 4(b), 5(a) and 5(b) give some typical cases.

a. The transition from stratified flow to plug and slug flow. This occurs at superficial liquid velocities v_{sl} of about 0·2 m/sec independent of superficial air velocity. For

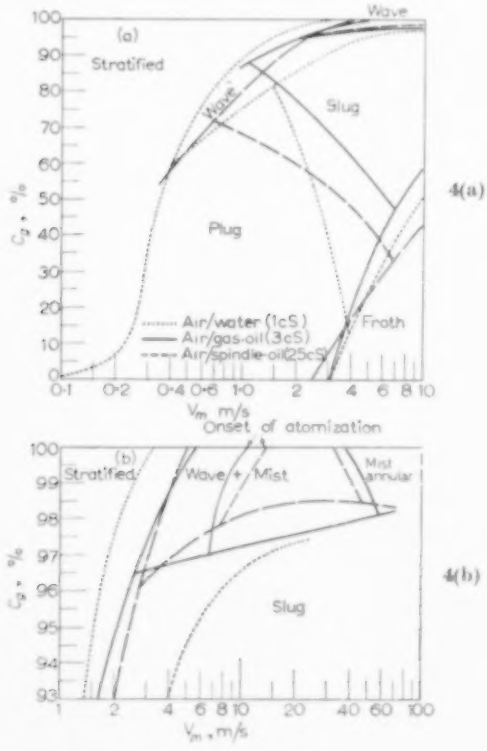

4(a)

4(b)

Fig. 4 (a). Flow regions in 91 mm I.D. pipe.

Fig. 4 (b). Flow regions for high c_g's in 91 mm I.D. pipe.

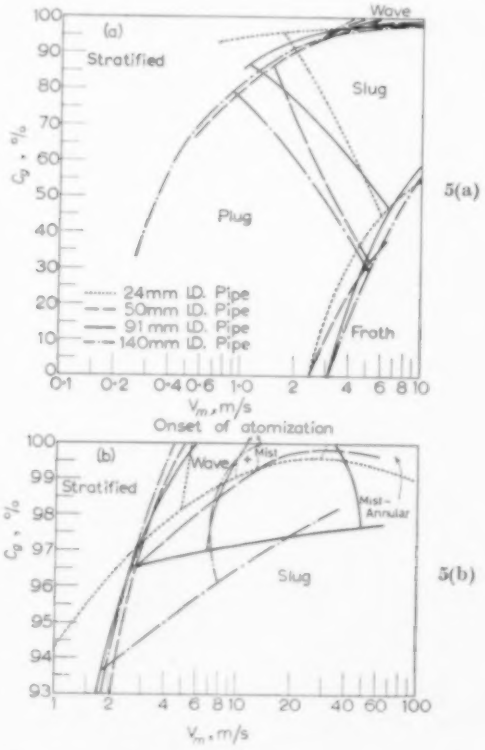

5(a)

5(b)

Fig. 5 (a). Flow regions for air–gas-oil flow.

Fig. 5 (b). Flow regions for high c_g's for air–gas-oil flow.

the smaller diameters the transition occurs at somewhat lower velocities, because instabilities in the liquid surface can easily reach the wall at the top of the pipe (see Fig. 5(a), 24 mm pipe).

b. The transition from wave + mist flow to slug flow. For the largest pipe diameter (140 mm) this occurs at an air percentage of between 94–97 per cent. For the smaller diameters the waves reach the wall at the top of the pipe more easily; therefore here again the transition occurs at higher air percentages. There is, moreover, the influence of surface tension. For air–water flow the wave flow region is greater than for air–oil flow (Fig. 4(a)).

c. The transition from wave flow to wave + mist flow. Atomization of the waves begins in all cases for $v_m \sim 11$ m/sec.

d. The transition from wave + mist flow to mist–annular flow. The liquid droplets formed by atomization of the liquid in the lower part of the pipe are deposited on the pipe wall and form a film of liquid. For $v_{sg} > 30$ m/sec, this film and the liquid layer in the lower part of the pipe form one fully developed liquid annulus. Thus generally the liquid annulus co-exists with a mist in the gas phase. We observed a tendency for the surface to curve upwards in the neighbourhood of the pipewall at $v_{sg} > 15$ m/sec. However, at these velocities we always found atomization, even at the lowest oil flow rates ($v_{sl} = 0{\cdot}002$ m/sec). This contradicts results of KRASYAKOVA [11] for air–water flow in 30 mm pipes.

e. The transition from mist–annular flow to slug flow. This occurs at air percentages of about 98 per cent. Again for the small pipe diameters the transition occurs at somewhat higher air percentages.

f. The transition from plug flow to slug flow. This zone is very wide; no general conclusion can, therefore, be given.

g. The transition from plug flow and slug flow to froth flow. This occurs at $v_{sl} \simeq 3$ m/sec. Here the pipe diameter shows the effect of shifting the transition to higher velocities for the greater pipe diameters.

3.2 *Pressure drop.*

The correlation generally used for two-phase pressure drop is the one given by LOCKHART and MARTINELLI [13], based on their results with air–liquid flow in 0·06–1 in. pipes at atmospheric pressure. They use the parameters Φ_g and x, given by:

$$\Phi_g^2 = \frac{\Delta P_{tp}}{\Delta P_g}\,;\quad \mathrm{x}^2 = \frac{\Delta P_l}{\Delta P_g}\,. \tag{2}$$

Here: ΔP_{tp} = pressure drop over pipe length ΔL for two-phase flow.

ΔP_g = pressure drop over pipe length ΔL for the gas-phase flowing alone through the pipe.

ΔP_l = pressure drop over pipe length ΔL for the liquid-phase flowing alone through the pipe.

Our results with smooth pipes showed that for plug, slug, and froth flow under atmospheric conditions their correlation also holds for the larger pipe diameters. The standard deviation between our pressure drop data and their correlation was 13 per cent, while maximum deviations of $\pm$ 30 per cent occurred. Our results showed, however, that in other cases the deviations were rather appreciable, for all pipe diameters. Closer examination of the relevant data indicated that the Lockhart-Martinelli correlation does not hold:

a. for plug, slug and froth flow if gas densities differ from that of air at atmospheric pressure.
b. for stratified flow and wave flow.
c. for mist-annular flow.

This probably explains the discrepancies as found by various authors when using this correlation (BERGELIN and GAZLEY [4], CHENOWETH and MARTIN [5], BAKER [3] and REID *et al.* [16]).

For the results in the 50 mm rough pipes comparison with the Lockhart-Martinelli correlation shows discrepancies when for ΔP_l and ΔP_g

in their parameter x the values for rough pipes are used. By using, however, in x the values for smooth pipes at the same conditions and in Φ_g the value for rough pipes reasonable agreement is again obtained for plug, slug, and froth flow at atmospheric pressure. This is also confirmed by CHISHOLM and LAIRD [6] in a recent paper on air–water flow in rough 1 in. pipes. They find, however, in addition that at larger values of ϵ/D an increase in pipe roughness has less influence with two-phase pressure drop than with one phase pressure drop. This did not appear from our measurements.

We developed new correlations for pressure drop for those cases where the existing ones appeared to be inadequate, as follows.

a. Plug, slug and froth flow; influence of air density

For plug, slug, and froth flow it was found that though the Lockhart-Martinelli correlation holds at atmospheric pressure, the values it gives for the pressure drop at higher air densities were too high. Consequently we tried – by using dimensionless groups – to develop a new correlation for these flow patterns, which would, in addition, reflect the influence of gas density.

The two-phase pressure drop is considered to be a function of the following quantities: pipe length ΔL, pipe diameter D, superficial liquid mass velocity m_l, superficial gas mass velocity m_g, liquid density ρ_l, gas density ρ_g, liquid dynamic viscosity η_l, gas dynamic viscosity η_g, surface tension σ, and acceleration of gravity g.

Since in the Lockhart-Martinelli correlation the influence of surface tension and gravity is neglected without loss of accuracy, it is felt that these quantities can be ignored for the flow patterns under consideration within the range of variables investigated. The following six dimensionless groups can then be formed:

$$\frac{\Delta P_{tp}}{\frac{1}{2}\, m_t^2/\rho_l}, \quad \frac{\Delta L}{D}, \quad \frac{m_t D}{\eta_l}, \quad \frac{m_g}{m_t}, \quad \frac{\eta_l}{\eta_g}, \quad \frac{\rho_l}{\rho_g},$$

where $m_t = m_g + m_l$ is the mass velocity of total gas and liquid flow.

Since the pressure drop is directly proportional to the pipe length (with the other variables constant) we have the following relationship:

$$\lambda_{tp} = F\left(Re_{tp},\ \frac{m_g}{m_t},\ \frac{\rho_g}{\rho_l},\ \frac{\eta_l}{\eta_g}\right). \tag{3}$$

Here:

$$\lambda_{tp} = \frac{\Delta P_{tp}}{\frac{1}{2}\,\frac{\Delta L}{D}\,\frac{m_t^2}{\rho_l}} \tag{4}$$

and

$$Re_{tp} = \frac{m_t D}{\eta_l}, \tag{5}$$

analogous to the friction factor and Reynolds number in one-phase flow. The choice of these groups based on m_t stemmed from the consideration of the flow of an evaporating medium in a pipe where the mass flow of liquid and gas separately is continually changing, but where the total mass flow is constant.

The influence of the gas density could be found by analysing our data for the 24 and 50 mm pipes taken over 3 separate sections of 4 m length each. Due to the pressure drop a difference in ρ_g/ρ_l existed between the 3 sections for each test condition the other dimensionless groups remaining constant. We assumed a power law to exist between λ_{tp} and ρ_g/ρ_l giving:

$$\lambda_{tp} = (\lambda_{tp})_n \left\{\frac{(\rho_g/\rho_l)_n}{(\rho_g/\rho_l)}\right\}^{\alpha}. \tag{6}$$

Here $(\lambda_{tp})_n$ is the value of λ_{tp} for the fixed value of $(\rho_g/\rho_l)_n = 1{\cdot}38 \times 10^{-3}$. Figure 6 gives some

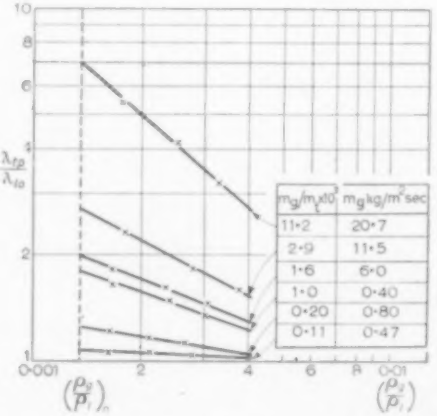

FIG. 6. Influence of air density on pressure drop with air–gas-oil flow in 24 mm pipe.

results showing the influence of gas density on λ_{tp}. Here a friction factor λ_{lo}, defined below and independent of the gas density, is used to bring the curves together in one figure. The exponent x is a function of other groups. Actually x was found to be a function of m_g/m_t alone. It is easily seen that in the case of all liquid flow ($m_g/m_t = 0$), x equals zero, in the case of all gas flow ($m_g/m_t = 1$), x equals unity. For intermediate values of m_g/m_t our results gave for x the empirical correlation:

$$x = 9{\cdot}5\left(\frac{m_g}{m_t}\right)^{0{\cdot}5} - 62{\cdot}6\left(\frac{m_g}{m_t}\right)^{1{\cdot}3} \quad \text{for } \frac{m_g}{m_t} < 0{\cdot}03$$
$$x = 1 \quad \text{for } \frac{m_g}{m_t} > 0{\cdot}03 \tag{7}$$

The influence of the other groups could be analysed separately from that of the gas density because

$$(\lambda_{tp})_n = f\left(Re_t, \frac{m_g}{m_t}, \frac{\eta_l}{\eta_g}\right) \tag{8}$$

Our data showed that curves could be plotted of $(\lambda_{tp})_n$ versus Re_{tp} and m_g/m_t (see Fig. 7), the influence of the viscosity ratio η_l/η_g could be neglected in the range of viscosities investigated (η_l/η_g from 60 to 1500). These curves can be represented by

$$\frac{(\lambda_{tp})_n - \lambda_{lo}}{\lambda_{lo}} = 230\left(\frac{m_g}{m_t}\right)^{0{\cdot}84} \tag{9}$$

for $\frac{m_g}{m_t} < 0{\cdot}05$ and $Re_{tp} > 3000$.

Here, λ_{lo} is the friction factor which would apply if the whole mass of gas and liquid were flowing in the liquid phase. Including the influence of density, this leads to the general correlation:

$$\lambda_{tp} = \lambda_{lo}\left\{1 + 230\left(\frac{m_g}{m_t}\right)^{0{\cdot}84}\right\}\left\{0{\cdot}00138\,\frac{\rho_l}{\rho_g}\right\}^{x}$$
$$\text{or } \Delta P_{tp} = \lambda_{lo}\left\{1 + 230\left(\frac{m_g}{m_t}\right)^{0{\cdot}84}\right\}\left\{0{\cdot}00138\,\frac{\rho_l}{\rho_g}\right\}^{x} \tag{10}$$

For: $\frac{m_g}{m_t} < 0{\cdot}05$, $Re_{tp} > 3000$.

Here ΔP_{lo} = pressure drop over pipe length ΔL which would occur if the whole mass of gas and liquid were flowing in the liquid phase through the pipe.

Furthermore x is given by (7).

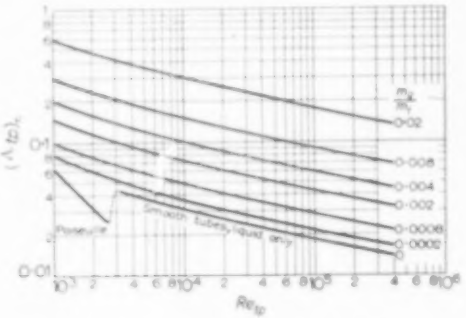

FIG. 7. New pressure drop correlation for plug, slug and froth flow.

The standard deviation for our 492 test data obtained in 24, 50, 91 and 140 mm smooth pipes with air–water, air–gas-oil and air–spindle-oil flow compared with this new correlation was 6 per cent for $m_g/m_t < 0{\cdot}001$ and 14 per cent for $0{\cdot}001 < m_g/m_t < 0{\cdot}05$; in the second range most data were for slug flow type where the pressure fluctuates strongly and an accurate determination of the pressure drop is impossible.

The influence of gas density was investigated over a range of $1{\cdot}1 - 3{\cdot}3\ \text{kg/m}^3$, the factor $0{\cdot}00138\,(\rho_l/\rho_g)$ then varies from 1–3. In Fig. 6 this influence on $\lambda_{tp}/\lambda_{lo}$ is shown for some test data at various values of m_g/m_t, it is seen that extrapolation to much higher densities is not permissible, since the curves would intersect the line $\lambda_{tp}/\lambda_{lo} = 1$. Further research at high gas densities would be required.

The data obtained in the 50 mm rough pipes with air–gas-oil flow were analysed in the same way as those of the smooth pipes. Pipe roughnesses studied were $\epsilon/D = 0{\cdot}030$ and $0{\cdot}019$ (cast iron pipe) and $\epsilon/D = 0{\cdot}0030$ and $0{\cdot}0612$ (ground cast iron pipe). The same correlation formula (10) as developed for smooth pipes holds with the same restrictions for all values of ϵ/D, if for λ_{lo} the value is taken corresponding to the ϵ/D of the rough pipe.

b. Stratified flow and wave flow

For stratified flow and wave flow the pressure drop was lower than predicted by the Lockhart-Martinelli correlation, as can be seen for wave flow in Fig. 8. For stratified flow only a few data are available, indicating the same trend as for wave flow. For various superficial liquid mass velocities different curves are found when the Lockhart-Martinelli parameters are used. This

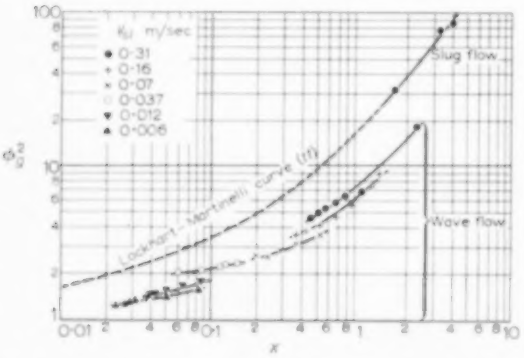

Fig. 8. Data for air–gas-oil flow in 140 mm pipe correlated with Lockhart-Martinelli parameters.

shows that these parameters are inadequate for correlating the pressure drop in the region of wave flow. This behaviour coincides with the transition to a different flow pattern as can also be seen in Fig. 8. The curve for the constant superficial liquid velocity $v_{sl} = 0{\cdot}31$ m/sec consists of 2 parts. For $X > 2$ the air mass velocity is small and slug flow exists, the results being in agreement with the Lockhart-Martinelli correlation. With increasing air velocity the flow pattern changes to wave flow this being the part corresponding to $X < 1$. The pressure drop shows a sharp decrease there. For $1 < X < 2$ the conditions just cover the transition from wave to slug flow. By using different inflow devices it was possible to obtain either slug or wave flow, the other conditions being the same. In this way the overlap in the two parts of this curve was found; this clearly showing the influence of flow pattern on pressure drop.

The results for the pressure drop with wave flow were analysed separately. It was found that the dimensionless group $\dfrac{\Delta P_{tp}}{\frac{1}{2}\dfrac{\Delta L}{D}\dfrac{m_l^2}{\rho_g}}$ could be correlated with m_g/m_t (see Fig. 9) giving:

$$\frac{\Delta P_{tp}}{\frac{1}{2}\dfrac{\Delta L}{D}\dfrac{m_l^2}{\rho_g}} = C\left(\frac{m_g}{m_t}\right)^{1{\cdot}45} \qquad (11)$$

for $\dfrac{m_g}{m_t} < 0{\cdot}8$.

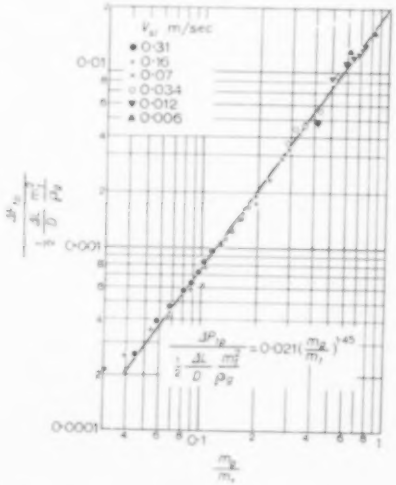

Fig. 9. Pressure drop correlation for wave-flow results in 140 mm tube with air–gas-oil flow.

Here C was found to depend slightly on pipe diameter and liquid viscosity, see Table 3. The air density could not be varied during these tests and amounted to $1{\cdot}2$ kg/m^3.

Table 3. Influence of pipe diameter and liquid viscosity on C

Diameter	*Air–gas-oil*	*Air–spindle-oil*
0·050 m	$C = 0{\cdot}026$	$C = 0{\cdot}028$
0·091 m	$C = 0{\cdot}022$	
0·140 m	$C = 0{\cdot}021$	$C = 0{\cdot}022$

In this case again a marked influence of pipe roughness on the two-phase pressure drop was found. The experiments with air–gas-oil flow in the rough 50 mm pipes showed that the same correlation formula (11) could be used, with the constant C_r depending on the pipe roughness as given in Table 4.

Table 4. Influence of pipe roughness on C_r for air–gas-oil flow in 50 mm pipes

Pipe roughness ϵ/D	C_r	C_r/C
0·0012	0·026	1·0
0·0039	0·032	1·2
0·019	0·045	1·7
0·030	0·052	2·0

c. *Mist-annular flow*

For this flow pattern measurements were made only in the $D = 24$, 50 and 91 mm pipes for air–gas-oil flow and in the 50 mm pipes for air–spindle-oil flow. Here again the Lockhart-Martinelli parameters were found to be inadequate for the correlation of our data, see Fig. 10. This contradicts LEVY's [12] theoretical prediction.

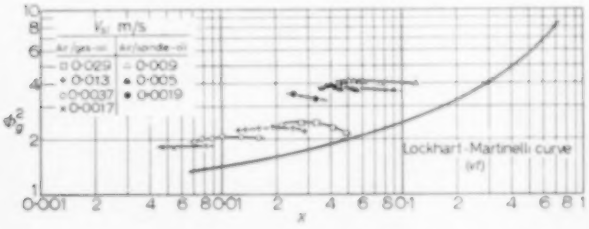

FIG. 10. Data for mist-annular flow in 50 mm pipes correlated with Lockhart-Martinelli parameters.

For mist–annular flow the gas is the continuous phase. Therefore a new dimensionless group was based on the gas flow alone:

$$\lambda'_{tp} = \frac{\Delta P_{tp}}{\frac{1}{2}\frac{\Delta L}{D}\frac{m_g^2}{\rho_g}}. \qquad (12)$$

The results are thus correlated with a Reynolds number based on the gas flow alone, see Fig. 11.

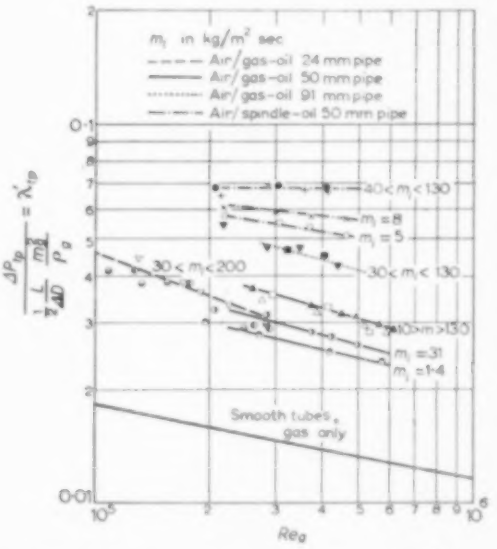

FIG. 11. Experimental pressure drop curves for mist-annular flow.

It was found that for liquid flow rates which are not too low, the friction factor λ'_{tp} becomes independent of this rate. For the case of air–gas-oil flow λ'_{tp} could then be correlated with m_g alone giving

$$\lambda'_{tp} = a\,(m_g)^{-\frac{1}{2}} \qquad (13)$$

$a = 0{\cdot}12$ kg$^{\frac{1}{2}}$ m$^{-\frac{1}{2}}$ sec$^{-\frac{1}{2}}$. This result holds for $30 < m_l < 200$ kg/m² sec. No influence of the air density on λ'_{tp} was found over the experimental range of air densities of 1·2–3 kg/m³. For lower superficial liquid mass velocities λ'_{tp} decreases with m_l.

For rough 50 mm pipes with air–gas-oil flow it was found that in the case of not too great roughness $\left(\frac{\epsilon}{D} = 0{\cdot}0012 \text{ and } 0{\cdot}0030\right.$, or ϵ of 0·06 and 0·15 mm$\left.\right)$

the pressure drop was nearly equal to that for mist–annular flow in smooth pipes. For great roughness $\left(\frac{\epsilon}{D} = 0{\cdot}030 \text{ and } 0{\cdot}019 \text{ or } \epsilon = 1{\cdot}5 \text{ and } 0{\cdot}95 \text{ mm}\right)$ the pressure drop was about 10 per cent higher than for air flowing alone.

3.3 *Holdup*

In most of our experiments with air–oil flow the holdup was measured. This was done to obtain a more accurate compressibility correction for the pressure drop and more information about the gas–liquid flow. In the literature data for the holdup are reported by Lockhart and Martinelli [13], Johnson and Abou Sabe [8] Alves [1] and Kozlov [10]. These results were all obtained with the quick closing valve technique, and they mutually show differences when correlated with the Lockhart-Martinelli parameter x as is done by most authors. Our results for the 50, 91 and 140 mm pipes obtained with the capacitance method also showed deviations from this correlation at various liquid mass velocities, indicating that x, which is only determined by the ratio v_{sl}/v_{sg}, is inadequate and that both v_{sl} and v_{sg} have to be accounted for.

For vertical two-phase flow it is found by Schmidt *et al.* [17], Moore and Wild [15] and by Bailey *et al.* [2] that the holdup is mainly a function of the slip velocity (v') between both phases, where:

$$v' = \frac{v_{sg}}{R_g} - \frac{v_{sl}}{1 - R_g} \cdot \tag{14}$$

The use of this type of correlation for our horizontal test results was found to be successful, and gave for the gas holdup R_g with air–oil flow:

$$\frac{R_g}{1 - R_g} = A \left[R_g v'\right]^{0{\cdot}85} = A \left[v_{sg}\left(1 - \frac{R_g}{1 - R_g}\frac{v_{sl}}{v_{sg}}\right)\right]^{0{\cdot}85} \tag{15}$$

Here $A = 0{\cdot}60\ (\text{m/sec})^{-0{\cdot}85}$. Figure 12 gives some test data.

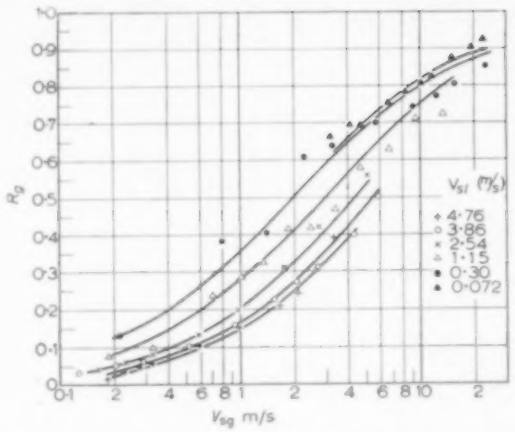

Fig. 12. Gas holdup for air–spindle-oil flow in 140 mm pipe.

No significant effect of pipe diameter or liquid viscosity was found in our velocity ranges. The gas density influence was not investigated. The standard deviation in R_g for our 444 data compared with this correlation was 0·04 (absolute value).

4. Conclusions

1. The flow patterns occuring with gas–oil flow can be predicted from one diagram, the influence of pipe diameter and liquid viscosity being small. For gas–water flow the same diagram with an enlarged wave flow region can be used.
2. The Lockhart-Martinelli correlation has 3 limitations; it cannot be used:
   a. for plug, slug and froth flow, if gas densities differ from that of air at atmospheric pressure.
   b. in the stratified and wave flow regions,
   c. in the mist–annular flow region.
3. For plug, slug and froth flow a new experimental correlation which includes the influence of gas density and pipe roughness gives:

$$\Delta P_{tp} = \Delta P_{lo}\left[1 + 230\left(\frac{m_g}{m_t}\right)^{0{\cdot}84}\right]\left[0{\cdot}00138\,\frac{\rho_l}{\rho_g}\right]^{\alpha}$$

with:

$$\alpha = 9{\cdot}5\left(\frac{m_g}{m_t}\right)^{0{\cdot}5} - 62{\cdot}6\left(\frac{m_g}{m_t}\right)^{1{\cdot}3}$$

for

$$\frac{m_g}{m_t} < 0{\cdot}05\,; \quad Re_{tp} > 3000.$$

4. For wave flow a new correlation gives:

$$\frac{\Delta P_{tp}}{\frac{1}{2}\frac{\Delta L}{D}\frac{m_t^2}{\rho_g}} = C\left(\frac{m_g}{m_t}\right)^{1{\cdot}45}$$

$$\text{for } \frac{m_g}{m_t} < 0{\cdot}8.$$

Here C depends mainly on pipe diameter and pipe roughness (Tables 3 and 4).

5. For mist–annular flow ΔP_{tp} is independent of the liquid flow rate if this is greater than 30 kg/m² sec; for air–gas-oil flow a new correlation then gives:

$$\frac{\Delta P_{tp}}{\frac{1}{2}\frac{\Delta L}{D}\frac{m_g^2}{\rho_g}} = 0{\cdot}12\,(m_g)^{-\frac{1}{4}}.$$

6. The gas holdup correlates with the slip velocity between both phases:

$$\frac{R_g}{1-R_g} = 0{\cdot}60\left[R_g\,v'\right]^{0{\cdot}83} = A\left[v_{sg}\left(1-\frac{R_g}{1-R_g}\frac{v_{sl}}{v_{sg}}\right)\right]^{0{\cdot}85}$$

NOTATION

C = empirical constant in equation (11)
c_g = air percentage
D = pipe diameter (m)
g = acceleration of gravity (m/sec²)
ΔL = length of measuring section (m)
m = superficial mass velocity (kg/m² sec)
ΔP_{tp} = two-phase pressure drop over measuring section (N/m²)
ΔP_l = pressure drop over measuring section if the liquid were flowing alone (N/m²)
ΔP_{lo} = pressure drop over measuring section which would occur if the whole mass of gas and liquid were flowing in the liquid phase (N/m²)
ΔP_g = pressure drop over measuring section if the gas were flowing alone (N/m²)
ΔP_c = pressure drop over measuring section due to the expansion of the gas phase (N/m²)
Q = flow rate by volume (m³/sec)
R = holdup
Re = Reynolds number
Re_{tp} = Reynolds number defined by equation (5)
v_m = mixture velocity (m/sec)
v_s = superficial velocity (m/sec)
v' = slip velocity (m/sec)
X^2 = Lockhart-Martinelli parameter
x = empirical exponent in equation (6)
ϵ = equivalent sand grain roughness (m)
η = dynamic viscosity (Ns/m²)
λ_{tp} = friction factor for two-phase flow defined by equation (4)
$(\lambda_{tp})_n$ = friction factor λ_{tp} for two-phase flow at $\rho_g/\rho_l = 0{\cdot}00138$
λ'_{tp} = friction factor for mist–annular flow defined by equation (12)
λ_{lo} = friction factor which would apply if the whole mass of gas and liquid were flowing in the liquid phase
ν = kinematic viscosity (m²/sec)
ρ = fluid density (kg/m³)
σ = surface tension (N/m)
Φ_g = Lockhart-Martinelli parameter

Subscripts
l = liquid
g = gas
t = total of gas and liquid

REFERENCES

[1] ALVES G. E. *Chem. Engng. Progr.* 1954 **50** 449.

[2] BAILEY R. V., ZMOLA P. C., TAYLOR F. M. and PLANCHET R. J. *Tulane University and Oak Ridge National Laboratory* 1956.

[3] BAKER O. *Oil–Gas J.* 1954 **53** 185.

[4] BERGELIN O. P. and GAZLEY C. *Proc. Heat Transfer Fluid Mech. Inst.*, Berkeley 1949.

[5] CHENOWETH J. M. and MARTIN M. W. *Petroleum Engng.* 1956 **28** C-42.

[6] CHISHOLM D. and LAIRD A. D. K. *Amer. Soc. Mech. Engr.* 1957 paper 57–SA–11.

[7] ISBIN H. S., MOEN R. H. and MOSHER D. R. *U. S. Atomic Energy Comm.* 1954 AECU–2994.

[8] JOHNSON H. A. and ABOU SABE A. H. *Trans. Amer. Soc. Mech. Engrs.* 1952 **74** 977.

[9] KOSTERIN S. I. *Izvest. Akad. Nauk SSSR. Otdel. Teckh. Nauk* 1949 **12** 1824.

[10] KOZLOV B. K. *Doklady Akad. Nauk SSSR.* 1954 **97** 987.

[11] Krasyakova L. Y. *J. Tech. Phys. USSR.* 1952 **22** 656.

[12] Levy S. *Proc. 2nd Midwestern Conf. Fluid Mech.* 1952 337.

[13] Lockhart R. W. and Martinelli R. C. *Chem. Engng. Progr.* 1949 **45** 39.

[14] Moody L. F. *Trans. Amer. Soc. Mech. Engrs.* 1944 **66** 671.

[15] Moore R. V. and Wilde H. D. *Trans. Amer. Inst. Mining Engrs.* 1931 **92** 296.

[16] Reid R. C., Reynolds A. B., Klipstein D. H., Diglio A. J. and Spiewak I. *Amer. Inst. Chem. Engrs. J.* 1957 **3** 321.

[17] Schmidt E., Behringer P. and Schurig W. *V.D.I. Forschungsheft* 365 1934 **5** 1.

[18] White P. D. and Huntington R. L. *Petroleum Engr.* 1955 **27** D–40.

Chemical Engineering Science, 1959, Vol. 9, pp. 218 to 224. Pergamon Press Ltd. London. Printed in Great Britain

Mass-transfer from single solid spheres—II

Transfer in free convection

F. H. Garner and R. B. Keey
Chemical Engineering Department, Birmingham University

(*Received* 13 *January* 1958)

Abstract—A theoretical analysis of the problem of free convection shows that for Schmidt numbers exceeding 100 :

$$N_{Sh} \propto (N'_{Ra})^{1/4} \quad \text{—} \quad \text{laminar convection}$$

$$N_{Sh} \propto (N'_{Ra})^{1/3} \quad \text{—} \quad \text{turbulent convection}$$

where N'_{Ra} is the mass-transfer Rayleigh number, defined by $N'_{Ra} = \dfrac{gd^3\,\Delta\rho}{\mu\,\mathscr{D}}$.

Preliminary experimental observations, employing the dissolution of compressed spheres of adipic and benzoic acids between $\frac{1}{2}$ in. and $\frac{3}{4}$ in. in diameter, confirm the above relationship for laminar convection. There is a small difference between the mean curve through the results and the limiting value of N_{Sh} at low Reynolds numbers found previously by the authors (Part I*). It seems that turbulence sets in over the lower hemisphere at a critical Rayleigh number of 3.5×10^8, where the characteristic dimension is based upon the length measured along the surface from the upper pole.

Résumé—Une analyse théorique du problème de convection libre montre que pour des indices de Schmidt supérieurs à 100 :

$$N_{Sh} (N'_{Ra})^{1/4} \text{ — convection laminaire}$$

$$N_{Sh} (N'_{Ra})^{1/3} \text{ — convection turbulente}$$

où N'_{Ra} représente l'indice de transfert massique de Rayleigh défini par $N'_{Ra} = \dfrac{gd^3\,\Delta\rho}{\mu\,\mathscr{D}}$.

Des observations expérimentales préliminaires utilisant la dissolution de sphères comprimées des acides benzoïques et adipiques d'un diamètre compris entre $\frac{1}{2}$ in. et $\frac{3}{4}$ in., confirmèrent la relation ci-dessus. Il y a une faible différence entre la courbe moyenne passant par les résultats et la valeur limite de N_{Sh} pour les nombres de Reynolds faibles, trouvée précédemment par les auteurs (Part I*). Il semble que la turbulence commence sur l'hémisphère inférieure pour un nombre critique de Rayleigh de $3{\cdot}5 \times 10^8$, où la dimension caractéristique s'établit d'après la longueur mesurée le long de la surface à partir du pôle supérieur.

Zusammenfassung—Aus einer theoretischen Untersuchung über die freie Konvektion ergeben sich folgende Proportionalitäten für Schmidtzahlen über 100 :

$$N_{Sh} \sim (N'_{Ra})^{1/4} \text{ – laminare Konvektion}$$

$$N_{Sh} \sim (N'_{Ra})^{1/3} \text{ – turbulente Konvektion,}$$

worin N'_{Ra} die Rayleighzahl der Stoffübertragung bedeutet, definiert durch $N'_{Ra} = \dfrac{gd^3\,\Delta\rho}{\mu\,\mathscr{D}}$.

Frühere Versuche über die Auflösung von komprimierten Kugeln aus Adipin – und Benzoesäure von 9,5 bis 19 mm Durchmesser haben die obigen Beziehungen im laminaren Bereich bestätigt. Zwischen der mittleren, durch die Messpunkte gelegten Kurve und dem Grenzwert von N_{Sh} bei kleinen Reynoldszahlen, wie er früher von den Autoren gefunden wurde (Teil I*) besteht ein geringer Unterschied. Es scheint, dass an der unteren Halbkugel bei einer kritischen Rayleighzahl von $3{,}5 \cdot 10^8$ Turbulenz einsetzt, wenn als charakteristische Länge die Bogenlänge vom oberen Pol eingesetzt wird.

*Chem. Engng. Sci. 1958 **9** 119.

Introduction

In Part I of this paper it was shown that forced convection could be assumed to predominate, when the Reynolds number had reached a certain critical value defined by :

$$N_{Re} > 0{\cdot}4\,(N'_{Gr})^{\frac{1}{2}}\,N_{Sc}^{-1/6}.$$

In the case of $\frac{3}{4}$ in. diameter benzoic acid spheres dissolving in water at 30·0°C free-convective effects were still discernable up to Reynolds number of 750 and at Reynolds numbers below 10 the variation of the Sherwood number with Reynolds number is small. Thus a study of free convection should help to evaluate more accurately mass-transfer at low flows.

Apart from the recent work of Mathers *et al.* [8], there seem to be no data on mass-transfer from spheres in free convection. (Problems of transfer from very small spherules in still media are those of molecular diffusion). Thus a preliminary investigation was undertaken to find out the factors of significance.

Theory

A dimensional analysis of the problem yields :

$$\frac{K_L d}{\mathscr{D}} = f\left[\frac{g d^3\,\Delta\rho}{\nu^2\,\rho}, \frac{\nu}{\mathscr{D}}\right], \qquad (1)$$

where the dimensionless groups are respectively the Sherwood number, the modified Grashof number and the Schmidt number. It is convenient to rewrite this relationship in the form :

$$N_{Sh} = f\,(N'_{Ra}\,N_{Sc})\,; \quad N_{Ra} = N'_{Gr} \times N_{Sc}, \qquad (2)$$

since for practical purposes the Sherwood number is dependent only upon the modified Rayleigh number when the Schmidt number exceeds 100.

It was Schmidt and Beckmann [11] who first suggested that the problem could be solved by using boundary-layer theory, in which all velocity and concentration changes are confined to a thin zone near the surface. There are two principal differences between this layer and the one associated with forced convection. Firstly we have to consider an extraneous force F, where $F = g\,\Delta\rho/\rho$. Secondly, the radial concentration and velocity profiles will each show a maximum within the layer and the parameters at the boundaries will be zero. By comparing buoyancy forces with viscous forces over a slab, we find

$$\frac{\delta_M}{L} \sim \left[\frac{x_0}{L N'_{Ra}}\right]^{1/4},$$

where x_0 is the distance from the leading edge and L the total length. Since x_0/L is never greater than unity and if δ_M is to be of an order less than L then

$$N'_{Ra} > 10^4.$$

From equations (1), (2) and (9) in (Part I) we can get the boundary-layer equations for free convection :

$$\left.\begin{aligned} &\frac{\partial\,(ru)}{\partial x} + \frac{\partial\,(rv)}{\partial y} = 0, \\ &u\frac{\partial u}{\partial x} + v\frac{\partial u}{\partial y} = g\frac{\Delta\rho}{\rho}\sin\epsilon + \nu\frac{\partial^2 u}{\partial y^2}, \\ &u\frac{\partial c}{\partial x} + v\frac{\partial c}{\partial y} = \mathscr{D}\frac{\partial^2 c}{\partial y^2}, \end{aligned}\right\} \qquad (3)$$

where ϵ is the angle between the normal to the surface and the vertical. By integrating from $y = 0$ to $y = h$ $(h > \delta)$, we get

$$\frac{1}{r}\frac{d}{dx}\int_0^h ru^2 dy = g\sin\epsilon\int_0^h \psi\,dy - \nu\left(\frac{\partial u}{\partial y}\right)_{y=0}$$

and

$$\frac{1}{r}\frac{d}{dx}\,r\int_0^h u\,\psi\,dy = -\mathscr{D}\left(\frac{\partial\psi}{\partial y}\right)_{y=0}, \qquad (4)$$

in which $\psi = (c - c_1)/(c_0 - c_1)$. The equivalent pair of equations for heat-transfer has been solved by Merk and Prins [9] by substituting the polynomials in $\eta = y/\delta$ for u and $\theta = (T - T_1)/(T_0 - T_1)$. To a first approximation these are :

$$\theta = (1 - \eta)^2 \text{ and } u = u_1\,\eta\,(1 - \eta)^2.$$

A further approximation is given. Their mathematical argument is not given here. The method of solution is similar except that θ and N_{Pr} are replaced everywhere by ψ and N_{Sc}. Their final result may be written as :

$$\overline{N}_{Sh} = 0{\cdot}559\,N'^{1/4}_{Ra}\,N_{Sc} > 1. \qquad (5)$$

Graphs showing the variations of local transfer rates and variation of maximum tangential velocity in the boundary-layer are given in Figs. 1 and 2.

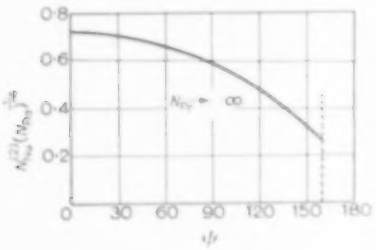

Fig. 1. Local heat transfer rates.

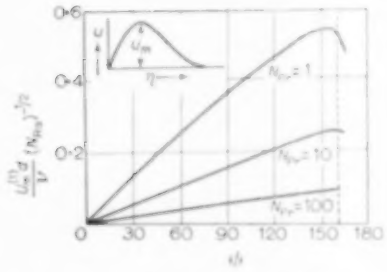

Fig. 2. Maximum velocity boundary layer.

The method breaks down towards the lower pole, as the boundary-layer thickens rapidly in this region and is infinite at $\phi = 180°$. Furthermore it is assumed that there is no difference between the momentum and mass-transfer film. Theoretically this is only true when $\nu = \mathscr{D}$ i.e. at a Schmidt number of unity, although the solutions obtained by Merk and Prins' method for a flat plate agree quite well with Schuh's more rigorous calculations [12]. In the case of heat-transfer, the theoretical expression predicts Nusselt numbers about $7\frac{1}{2}$ per cent lower than those obtained experimentally by Jakob and Linke [7].

If the Rayleigh number is large enough transition to turbulence in the boundary-layer takes place ($10^8 < N_{Ra} < 10^9$). Measurements of Griffiths and Davies [5] suggest a profile :

$$u = u_1 \eta (1 - \eta)^4$$

in this case. Differentiation of this expression gives an infinite velocity gradient at the surface and to give a finite value to the skin-friction, a laminar sub-layer can be postulated. Zijnen's data [14] show that this sub-layer extends up to $y^* = 12$, where y^* is a dimensionless radial distance, based upon the friction velocity u^* :—

$$y^* = \frac{u^* y}{2\nu} \text{ and } u^* = \sqrt{\frac{\tau_0}{\rho}}$$

Between this laminar layer and the fully turbulent core is a quasi-turbulent " buffer " zone and for calculation purposes an effective laminar film can be assumed up to $y^* = 13$. Using this concept Bayley [1] has obtained an expression for free-convective heat-transfer in two-dimensional flow, which can be written in the form for mass-transfer :

$$\overline{N}_{Sh} (N'_{Ra})^{-1/3} = 1{\cdot}10 \; ; \quad 10^9 < N_{Ra} < 10^{12}. \quad (6)$$

It is seen that this relationship is independent of the characteristic dimension of the body. Thus equation (6) should be applicable in the case of the dissolution of spheres in turbulent free convection.

Experiment

The apparatus which was described in Part 1 was used. Pellets of 'Analar' grade adipic and benzoic acid, ranging in four sizes from $\frac{3}{8}$ in. to $\frac{3}{4}$ in. in diameter, were compressed in the hand-press, described in Part I. As before, photographic plates were exposed at suitable time intervals during the dissolution period. After development these were subsequently projected in a diascope and superimposed to obtain the diminution of the sphere. From the radial diminution local mass-transfer coefficients and overall transfer coefficients can be estimated.

The following data are required : pellet density, the solubility and diffusivity of the solute in the solvent and the density and viscosity of the saturated solutions. Pellet densities were found by Archimedes' principle. Solubilities and diffusivities were calculated from information in the literature [2, 3, 13]. Viscosities of the saturated solutions were assumed to be the same as that of pure water at the same temperature. Densities of the saturated solutions were

measured in a 10 ml pycnometer, which enabled densities to be measured to 1 part in 10,000. The mean results of three determinations at each temperature are given underneath.

Table 1. *Saturation densities* (*g*/*ml*)

t (°C)	*Distilled water*	*Adipic acid in water*	*Benzoic acid in water*
15	0·9991	1·0026	0·9956
20	0·9982	1·0023	0·9986
25	0·9970	1·0019	0·9974
30	0·9960	1·0014	0·9963

The average accuracy of the difference in density between a saturated solution of adipic acid and water is ± 2 per cent and that between a saturated solution of benzoic and water is ± 25 per cent. The latter inaccuracy is not as serious as it would appear on first sight, for the mass-transfer coefficient is proportional to the fourth root of the density difference. This reduces the significance of the error by a factor of about four.

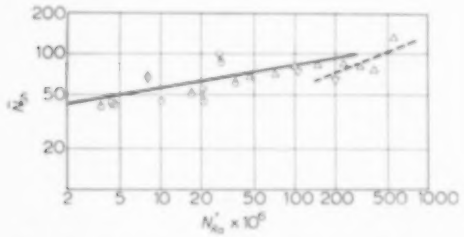

Fig. 3. Free convection overall transfer rates.
△ Adipic acid upper pole support.
▽ Adipic acid lower pole support.
○ Benzoic acid upper pole support.
○ Benzoic acid lower pole support.

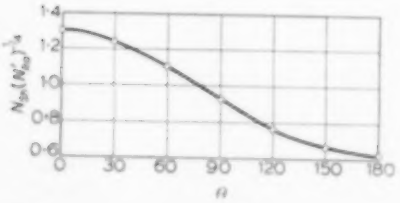

Fig. 4. Local mass-transfer rates in laminar free convection
$3{\cdot}62 < N'_{Ra} \times 10^6 < 106{\cdot}2$.

The results are presented graphically in Figs. 3, 4 and 5. The overall transfer results are applied to the region defined by

$$3{\cdot}1 < N'_{Gr} \times 10^3 < 583 \text{ and } 798 < N_{Sc} < 2{,}200.$$

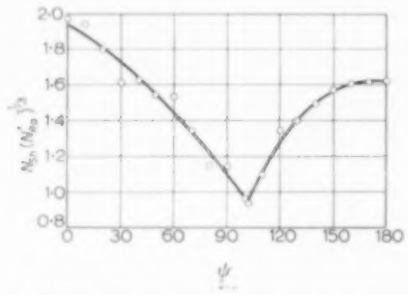

Fig. 5. Local mass-transfer rates in turbulent free convection
$N'_{Ra} = 2{\cdot}32 \times 10^8$.

Discussion

Experiments were performed with the support both at the upper and lower pole of the sphere. From Fig. 3 there is seen to be no significant difference between the effects of the two methods of support. Unlike forced convection, in free convection there is no back-flow region, where a support can hinder or promote separation of the forward-flow. The effect of the support in free-convective flow is to add vorticity into the boundary-layer and the resultant effect is independent of the point where vorticity is added.

Theory suggests that there is a linear relationship between N_{Sh} and $N'^{-1/4}_{Ra}$. Based on this assumption, the results for the overall transfer rate were correlated by the principle of least squares. The correlation coefficient of the line so obtained was 0·59. As this represents a low degree of correlation, individual points were re-examined. It was noticed that all spheres with a modified Rayleigh number exceeding 149×10^8 showed a pronounced minimum in the local mass-transfer rate as some position other than the rear pole. Accordingly it was decided to neglect these in the general correlation. The new correlation coefficient was 0·68 and the regression line so obtained is :—

$$\overline{N}_{Sh} = 0{\cdot}58_5 (N'_{Ra})^{1/4} + 23. \qquad (7)$$

The t-value of this correlation is 3·20. This may be compared to the t-value for a probability of 1 per cent that this had occurred from chance; the value so obtained is 2·92. We thus conclude that the correlation is significant. It will be noticed that there are four points which fall somewhat higher than the remainder. It is these which render the correlation coefficient so low. This could not be ascribed to any physical cause and the points remain anomalous, especially since these are more consistent with the limiting value of the Sherwood number reported in Paper 1. However, the mean probable error of *all* the results is $\pm$ 14·2 per cent, which is of the same order as the maximum error attributable to the experimental technique ($\pm$ 16 per cent). To reduce these unavoidable errors, greater magnification of the processed plates is required and solvents are needed, in which the saturation densities are much different from the solvent density. In connexion with the latter condition, however, solutes of high solubility generally tend to dissolve somewhat irregularly. More accurate work is contemplated.

It is seen from equation (7) that the experimental value of the coefficient of the Rayleigh number agrees well with MERK and PRINS' [9] theoretical value. That the condition:

$$\begin{matrix} \text{Lim} & N_{Sh} & \rightarrow & 2 \\ N'_{Ra} & \rightarrow & 0 \end{matrix}$$

is not satisfied is not surprising, since the lowest Rayleigh number used in this work is $3{\cdot}62 \times 10^6$. Data are given by MATHERS and *et al.* [8] on the sublimation of benzene- and naphthalene-coated spheres at reduced pressures, when thermal gradients are insignificant. The results therein covered a much lower Rayleigh number range than those of the present work and thus form a useful comparison (Fig. 6). The two sets of data seem to be consistant.

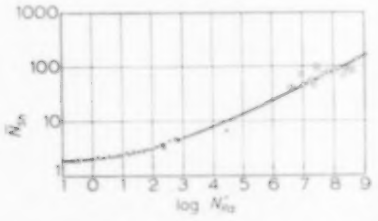

FIG. 6. Isothermal mass-transfer in free convection
× MATHERS *et al.*[8]
o Present work.

The results for the local mass-transfer rate scatter more than those for the overall rate, since the latter approximates to the transfer rate at the great circle ($\phi = 90°$) and superimposition errors here are at a minimum. To overcome this difficulty local mass-transfer rates (for $N'_{Ra} < 1{\cdot}49 \times 10^8$) were expressed in terms of the product $N_{Sh} N'^{-1/4}_{Ra}$, which according to theoretical reasoning should be almost independent of Rayleigh number, (see Theory). Based on this assumption the mean probable errors of transfer rates at successive angles, 60° apart, beginning at the upper pole, are: $\pm$ 15·9 per cent, 16·7 per cent, 17·3 per cent and 24·8 per cent. These errors are of the same order as that of the overall transfer rate and the above assumption is considered justifiable.

The maximum mass-transfer rate occurs at the upper pole and progressively decreases around the surface with a point of inflexion at $\phi = 110°$ until it is a minimum at the rear pole. Over the majority of the sphere surface (up to $\phi = 140°$) the shape, though not the magnitude, agrees well with that predicted from laminar boundary-layer theory. There is a very rapid increase in the boundary-layer thickness over the rear hemisphere until it is infinitely thick at the rear pole. This thickening gives rise to the formation of a characteristic tail, which is sometimes rendered visible by the density striae. Photograhs of the dissolution of sugar-coated spheres in Fig. 7 illustrate the higher transfer rate over the upper hemisphere and show that the boundary layer is infinitely thick at the rear pole.

This distribution of mass-transfer rate over the surface can be explained by considering the nature of the free-convective flow. This flow is set up due to a difference in concentration, which gives rise to a density difference between the sphere and the surrounding fluid. It is thus expected that there is a general inflow, roughly radially towards the upper surface. From considerations of continuity the heavier fluid must fall downwards around the surface. Solute

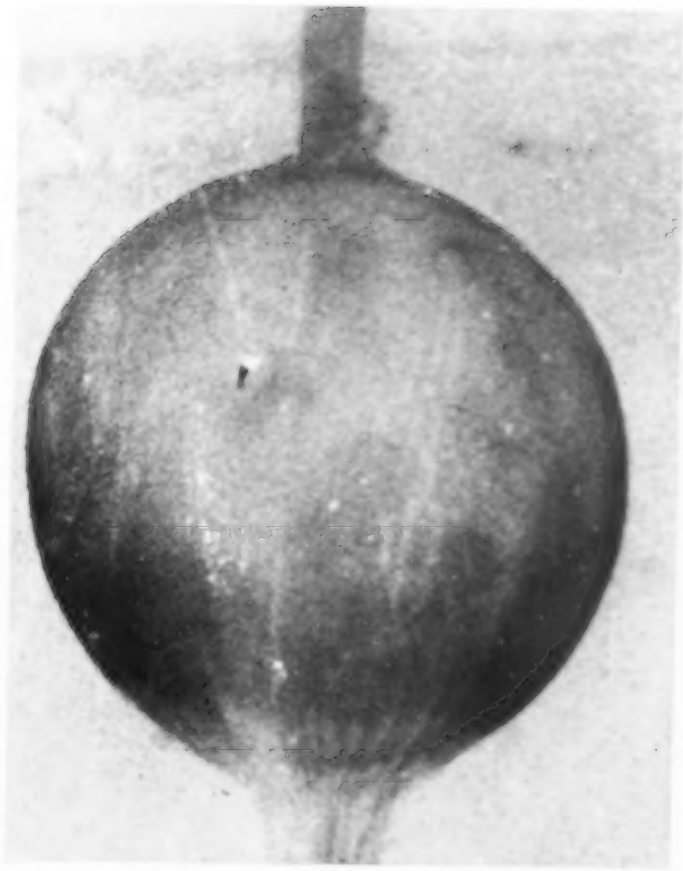

FIG. 7. Dissolution of sugar-coated spheres.

-free fluid will then stream upwards to take the place of the inflowing fluid, giving a general circulation as shown in Fig. 11 (Part I), which has no effect at infinity upstream. Hence the boundary-layer is finite at the upper pole and progressively thickens as the fluid diverges from the sphere surface until it is infinite at the rear pole. Since the driving force for mass-transfer remains the same, this means that the concentration gradients become less, whence the mass-transfer rate decreases. Boundary-layer theory predicts that the tangential velocities increase with increasing ϕ. If this condition holds when boundary-layer theory fails, then the increasing rate at which material can be convected from the surface would tend to counterbalance the thickening of the boundary-layer. This would explain the point of inflexion.

Table 2 summarizes the data for those points, which were neglected in the general correlation. The third column $(N'_{Ra})_c$ gives the Rayleigh number based upon a characteristic length, measured from the upper pole to the ring of minimum transfer.

Table 2. Overall transfer rates at high Rayleigh numbers

$N_{Ra}' \times 10^6$	ϕ_c	$(N_{Ra}')_c \times 10^6$	N_{Sh}
149_5	154	394	83
201	$146\frac{1}{2}$	329	64
232	102	206	84
316	$118\frac{1}{2}$	351	80
399	118	438	76
550	100	364	131

If $(N'_{Ra})_c$ is assumed to be independent of Rayleigh number, the mean probable error of these values is $\pm$ 13·9 per cent, which is of the same order as that for the overall transfer results. Thus either $(N'_{Ra})_c$ is a constant (approximately $3{\cdot}5 \times 10^8$) or else the variation thereof is masked by the scatter. This value is the same as that which accompanies the onset of turbulence in the free-convective flow around a horizontal cylinder [6]. Eckhert and Soehngen [4] have studied the flow around a heated, vertical aluminium plate in air with an interferometer and found that at small thermal potentials, transition to turbulence took place at $N_{Gr} = 4 \times 10^8$. Schmidt [10] was able to correlate heat-transfer from spheres by a linear plot of N_{Nu} against $N_{Ra}^{1/3}$ over the range $10^8 < N_{Ra} < 10^{13}$. Thus in the present case turbulence may be present over the rear hemisphere. It would be expected that turbulence would set in in this manner, as maximum tangential velocities occur here.

A typical distribution of local mass-transfer rates is given in Fig. 3. The pronounced minimum evidently corresponds to the onset of turbulence. The eddies within the boundary-layer enable material to be convected more rapidly, whence the increase in mass-transfer rate below this position.

Conclusions

Mass-transfer in laminar free convection can be correlated by a linear relationship between N_{Sh} and $N_{Ra}'^{1/4}$, where $N'_{Ra} = \dfrac{gd^3\,\Delta\rho}{\mu\,\mathscr{D}}$. Maximum transfer takes place over the upper hemisphere. At a critical Rayleigh number of $3{\cdot}5 \times 10^8$ (where the characteristic dimension is given by $\phi\,d/2$), it appears that turbulence sets in. This causes an increase in the mass-transfer rate over the lower hemisphere.

Notation

c	= concentration	ML^{-3}
d	= sphere diameter	L
$\mathscr{D}$	= diffusivity	L^2T^{-1}
g	= gravitational acceleration	LT^{-2}
K_L	= mass- transfer coefficient	LT^{-1}
L	= distance along the surface of the sphere from the upper pole	L
N_{Gr}	= Grashof number	—
N_{Nu}	= Nusselt number	—
N'_{Ra}	= Rayleigh number	—
$(N'_{Ra})_c$	= a critical Rayleigh number (defined in Text)	—
N_{Re}	= Reynolds number	—
N_{Sc}	= Schmidt number	—
N_{Sh}	= Sherwood number	—
r	= radial distance	L
r_0	= distance from axis of rotation	L
u, v	= velocities in x and y directions	LT^{-1}
T	= temperature	θ
u^*	= friction velocity (defined in text)	—

x, y = distances mutually at right-angles — L
y^* = dimensionless distance, normal to surface (defined in text) — —
δ = boundary-layer thickness — L
ϵ = angle (defined in text) — —
η = dimensionless distance, normal to surface (defined in text) — —
μ = shear viscosity — $ML^{-1}T^{-1}$
ν = kinematic viscosity — L^2T^{-1}
ρ = fluid density — ML^{-3}
τ_0 = skin-friction intensity — $ML^{-1}T^{-2}$
ϕ = dimensionless concentration (defined in text) — —
ϕ = angle, from upper pole — —

Subscripts —
$^\circ$ = at surface
1 = at edge of boundary-layer

Operators —
∂ = partial differential
d = total differential
Δ = finite-difference

Superscribed dashes indicate the dimensionless groups are modified for mass-transfer.

References

[1] Bayley F. J. *Proc. Inst. Mech. Engrs.* 1955 **169** 361.

[2] Bougoin R. *Ann. Chim. (Phys.)* 1878 **15** 161.

[3] Davies J. and Griffiths E. *Trans. Faraday. Soc.* 1953 **49** 1405.

[4] Eckhert E. R. G. and Soehngen E. *Trans. Inst. Mech. Engrs.* 1951 **32** 381-387.

[5] Griffiths E. and Davies A. H. Food Investigation Board, S.R.9. D.S.I.R. 1922.

[6] Hermann R. *Forsch. Ver. Dtsch. Ing.* 1936 379.

[7] Jakob M. and Linke W. *Forsch. Geb. Ing.* 1933 **4** 75.

[8] Mathers W. G., Madden A. J. and Piret E. L. *Ind. Engng. Chem.* 1957 **49** 961.

[9] Merk H. J. and Prins J. A. *Appl. Sci. Res. Hague* 1953-54 **A4** 11, 195, 207.

[10] Schmidt E. *Chem.-Ing.-Tech.* 1956 **28** 175.

[11] Schmidt E. and Beckmann W. *Tech. Mech. Thermodyn.* 1930 **1** 391.

[12] Schuh H. *Temperaturgrenzschichten*, Göttinger Monographien, B6, 1946.

[13] Wilke and Pin Chang. *Amer. Inst. Chem. Engrs. J.* 1955 **1** 264.

[14] Zijnen B. G. van der Hegge Thesis, Delft University 1924.

Chemical Engineering Science, 1959, Vol. 9, pp. 225 to 241. Pergamon Press Ltd. London. Printed in Great Britain

On the action of surface active agents on mass transfer in liquid–liquid extraction

G. Boye-Christensen* and S. G. Terjesen

The Technical University of Norway, Chemical Engineering Laboratory, Trondheim, Norway

(*Received* 28 *April* 1958)

Abstract—The effect of the surface active agents sodium hexadecanyl sulphate and sodium undecanyl sulphate on the rate of mass transfer, droplet oscillation and terminal velocity has been studied during extraction of *o*-nitrophenol and iodine from aqueous solutions by single drops of carbon tetrachloride. The effect is caused by the pure surface active agents and does not depend on the presence of impurities. The hydrodynamic character of the effect has been confirmed. A comparison with solid spheres shows that the surface active agents can make the rates of mass transfer and the terminal velocities equal to those for solid bodies, internal circulation, oscillation and the zig-zag path being completely eliminated. Evidence is presented indicating that the high rates of mass transfer obtained in the absence of surface active agents, about three times that for solid spheres, are not caused by the droplet oscillation, and that, at the most, they can be accounted for only partly by internal circulation. It is suggested that the explanation must be sought in the micro structure of the flow pattern.

Résumé—Les auteurs étudient au cours de l'extraction de l'*o*-nitrophenol et de l'iode à partir des solutions aqueuses par gouttes individuelles de tétrachlorure de Carbonne l'effet des agents tensio actifs hexadecanyle sulfate de Na et undecanyle sulfate de Na sur la vitesse de transfert massique, l'oscillation des gouttes et les vitesses à l'équilibre. L'effet est produit par les agents tensio actifs purs et ne dépend pas de la présence d'impuretés. Le caractère hydrodynamique a été confirmé. Une comparaison avec les sphères solides montre que les agents tensio actifs peuvent donner des vitesses de transfert massique et des vitesses à l'équilibre égales à celles obtenues avec des corps solides, la circulation interne l'oscillation et la direction en zig-zag étant complétement éliminées. Les auteurs prouvent que les vitesses de transfert de masse élevés obtenues en l'absence d'agents tensio actifs trois fois plus plus environ qu'avec les sphères solides, ne sont pas occasionnées par l'oscillation des gouttelettes, et, au plus, elles peuvent être interprétées en partie seulement par la circulation interne. Ils suggèrent que l'explication peut être cherchée dans la micro structure du modèle d'écoulement.

Zusammenfassung—Die Wirkung der oberflächenaktiven Stoffe Natriumhexadekanyl-sulfat und Natriumundekanylsulfat auf die Grösse der Stoffübertragung, Tropfenschwingung und Endgeschwindigkeit wurde bei der Extraktion von *o*-Nitrophenol und Jod aus wässrigen Lösungen durch einzelne Tropfen von Tetrachlorkohlenstoff untersucht. Die Wirkung wurde durch die reinen oberflächenaktiven Stoffe verursacht und hing nicht ab von der Anwesenheit von Verunreinigungen. Der hydrodynamische Charakter de Wirkung wurde bestätigt. Ein Vergleich mit festen Kugeln zeigt, dass die oberflächenaktiven Stoffe die Gross der Stoffübertragung und der Endgeschwindigkeiten gleich denen für feste Körper machen können, wobei inner Zirkulation, Schwingung und Zick-Zack-Bahn vollständing ausgeschaltet wurden. Es wird nachgewiesen, dass die hohen Beträge der Stoffübertragung ohne oberflächenaktive Stoffe, die etwa dreimal so gross sind als für feste Kugeln, nicht durch die Tropfenschwingung verursacht werden und dass man sie in den meisten Fällen nur teilweise der inneren Zirkulation zuschreiben kann. Es wird empfohlen, die Erklärung in der Mikrostruktur des Strömungsbildes zu suchen.

* Present address: N. V. De Bataafsche Petroleum Maatschappij, The Hague, Netherlands.

Introduction

Previous papers in this series [12], [19], [1] and [20] have dealt with the effect of the surface active agent sodium oleyl-*p*-anisidine sulphonate on the rate of extraction of iodine or *o*-nitrophenol from aqueous solutions with single drops of carbon tetrachloride. The results were given in terms of an interfacial resistance coefficient which was defined simply as the difference between the resistance to mass transfer in the presence and absence of the surface active agent. This additional resistance was shown to be closely related to the concentration of surface active molecules adsorbed at the interface, and as a first approximation these two quantities were assumed to be proportional. Evidence was also presented indicating that the additional resistance caused by the surface active agent is in effect the result of some modification to the normal mechanism of mass transfer, and does not involve specific physical or chemical forces acting between the surface active molecules and the diffusing solute. It was suggested that the general nature of this additional resistance could be explained by assuming that the adsorbed surface active molecules somehow are capable of modifying the hydrodynamic conditions in the vicinity of the interface. The term hydrodynamic is in this context to be interpreted in its widest sense as involving any movement of aggregates of solvent molecules, however small.

In the present investigation other surface active agents have been used in an attempt to correlate interfacial resistance with the character of the adsorbed layer of surface active molecules. Lewis [17] has already from results obtained with his transfer cell suggested that only rigid films are capable of reducing the rate of mass transfer. Under the particular experimental conditions prevailing in his transfer cell, Lewis considers transfer of turbulence through the interface to be the predominant mechanism of mass transfer, and that rigid layers of surface active molecules interfere with this.

The second object of the present work is to clarify the effect of impurities on the action of surface active agents. This is particularly important, since the results of Cullen and Davidson [2], appertaining to the effect of surface active agents on the absorption of carbon dioxide in water, point to the conclusion that pure surface active agents cannot alone produce interfacial resistance. The results of Lindland and Terjesen [19] and Boye-Christensen and Terjesen [1] with purified sodium oleyl-*p*-anisidine sulphonate seem, however, to contradict this idea. It must be pointed out, however, that, whereas Cullen and Davidson consider their effect to be of the barrier type, the latter authors interpret theirs in purely hydrodynamic terms. Although subjected to repeated recrystallizations, the surface active agent used by the latter authors cannot be claimed to have a really high degree of purity. On the other hand, it seems unlikely that impurities could be responsible for the effect of an agent which is active in concentrations as low as 10^{-7} mole/l. To settle the point conclusively it was nevertheless considered necessary to synthesize surface active agents with less complex molecules, using routes which ensure the greatest possible freedom from homologues and other impurities. Results obtained during the present work with highly pure sodium hexadecanyl sulphate ($C_{16}H_{33}SO_4^-Na^+$) show that impurities do not contribute noticeably to the effect of strong surface active agents on the type of resistance to mass transfer encountered with our system.

There remains the important question of the nature of the hydrodynamic effect responsible for the retardation of mass transfer, and more particularly, of the part played by the internal circulation in the falling drops. Garner and Skelland [9] have shown that surface active agents can stop this internal circulation and thereby reduce both the rate of fall of the drops and the rate of mass transfer. Garner and Hale [6], however, have reported that in extracting diethylamine from toluene by drops of water in the presence of *Teepol*, their technique of visual observation failed to reveal any internal circulation even in the absence of the surface active agent. These findings led them to conclude that the retardation of mass transfer was a true barrier-effect. Lindland and Terjesen [19] have pointed out that with the system water-

carbon tetrachloride with iodine or *o*-nitrophenol as solute the partition coefficients are so greatly in favour of the solvent phase that the resistance to mass transfer is almost exclusively located in the continuous aqueous phase outside the drops. These authors did, however, stress that, although internal circulation therefore cannot directly assist in the mass transfer it might well do so indirectly by altering the hydrodynamic conditions outside the drops. It has been made the third object of the present work to provide further evidence on this question. The effect of the surface active agents on the rate of fall of the drops will be taken as an indication of their effect on the internal circulation, and will be compared with the effect on the rate of mass transfer. If the rate of fall and the rate of mass transfer both decrease in a similar manner with increasing concentration of surface active agents it is reasonable to assume that the surface active agents in both cases act through a retardation of the internal circulation. If, on the other hand, they vary in fundamentally different ways, it must be assumed that retardation of internal circulation and of mass transfer are different, and largely independent manifestations of the adsorbed surface active molecules. Already LINDLAND and TERJESEN [19] have pointed out that the sharp primary retardation in the rate of fall of the drops appear to reach its maximum value at a concentration of surface active agent about one-third to one-half of that necessary to develop fully the additional resistance. It was not at the time considered safe to draw any conclusions from this observation, but the results of the present investigation confirm and extend this finding and make it unlikely that surface active agents reduce the rate of mass transfer mainly through their action on internal circulation. This conclusion is, of course, limited to cases where the normal resistance to mass transfer is located almost exclusively in the continuous phase outside the drops.

GARNER [5] has also pointed to the effect of surface active agents on the oscillation of the drops as another possible mechanism for their ability to slow down the rate of mass transfer. It will be shown that with the present system the intensity of oscillation increases with increasing concentration of surface active agents, reaches a maximum and then disappears completely, the whole cycle being completed at concentrations much lower than those necessary to give the full reduction in the rate of mass transfer. Again, no correlation appears to exist.

EXPERIMENTAL

The apparatus and experimental procedure have been described in detail elsewhere [19]. The glass rod in the adsorption section of the column was rotated at 750 r.p.m., and the effective length of the extraction section proper was 143 cm. The stop-cock on the collecting burette at the bottom of the column was fitted with a *Teflon* plug which did not require lubrication. The drops were formed at the comparatively slow rate of 1·25 per sec in accordance with the observation of GARNER and SKELLAND [8] that slow rates of formation promote constant drop size. As before [19], capillaries of thin wall glass tubing were found most satisfactory.

The greatest care was taken to avoid contamination which, even in minute quantities, interfered with the results. Wherever practical considerations made it essential to use flexible connexions the joints were so designed that the rubber or plast was always separated from the fluid by a cushion of air as described previously [19]. An improved version of the drop-forming apparatus

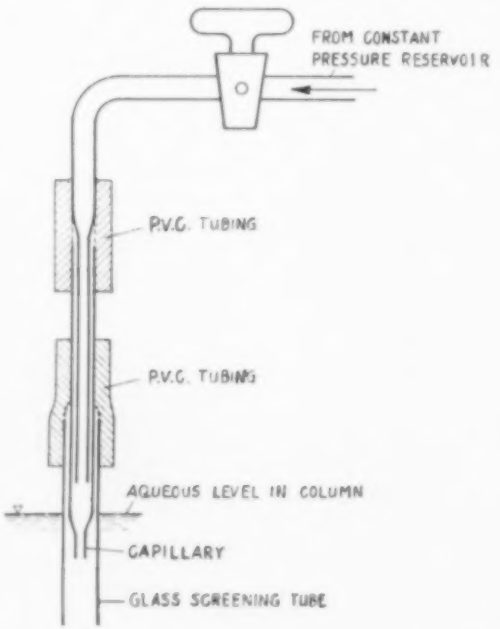

FIG. 1. Improved arrangement for droplet formation.

shown in Fig. 1 was used. This allowed easy change of capillary without danger of contamination.

The column and auxiliary equipment were thoroughly cleaned with a mixture of chromic and sulphuric acids followed by rinsing with distilled water. But even with these precautions it occasionally proved impossible for considerable periods to reproduce the high transfer rates obtained without addition of surface active agent, this being by far the most susceptible condition.

For the bulk of the experiments the temperature was maintained at 25°C by circulating thermostatically controlled water through the column jackets.

When the drops passed the restriction between the adsorption and extraction sections of the column they were slowed down and subsequently accelerated in the extraction section. The drop velocities determined in the extraction section do not therefore represent terminal velocities. These were determined in a column 450 cm long with internal diameter 7·5 cm by timing the drops over a distance of 180 cm after they had fallen 200 cm. According to Lapple [16] the column diameter used is not quite sufficient to eliminate the wall effect.

Materials

Synthesis of sodium undecanyl sulphate : $C_{11}H_{23}SO_4^-Na^+$.

Undecenoic acid derived from castor oil by distillation *in vacuo* was used as a starting material. According to Jones and Pyman [14] this process gives an acid practically free from homologues. The crude acid was re-distilled *in vacuo*, re-crystallized five times from petroleum ether (40-60°C), once from ethanol and once from acetone. The crystallizations were carried out at − 18°C with one part of acid to one part of solvent, and the mother liquor was removed by hydraulic pressure. After a final distillation *in vacuo* the melting interval was 24·1–24·9°C* with about 80 per cent melting within 24·5–24·8°C as compared with the m.p. of 24·5 given by Jones and Pyman [14].

The undecenoic acid was hydrogenated according to Kern *et al.* [15] to undecanoic acid which after three re-crystallizations from petroleum ether as described above, melted over the interval 28·4–28·8°C with 80 per cent within 28·6–28·8°C as compared with Ralston and Hoerr's melting point of 28·13°C [24].

Reduction to alcohol was effected with lithium aluminium hydride according to Nystrom and Brown [22]. After repeated washing with alkali and acid, followed by a distillation *in vacuo*, the undecanol melted in the interval 14·9–16·4°C with 80 per cent within 15·9–16·3°C. This melting point appears to be exceptionally difficult, and Beilstein gives values ranging from 11 to 19°C, while Verkade *et al.* [29] obtained 16·3°C.

*The melting intervals were determined by the capillary method, the material being observed through a lens. The temperature of the water flowing passed the capillary was never raised faster than 0·1°C/min. Around the melting point the rate was reduced to 0·1°C/3 min. Still slower rates of heating made no difference to the results.

The undecanol was sulphated with chlorosulphonic acid in glacial acetic at 4°C by the procedure of Dreger *et al.* [4], and the resulting sodium undecanyl sulphate extracted twice for eight hours with ether in a Soxhlet apparatus. It had the form of skinny crystalline plates.

Synthesis of sodium hexadecanyl sulphate : $C_{16}H_{33}SO_4^-Na^+$.

Palmitic acid was prepared by the method of Plešek [23]. The chloride of the undecanoic acid obtained above was condensed by a Grignard reaction with the ethyl ester of *cyclo*pentanone carboxylic acid to 5-hydroxy hexadecanoic acid (m.p. 79·5–79·7°C). The *cyclo*pentanone carboxylic acid was made from purified adipic acid with melting interval 151·7–152·6°C as compared with the m.p. of Verkade *et al.* [29] of 153°C. The adipic acid was esterified, distilled *in vacuo*, and treated with sodium and dry toluene as described in *Organic Synthesis* [30]. The hydroxy-acid obtained from the main reaction was reduced to palmitic acid with hydrazine hydrate according to Plešek [23]. After five recrystallizations from ethanol, one from carbon tetrachloride and one from acetone, as described for undecanoic acid, the palmitic acid melted over the interval 62·55–62·75°C as compared with the highest m.p. of 62·82°C given by Timmermans [28]. The reduction to alcohol was carried out as described for undecanoic acid, and after two re-crystallizations from acetone the melting interval was 49·15–49·3°C, whereas Timmermans [28] gives m.p. 49·27°C. The sulphate was finally prepared and purified as described for sodium undecanyl sulphate, and its appearance was similar.

Carbon tetrachloride

For the majority of experiments the carbon tetrachloride was purified by distillation as described previously [19], but in some cases it was treated with chlorine and chlorine dioxide according to Dickinson and Leermakers [3]. This elaborate purification did not affect the results, and was consequently discontinued.

Other materials

The *o*-nitrophenol was a crystalline Merck product, with a melting point of 45°C. The iodine was of Pro Analysi quality. Both substances were dissolved in distilled water containing 0·002 mole/l of citric acid giving a pH of 3·15.

Methods of Analysis

Solutions of iodine and *o*-nitrophenol in water and in carbon tetrachloride were analysed photometrically as before [19] and [1], using a Beckman DU Quartz Spectrophotometer.

Results and Discussion

A few exploratory experiments were carried out with *n*-valeric and lauric acids as surface active agents, but the sodium salts of hexadecanyl

sulphate and undecanyl sulphate were used for the bulk of the work. In all cases the solvents were water and carbon tetrachloride with the former as the continuous phase. The diffusing solute was mainly *o*-nitrophenol, but iodine was used for a few experiments. The transfer was always from the continuous aqueous phase to falling droplets of carbon tetrachloride, and the temperature was maintained at 25°C.

n-Valeric acid

n-Valeric acid had no effect on the rate of mass transfer in the concentration range investigated, viz. $7{\cdot}5 \times 10^{-5}$ to $2{\cdot}3 \times 10^{-2}$ g/100 ml aqueous

Table 1. *Extraction of o-nitrophenol in presence of highly pure, synthetic sodium hexadecanyl sulphate and* 0·002 *M citric acid*

$n_S \times 10^7$ (mole/l)	V (mm³)	v (cm/sec)	$p = \frac{C_E \times 100}{m \times C_{RA}}$	R_R (sec/cm)	R_{Ri} (sec/cm)
	Average droplet volume: 18·1 ± 0·2 mm³				
0	18·2*	21·8*	—	45·8*	0
0·29	17·9	22·1	1·93	48·6	2·8
0·29	18·0	22·1	1·91	48·9	3·1
0·58	18·2	21·8	1·77	53·4	7·6
0·58	18·0	22·0	1·71	55·0	9·2
0·87	17·9	21·2	1·62	60·1	14·3
0·87	18·5	21·2	1·53	63·3	17·5
1·16	17·9	19·7	1·47	71·9	26·1
1·16	17·9	19·7	1·40	75·4	29·6
1·45	18·2	19·85	1·43	72·6	26·8
1·45	18·5	19·85	1·50	69·0	23·2
1·75	18·2	19·85	1·39	74·6	28·8
1·75	18·2	19·85	1·27	81·8	36·0
2·62	18·0	20·1	1·25	82·8	37·0
2·62	18·2	20·1	1·27	81·2	35·4
2·91	17·9	19·85	1·12	92·9	47·1
2·91	17·9	20·0	1·13	91·7	45·9
4·36	17·9	19·6	0·96	110·5	64·7
	Average droplet volume: 19·1 ± 0·8 mm³				
0	19·1†	21·9†	—	48·1†	0
1·16	19·5	19·45	1·53	67·7	19·6
1·16	19·2	19·4	1·51	68·4	20·3
3·02	19·2	19·9	1·08	94·8	46·7
3·02	18·9	19·9	1·09	94·1	46·0
6·04	19·3	19·6	0·781	132·8	84·7
6·04	19·1	19·45	0·800	130·8	82·7
9·12	19·0	19·2	0·678	157·1	109·0
9·12	19·2	19·2	0·678	156·5	108·4
12·1	19·1	18·95	0·650	165·5	117·4
12·1	19·1	19·2	0·646	164·6	116·5
15·1	21·4	19·2	0·632	162·9	114·8
15·1	16·7	18·95	0·711	158·1	110·0
30·5	19·2	18·9	0·663	162·2	114·1
30·5	19·2	18·9	0·791	135·9	87·8
61·0	19·1	18·6	0·690	158·6	110·5

*Average of 13 observations. For R_{RO}: $\sigma = 1{\cdot}5$ and $\sigma/\sqrt{n} = 0{\cdot}4$.
†Average of 8 observations. For R_{RO}: $\sigma = 1{\cdot}8$ and $\sigma/\sqrt{n} = 0{\cdot}6$.

phase. The distribution coefficient for *n*-valeric acid between carbon tetrachloride and water was found to be approximately 1·55, and prior to the extraction experiments the corresponding amount of *n*-valeric was added to the solvent phase to prevent any appreciable net transfer of surface active agent across the interface.

Lauric acid

Lauric acid is sparingly soluble in water, and was consequently added to the solvent phase. An impure, commercial sample reduced the rate of mass transfer to approximately the same extent as sodium oleyl-*p*-anisidine sulphonate [19], but after purification the effect disappeared completely.

Sodium hexadecanyl sulphate

The results obtained with the highly pure, synthetic product are given in Table 1, and those obtained with a sulphate prepared from commercial cetyl alcohol in Table 2. Both series have been plotted in Fig. 2 which also shows the reduction in the rate of fall of the droplets caused by the surface active agent. As in the preceeding papers in this series the action of the surface active agent on the rate of mass transfer is expressed as an additional resistance defined as the difference between the resistance with and without the agent present:

$$R_{Ri} = R_R - R_{RO} \qquad (1)$$

The resistances are calculated on a raffinate or aqueous basis. Only averages for each concentration of surface active agent are plotted to avoid overloading the figure.

It is evident from Fig. 2 that the action of the pure and impure hexadecanyl sulphates are identical. The suggestion by Cullen and Davidson [2] that the presence of impurities constitutes an essential condition for reduction in the rate of mass transfer is not therefore generally valid. However, impurities can have such an effect also in this case as shown by the results reported above for lauric acid. As pointed out earlier, the effect observed by the present authors is hydrodynamic in nature, whereas Cullen and Davidson claim to have a true barrier effect, and, whereas we use liquid-liquid extraction, their system is gas absorption.

The fully drawn curve in the lower part of Fig. 2 represents equation (2) and is seen

$$n_S = 6{\cdot}4 \times 10^{-9} \frac{R_{Ri}}{(1 - R_{Ri}/112)^{0{\cdot}1}} \qquad (2)$$

Table 2. Extraction of o-nitrophenol in presence of sodium hexadecanyl sulphate prepared from commercial cetyl alcohol, and 0·002 M citric acid

$n_S \times 10^7$ (mole/l)	V (mm^3)	v (cm/sec)	$p = \frac{C_E \times 100}{m \times C_{RA}}$	R_R (sec/cm)	R_{Ri} (sec/cm)
		Average droplet volume: 18·0 mm^3			
0	18·2*	21·8*	—	45·8*	0
5·6	18·0	—	0·895	120·0	74·2
5·6	17·95	—	0·903	119·2	73·4
5·6	18·0	—	0·917	117·3	71·5
5·6	17·95	—	0·900	119·5	73·7
5·6	18·2	—	0·878	122·1	76·3
11·2	18·1	—	0·662	166·4	120·6
16·3	16·0	18·9	0·743	153·9	118·1
16·8	18·1	—	0·735	145·7	99·9
28·0	17·85	—	0·718	157·7	111·9
32·5	13·1	18·3	0·794	158·6	112·8
32·5	17·55	18·9	0·701	158·5	112·7
56·0	17·55	—	0·713	161·4	115·6
84·0	17·65	—	0·689	167·4	121·6

*As for Table 1.

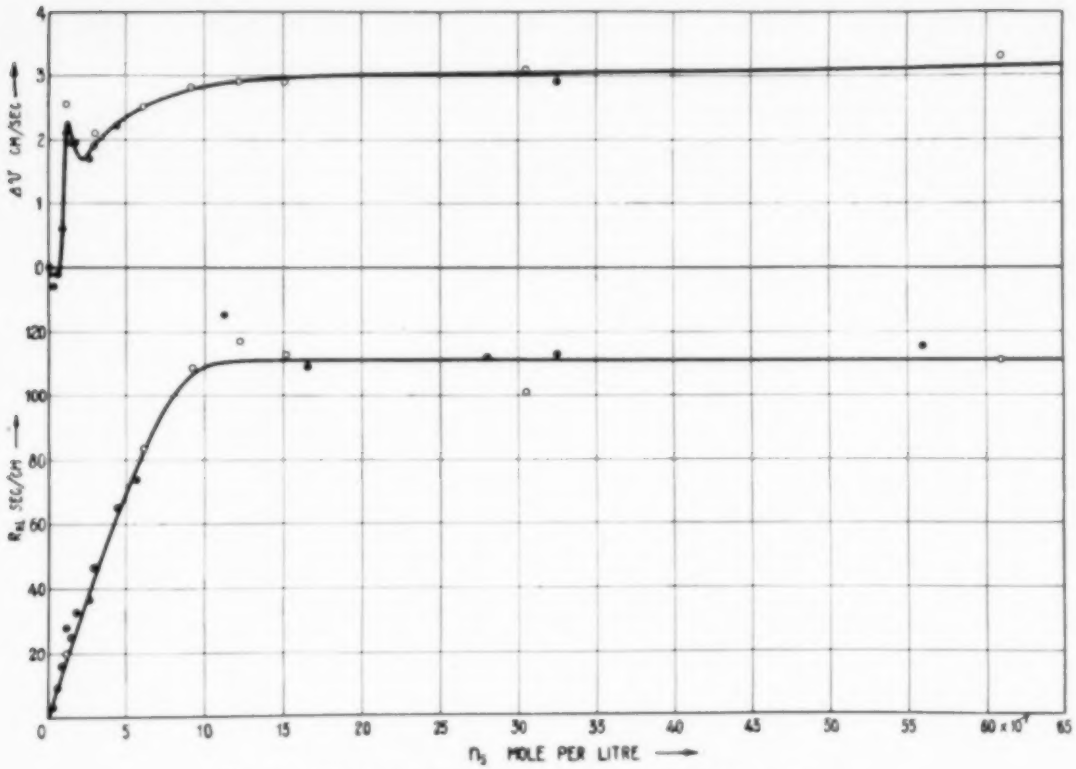

FIG. 2. Additional mass transfer resistance R_{Ri} and reduction in rate of fall Δv with sodium hexadecanyl sulphate and 0·002 M citric acid.

◗ Droplet size : 18·1 mm³; pure agent
○ Droplet size : 19·1 mm³; pure agent
● Droplet size : 18·2 mm³; impure agent.

to fit the observations within the limits of the experimental error. This equation is very similar to that previously found for sodium oleyl-*p*-anisidine sulphonate [1] and given below on a molar basis (3)

$$n_S = 6{\cdot}7 \times 10^{-9} \frac{R_{Ri}}{(1 - R_{Ri}/101)^{0{\cdot}1}} \qquad (3)$$

The slopes are practically identical, but the limiting values for the additional resistance R_{Ri} differ by about 10 per cent. This discrepancy appears to be too large to be attributed to experimental error, but no explanation for it can be advanced at present.

The plot of the reduction in the rate of fall of the droplets exhibits a complex pattern. It appears that additions of surface active agent less than about $0{\cdot}5 \times 10^{-7}$ mole/l have no effect on the rate of fall although they appreciably reduce the rate of mass transfer. With additions greater than 1×10^{-7} mole/l, however, the reduction in the rate of fall increases very sharply with increasing concentration up to a local maximum, whereupon it falls and passes through a minimum. Subsequently it rises slowly and becomes ultimately constant. The local maximum and minimum can be explained by the action of the surface agent on the oscillation of the droplets. It was observed that the intensity of oscillation was slight in the absence of surface active agent, but increased strongly along the rising branch of the curve. The maximum oscillation and the maximum reduction in the rate of fall occurred at about the same concentration of surface active

Table 3. Extraction of o-nitrophenol in presence of highly pure, synthetic sodium undecanyl sulphate and 0·002 M citric acid

$n_S \times 10^7$ (mole/l)	V mm^3	v cm/sec	$p = \frac{C_E \times 100}{m \times C_{RA}}$	R_R (sec/cm)	R_{Ri} (sec/cm)
3·7	18·8	21·35	1·70	56·0	8·7
3·7	18·5	21·35	1·77	54·1	7·5
3·7	18·2	21·2	1·79	54·4	8·6
4·1	18·4	20·55	1·71	58·3	12·0
4·1	18·4	19·8	1·65	62·8	16·5
4·1	18·15	20·4	1·76	57·3	11·5
7·3	18·5	19·95	1·52	67·4	20·8
7·3	18·5	19·95	1·62	63·6	17·0
7·3	18·75	19·8	1·59	64·9	17·8
11·0	18·65	19·3	1·54	68·7	21·7
11·0	19·10	19·4	1·56	67·2	19·1
12·2	18·5	19·4	1·48	71·6	25·0
12·2	18·2	19·7	1·45	72·0	26·2
12·2	18·3	19·4	1·53	69·3	23·3
14·6	18·75	19·7	1·45	71·2	24·0
21·9	20·0	19·7	1·28	79·1	29·2
21·9	17·5	19·7	1·38	76·8	32·8
24·3	18·5	20·0	1·32	77·8	31·2
36·5	18·5	19·7	1·21	86·1	39·5
36·5	18·3	19·5	1·24	85·1	39·1
40·5	18·5	19·7	1·21	86·1	39·5
40·5	18·2	19·8	1·24	84·1	38·3
61·0	18·2	19·6	1·17	90·3	44·5
61·0	18·25	19·5	1·08	97·7	51·8
73·0	17·8	19·5	1·12	95·7	50·9
73·0	18·1	19·55	1·10	95·8	50·3
73·0	18·6	19·65	1·07	97·4	50·6
73·0	18·75	19·45	1·12	94·0	46·8
73·0	18·65	19·45	1·12	94·1	47·2
91·3	18·65	19·5	1·01	104·6	57·7
91·3	18·65	19·5	1·06	98·7	51·8
94·9	18·4	19·45	1·06	100·1	53·8
110	17·9	19·5	1·05	101·6	56·6
110	18·75	19·6	1·05	98·9	51·7
120	18·5	19·55	0·972	108·0	61·4
122	18·75	19·5	1·05	100·3	53·1
123	18·6	19·6	0·987	106·1	59·3
123	18·6	19·4	0·972	108·7	61·9
123	18·0	19·5	1·00	106·3	61·0
123	17·85	19·6	0·982	108·0	63·1
131	18·2	19·45	0·952	111·5	65·7
134	18·6	19·4	0·953	111·0	64·2
134	18·6	19·5	0·923	114·3	67·5
153	18·65	19·7	0·919	113·3	66·4
153	18·6	19·6	0·905	115·7	68·9
153	18·8	19·5	0·942	111·1	63·8
153	18·5	19·5	0·906	116·5	69·9
183	18·5	19·5	0·913	115·6	69·0
183	18·6	19·45	0·908	116·3	69·5
183	18·6	19·45	0·880	120·0	73·2
244	18·35	19·5	0·828	127·8	81·6
244	18·2	19·6	0·866	122·1	76·3
274	18·65	19·5	0·831	126·8	79·9
307	18·6	19·4	0·818	129·4	82·6
307	18·5	19·4	0·822	128·9	82·3
489	18·65	19·3	0·767	138·5	91·6
489	18·45	19·5	0·782	135·1	88·7
730	18·2	19·45	0·729	145·6	99·6
730	18·3	19·45	0·762	139·1	93·1
1100	18·1	19·3	0·735	145·9	100·4

agent, viz. $1{\cdot}2 \times 10^{-7}$ mole/l. With further additions the oscillations decreased and disappeared completely when the reduction in the rate of fall passed through its minimum. From there on the droplets fell in a perfectly quiet way. A reduction in the rate of fall due to oscillation has previously been reported by GARNER and SKELLAND [9]. The fact that the curve for the resistance coefficient exhibits no corresponding maximum and minimum shows that in this case the effect of oscillation on the rate of mass transfer is insignificant.

The complex pattern of the curve representing the reduction in the rate of fall is clearly due to the superposition of two separate effects, i.e. the action of the surface active agent on the oscillation and on the internal circulation. If the effect on oscillation could be eliminated the effect on the internal circulation would be expected to follow a steadily rising curve of a character not unlike that of the resistance curve. This similarity indicates that in this case the action of the surface active agent on internal circulation and on mass transfer is parallel. However, the results given below for sodium undecanyl sulphate show that this parallelism is fortuitous, and that the reduction in the rate of mass transfer is only partly, if at all, caused by suppression of the internal circulation.

Sodium undecanyl sulphate

The results obtained with highly pure, synthetic sodium undecanyl sulphate are given in Table 3 and the average resistances for each concentration plotted in Fig. 3. In this figure are also shown the results of Table 4 obtained when the aqueous solution was made 0·006 N with sodium chloride. It is clear that the reduction of the number of

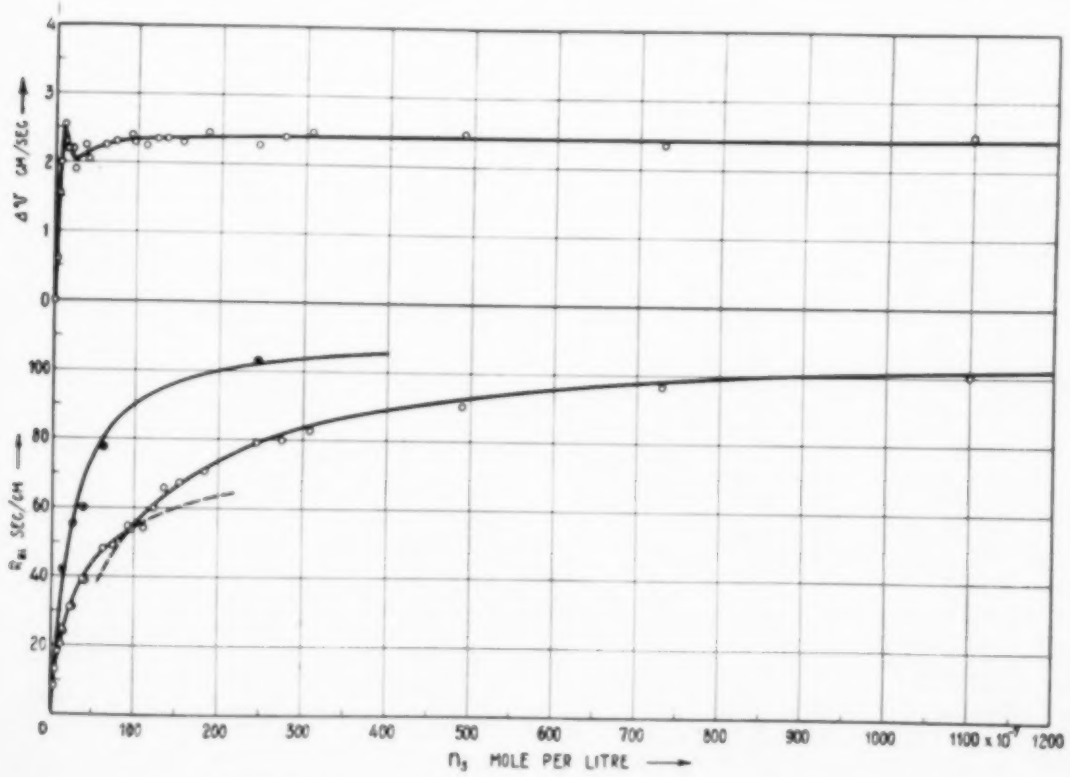

FIG. 3. Additional mass transfer resistance R_{Bi} and reduction in rate of fall Δv with sodium undecanyl sulphate and 0·002 M citric acid ○ ● 0·006 M sodium chloride also added.

Table 4. Extraction of o-nitrophenol in presence of specially pure, synthetic sodium undecanyl sulphate and 0·002 M citric acid + 0·006 M sodium chloride

$n_S \times 10^7$ (mole/l)	V (mm³)	v (cm/sec)	$p = \frac{C_E \times 100}{m \times C_{RA}}$	R_R (sec/cm)	R_{Ri} (sec/cm)
12·0	18·4	19·6	1·20	88·2	41·9
24·1	19·0	19·3	1·02	103·6	55·8
24·1	18·5	19·2	1·01	116·6	70·0
24·1	18·5	19·2	1·05	101·4	54·8
36·5	18·5	19·5	0·969	108·8	62·2
36·5	18·5	19·5	0·972	108·3	61·7
61·0	18·5	19·2	0·858	125·0	78·4
61·0	18·4	19·25	0·850	125·9	79·6
243	17·9	19·25	0·714	151·1	106·1
243	17·9	19·25	0·743	145·5	100·5

carbon atoms in the chain from 16 to 11 has greatly weakened the surface activity and changed the character of the curves. The results can no longer be described by equations of the type applicable to the sodium salt of oleyl-*p*-anisidine sulphonate and hexadecanyl sulphate. Two equations were necessary for the results obtained in the absence of sodium chloride, equation (4) for the lower branch and equation (5) for the upper, and these are shown as solid drawn lines in Fig. 4.

$$n_S = 36 \times 10^{-9} \frac{R_{Ri}}{1 - R_{Ri}/112} \exp\left(\frac{R_{Ri}/112}{1 - R_{Ri}/112}\right) \quad (4)$$

$$n_S = 92 \times 10^{-9} \frac{R_{Ri}}{1 - R_{Ri}/112} \quad (5)$$

In the presence of sodium chloride equation (6) was found to fit.

$$n_S = 21{\cdot}5 \times 10^{-9} \frac{R_{Ri}}{1 - R_{Ri}/112} \quad (6)$$

Equations (5) and (6) are straight Langmuir equations whereas equation (4) is a modified form. The equations can be seen to describe the results within the limits of experimental error. Without addition of sodium chloride there appears to be a break in the curve. This might be due to a phase transition, but since reproducibility was distinctly poorer with this surface active agent, restraint must be shown in drawing conclusions.

The curve for the reduction in the rate of droplet fall is similar to that obtained with hexadecanyl sulphate. The maximum and minimum are clearly visible, and variation in droplet oscillation in relation to these was also the same. The striking feature of the results is that the reduction in the rate of fall reaches its terminal value when 80×10^{-7} mole/l of surface active agent has been added, whereas the additional resistance to mass transfer at this concentration is only half developed. It is reasonable to conclude that the internal circulation has ceased when there is no further reduction in the rate of fall, and that the action of the surface active agent on the internal circulation therefore, at the most, can be only partly responsible for the reduction in the rate of mass transfer.

Transfer of iodine in presence of sodium undecanyl sulphate

It is of interest to compare the action of the weak surface active agent sodium undecanyl sulphate on the extraction of *o*-nitrophenol and iodine. Such a comparison has previously been reported for the strong surface active agent sodium oleyl-*p*-anisidine sulphonate [1]. The present results with the weak agent are given in Table 5. The ratio of the additional resistance caused by the surface active agent R_{Ri} to the resistance in the absence of the agent R_{RO} is plotted in Fig. 4 for the extraction of *o*-nitrophenol and iodine. The results obtained with iodine

Table 5. Extraction of iodine in presence of highly pure, synthetic sodium undecanyl sulphate and 0·002 N citric acid

$n_S \times 10^7$ (mole/l)	V (mm³)	v (cm/sec)	$p = \frac{C_E \times 100}{m \times C_{RA}}$	R_R (sec/cm)	R_{Ri} (sec/cm)
	Average droplet volume: 18·5 ± 0·2 mm³				
0	18·7*	21·9*	—	40·6*	0
16·4	18·5	19·6	2·16	68·1	17·5
29·2	18·7	20·0	1·91	75·2	34·6
29·2	18·5	20·0	2·05	70·2	29·6
58·4	18·7	19·45	1·63	90·8	50·2
58·4	18·7	19·6	1·63	89·8	49·2
58·4	18·7	19·6	1·62	90·7	50·1
168	18·5	19·45	1·49	99·6	59·0
168	18·5	19·45	1·40	106·3	65·7
566	18·5	19·3	1·09	137·8	97·2
566	18·5	19·45	1·11	133·6	93·0
1060	18·2	19·15	1·16	131·1	90·5
1060	18·2	19·15	1·18	128·5	87·9

*Average of 5 observations. For R_{RO}: $\sigma = 1{\cdot}4$ and $\sigma/\sqrt{n} = 0{\cdot}6$.

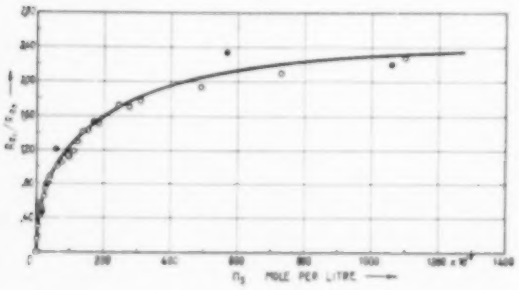

Fig. 4. The ratio R_{Ri}/R_{RO} plotted against concentration of sodium undecanyl sulphate.
● for iodine
○ for *o*-nitrophenol.

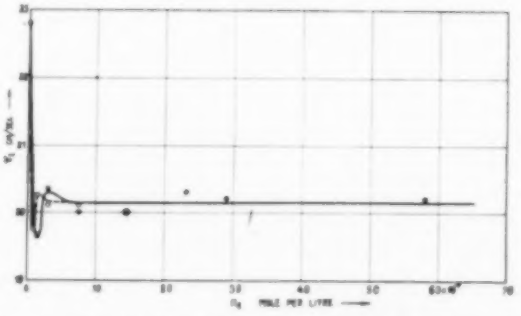

FIG. 5. Terminal velocities with sodium hexadecanyl sulphate.
● without citric acid ○ with 0·002 M citric acid.

were less reproducible, but the figure shows clearly that the action of sodium undecanyl sulphate is the same for both diffusing solutes. This confirms the previous results with the strong agent.

Terminal velocities in larger column. The effect of citric acid and salts

The reduction in the rate of fall observed with sodium hexadecanyl sulphate is shown in Fig. 5, and with sodium undecanyl sulphate in Fig. 6. The droplet volume was in all cases 20 mm³ with an equivalent diameter of 0·337 cm.

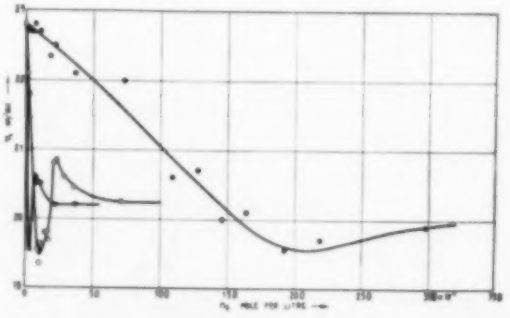

FIG. 6. Terminal velocities with sodium undecanyl sulphate.
○ without citric acid ● with 0·002 M citric acid
◑ with 0·002 M sodium citrate.

The rate of fall in the absence of surface active agent was 22·8 cm/sec at 25°C. With the extraction column the velocity was 21·9 cm/sec showing that the terminal velocity was not reached at the entrance to the extraction section of the column. The value of 22·8 cm/sec is considerably higher than the 19·8 cm/sec reported by Hu and Kintner [13] at 30·4°C. These authors found that when plotted against the droplet diameter the velocity reached a maximum of 20·2 cm/sec at an equivalent diameter of 0·35 cm. The difference in temperature does not explain the discrepancy between their results and those of the present authors. It is pertinent to point to the possibility that the terminal velocities might have been affected by surface active impurities present in the technical grade organic liquids.

On addition of sufficiently large quantities of surface active agents the terminal velocities in all cases appeared to approach 20·1 cm/sec irrespective of whether citric acid or sodium citrate were present as well.

All curves have maxima coinciding with maximum oscillation and minima where the oscillations have ceased completely. The characteristic shape of the curves is particularly well established in Fig. 6 containing a large number of observations. The oscillations are not just a continuation of the oscillations induced by internal currents during the formation of the droplets. This follows from the observation that in some cases the droplets fall fairly quietly at the start before the adsorption layer has been established, and then suddenly begin to oscillate violently further down the column.

In addition to internal circulation and oscillation the movement of the droplets is characterized by a zig-zag path. A similar behaviour has been observed by Garner and Hammerton [7] for gas bubbles. Whereas these authors found that the path became much more irregular on addition of vaseline, the present observations showed that additions of surface active agents reduce, and even eliminate this tendency. When the rate of fall has reached its minimum the path became practically straight.

There were some indications that a stationary adsorption state had not been established even after a fall of 200 cm. It was observed in some cases that oscillation started within the measuring distance, and in other cases that it died away.

The surface active agents became more effective on addition of sodium chloride, sodium citrate, and even citric acid. The effect on the terminal velocity can be seen from Figs. 5 and 6 which show that the weaker surface active agent is most strongly affected. The character of the curves with the maxima and minima remain essentially unaltered, and the terminal velocity appears to approach the same limiting value on addition of sufficiently large quantities of surface active agent. Particularly illustrating is Fig. 7, where the terminal velocity in the presence of $2{\cdot}2 \times 10^{-7}$ mole/l of sodium undecanyl sulphate has been plotted against the concentration of added sodium chloride. Even with this very

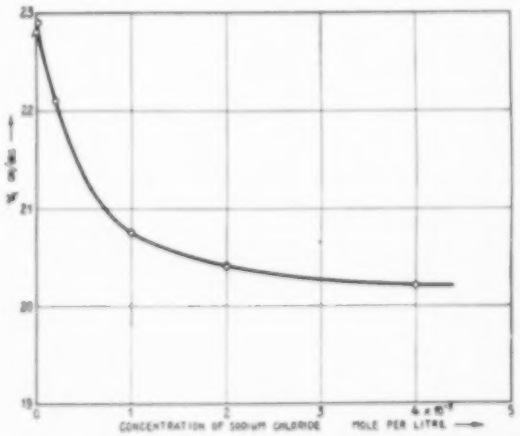

Fig. 7. Terminal velocities with $n_S = 2{\cdot}2 \times 10^{-7}$ mole/l of sodium undecanyl sulphate plus varying additions of sodium chloride.

low concentration of surface active agent the limiting condition is reached when the solution is made 0·004 M with respect to sodium chloride. In this connexion it must be remembered, that all experiments with *o*-nitrophenol as diffusing solute, and also the present experiments with iodine, have been carried out with solutions containing 0·002 mole/l of citric acid.

Comparison with solid spheres. The nature of the action of surface active agents

The terminal velocity of a sphere with a diameter of 0·337 cm was calculated to be 23·8 cm/sec by the method recommended by LAPPLE [16]. It is of interest to compare this figure with the average terminal velocity of 20·1 obtained on addition of comparatively large quantities of surface active agents. The results of MELHUS and TERJESEN [21] show that the shape of the droplets generally approximate to oblate spheroids. With sodium oleyl-*p*-anisidine sulphonate the ratio of the short to the long axis was $b/a = 0{\cdot}82$ at a concentration of $1{\cdot}2 \times 10^{-7}$ mole per litre and 0·78 at $8{\cdot}2 \times 10^{-7}$. The ratio of the terminal velocities for two bodies of the same material moving in the same medium is given by equation (7)

$$\frac{v_{t(1)}}{v_{t(2)}} = \sqrt{\frac{A_{p(2)}}{A_{p(1)}} \cdot \frac{C_2}{C_1}} \qquad (7)$$

where A_p is the projected area and C the drag coefficient. For an oblate spheroid and a sphere of the same volume this reduces to

$$\frac{v_{t\,(\text{sphere})}}{v_{t\,(\text{spheroid})}} \sqrt[3]{\frac{a}{b}} \cdot = \sqrt[2]{\frac{C_{\,(\text{spheroid})}}{C_{\,(\text{sphere})}}} \qquad (8)$$

As a first approximation the drag coefficients for spheres and spheroids at the same Reynolds' number are assumed to be the same. By interpolation in the table of drag coefficients given by LAPPLE the velocity ratios are calculated for the two additions of surface active agent to be 0·89 and 0·87 respectively, whereas the ratio between the observed terminal velocity and that calculated for an equivalent sphere is 0·84. This difference between the calculated and observed ratio of less than 5 per cent can probably be explained by the fact that the drag coefficients for oblate spheroids undoubtedly are larger than for spheres, but, unfortunately, measured drag coefficients for spheroids are not available in this range of Reynolds' numbers. However, the conclusion is justified that the movement of a droplet in the presence of sufficiently large amounts of surface active agents appears to differ from that of an equivalent sphere solely by its spheroid shape. All other effects such as internal circulation, oscillation and the zig-zag path have disappeared.

SIEMES [26], using the data of STUKE [27] on the rise of air bubbles in water containing various amounts of capronic acid, has shown that the limiting rate of rise on addition of sufficiently large quantities of the acid, about 0·01 mole/l, is approximately the same as for solid spheres, provided the Reynolds' number is below about 250. Above this value the deformation of the bubbles was too great and caused the drag coefficient to increase above that for solid spheres.

A similar comparison with solid spheres can be made with respect to mass transfer. Data for mass transfer to solid spheres in liquids do not seem to be available*, but SHERWOOD and PIGFORD [25] have correlated data for solid spheres and droplets falling in air by plotting N_{Sh} against $N_{Re} \times N_{Sc}^{2/3}$. The curve recommended by these authors is shown in Fig. 8 together with the corresponding curve recommended by McAdams for heat transfer. The results obtained with liquid droplets in the present and previous work in this series are also shown in Fig. 8. It can be seen that the limiting mass transfer coefficients obtained with comparatively large additions of surface active agents fall on the curve recommended by SHERWOOD and PIGFORD whereas the results without addition of surface active agents are about three times as high. The line through the points obtained without addition of surface active agents is drawn parallel to the SHERWOOD and PIGFORD line for solid spheres and in a distance of 2·8 on the logarithmic scale.

In Fig. 8 are also shown the results of GUYER and PFISTER [10] appertaining to absorption of carbon dioxide from gas bubbles rising through water. For bubble diameters larger than about 0·3 cm the points fall on the same line as the present extraction results without surface active agents present, but for smaller bubbles they fall considerably below and appear to approach the line for solid spheres.

The results have also been compared with those of HEERTJES, *et al.* [11]. These authors plotted N_{Sh} as a function of $N_{Re}^{0.5} \times N_{Sc}^{0.5}$ for the

*See note added in proof (p. 240).

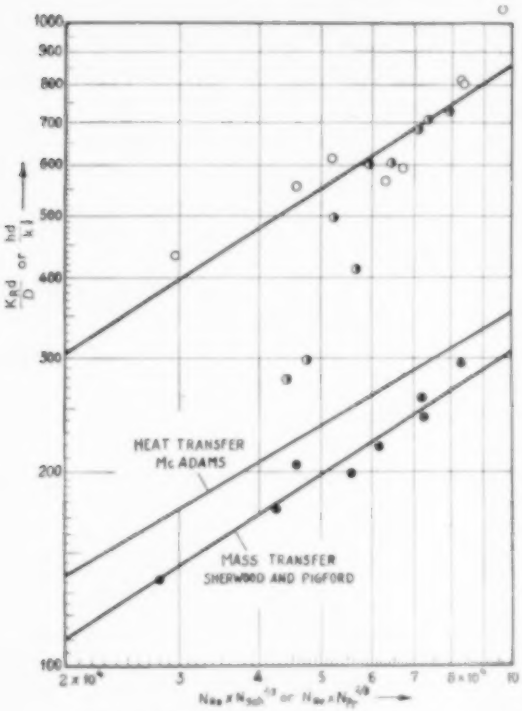

Fig. 8. Comparison with solid spheres.

- ○ without addition of surface active agents [19], [1] and [20]
- ● with comparatively large additions of surface active agents [19], [1] and [20]
- ◑ results of Guyer and Pfister with bubbles of carbon dioxide [10].

continuous phase for droplets of water in *iso*butanol and of *iso*butanol in water together with the observations of Guyer and Pfister referred to above. The present results fall among theirs, but on a much steeper curve, more in line with those for carbon dioxide. The points of Guyer and Pfister and of the present authors appear to correlate better by the plot proposed by Sherwood and Pigford, but further work is necessary before generally reliable correlations can be arrived at.

The nature of the action of the surface active agents can now be understood. It consists simply in eliminating all effects associated with the liquid boundary. The adsorbed molecules make the liquid droplets equivalent to solid spheres, except for the change in shape which appears to have little effect on mass transfer. These results rule out the possibility that the adsorbed surface active molecules form a barrier which interacts with the diffusing solute molecules and thus retards their passage through the interface. The previously reported conclusion that the effect is hydrodynamic in character has thus been confirmed.

The problem is no longer to explain why the rate of mass transfer is so slow in the presence of surface active agents, but to explain why it is so fast in the absence of these. The present results, and particularly those with sodium undecanyl sulphate, show that droplet oscillation has only an insignificant effect, and that internal circulation is at most capable of providing part of the explanation. This is in agreement with the observation by Garner and Hale that the surface active agent *Teepol* reduced the rate of transfer of diethylamine from toluene by drops of water, also when there was no internal circulation before the addition of the agent. The maximum in their resistance curve has been explained by Melhus and Terjesen [21] as being caused by impurities present in the *Teepol*, and there is no reason to doubt that the same mechanism is responsible in their case as in ours; that is that their effect is also of a hydrodynamic rather than of a barrier type.

The situation can be summed up in the form of a paradox: The high rates of mass transfer with pure systems must be due to some feature of the hydrodynamics of the falling droplets unconnected with oscillation and the zig-zag path and at least partly unconnected with the internal circulation. If the whole explanation cannot be found in the macro picture of the flow pattern it must be sought in its micro picture.

The concept of transfer of turbulence developed by Lewis [17] to explain the results with his transfer cell does not appear to be directly applicable to falling droplets. In his transfer cell the rate of mass transfer was independent of the molecular diffusivity, whereas the present results with iodine and *o*-nitrophenol show proportionality with the diffusivity to the power of about 0·4 also in the absence of surface active agents. The interfacial turbulence of Lewis and

PRATT [18] is not directly applicable either. These authors found that this effect occurred only when the transfer of the solute was accompanied by evolution of heat*, whereas the present results show no difference between the exothermic transfer of *o*-nitrophenol and the endothermic transfer of iodine except that which is caused by the difference in their molecular diffusivities.

The present results also throw some light on the more general question of establishment of equilibrium at phase boundaries. It is rather striking that the mass transfer coefficients for droplets in presence of surface active agents in Fig. 8 fall so well on the curve recommended by SHERWOOD and PIGFORD for solid spheres and droplets falling in air. These involve both evaporation and sublimation. The fact that so many different processes can be correlated by purely hydrodynamic variables indicate that, if true interfacial resistance of the barrier type exist at all, its contribution to the total resistance to mass transfer is unlikely to be greater than about 20 per cent, which is the spread of the experimental observations used by SHERWOOD and PIGFORD in establishing their correlation. At least some of this spread is due to experimental error and possible imperfections in the method of correlations.

CONCLUSIONS

(1) The action of strongly surface active agents on mass transfer does not depend on the presence of impurities, but is caused by the pure compounds.

(2) Whereas sodium oleyl-*p*-anisidine sulphonate and sodium hexadecanyl sulphate exert a strong action on both terminal velocity and rate of mass transfer, the action of sodium undecanyl sulphate is much weaker.

(3) The limiting values of the additional resistance to mass transfer and the reduction of the terminal velocities appear to be approximately the same for all surface active agents when sufficiently large quantities are added.

(4) In the case of strongly active agents the previously developed adsorption isotherm gives a satisfactory description of the mass transfer results, whereas equations of the Langmuir type are adequate for the weaker agents.

(5) The additional resistance to mass transfer caused by the relatively weak agent sodium undecanyl sulphate, expressed as per cent of the resistance without addition of this agent, is the same both with *o*-nitrophenol and iodine as diffusing solute.

(6) The surface active agents act strongly on the oscillation of the droplets, and this is reflected in the terminal velocities, but not in the rate of mass transfer, indicating that oscillation is of little or no importance for mass transfer.

(7) With sodium undecanyl sulphate the limiting terminal velocity is reached with much smaller concentrations than the limiting resistance to mass transfer. Taking the terminal velocity to be an indicator for the degree of internal circulation in the droplet, this shows that the reduction in mass transfer must at least partly be due to other factors than elimination of internal circulation.

(8) On addition of sufficiently large quantities of surface active agents the droplets behave as solid spheres or spheroids with respect to both terminal velocity and rate of mass transfer, confirming that the effect is hydrodynamic in character.

(9) The rate of mass transfer without surface active agents present is about 2·8 times that for equivalent solid spheres or about equal to that observed by GUYER and PFISTER [10] for transfer of carbon dioxide from gas bubbles with diameters above 0·3 cm.

(10) Conclusions (6), (7) and (8) imply that the high rates of mass transfer observed in the absences of surface active agents

*See note added in proof (p. 240).

are not due to droplet oscillation, and at the most only partly to internal circulation. The liquid-liquid boundary must give rise to a flow pattern which affects greatly the rates of mass transfer without affecting the terminal velocities.

(11) The phenomena of transfer of turbulence as described by Lewis [17] do not appear to be directly responsible.

*Since this paper was prepared the authors have received the paper by F. H. Garner and R. D. Suckling (*A. I. Ch. E. Journal*, 1958, **4**, 114) on mass transfer from soluble solid spheres. Their results fall close to the curve recommended by Sherwood and Pigford and shown on Fig. 8, and thus give strong support to the conclusions of the present paper.

The work of K. Sigwart and H. Nassenstein (*V.D.I. Zeitschr.* 1956, **98**, 453) has shown that the interfacial turbulence, first observed by Lewis and Pratt [18], occurs not only with exothermic extractions, but also with endothermic. Interfacial turbulence and "eruptions" cannot therefore be ruled out and must be further considered as possible explanations of the hydrodynamic type for the high transfer coefficients obtained in the absence of surface active agents.

Both these aspects have been discussed in some detail in a paper by S. G. Terjesen to be published in Dechema-Monographien Vol. 32.

The authors.

Acknowledgements—The authors wish to acknowledge the helpful assistance given by Professor N. A. Sorensen and Dr. T. Bruun of the Organic Chemical Laboratory with the planning of the synthetic work. The authors are indebted to the Royal Norwegian Council for Scientific and Industrial Research for a grant which has made this work possible.

Notation

A_p = projected area of droplet on plane vertical to direction of movement — cm²
a = long axis of oblate spheroid — cm
b = short axis of oblate spheroid — cm
C = drag coefficient — Dim. less
C_E = solute concentration in solvent phase — mg/cm³
C_E^* = equilibrium concentration in solvent phase — mg/cm³
C_R = solute concentration in aqueous phase — mg/cm³
C_{RA} = average of initial and final concentration in aqueous phase — mg/cm³
c_p = specific heat — cal/g°C
D = diffusivity — cm²/sec
d = diameter of equivalent sphere — cm
h = heat transfer coefficient — cal/cm² sec°C
K_R = extraction coefficient on a time and raffinate or aqueous basis — cm/sec
k = heat conductivity — cal/cm sec°C
m = distribution coefficient — $\frac{\text{mg solute/ml solvent}}{\text{mg solute/ml aqueous phase}}$
n_S = concentration of surface active agent — g mol/litre
p = per cent approach to equilibrium $= \frac{C_E \times 100}{m\, C_{RA}}$ — Dim. less
R_R = resistance on a time and raffinate or aqueous basis — sec/cm
R_{RO} = resistance without surface active agent — sec/cm
$R_{R\infty}$ = limiting resistance on addition of relatively large amounts of surface active agents — sec/cm
R_{Ri} = additional resistance caused by the surface active agent $= R_R - R_{RO}$ — sec/cm
V = droplet volume — mm³
v = velocity of fall — cm/sec
Δv = reduction in velocity of fall — cm/sec
v_t = terminal velocity — cm/sec
ρ = density — g/cm³
μ = viscosity — g/sec cm

N_{Re} = Reynold's number $= \frac{\rho v d}{\mu}$

N_{Pr} = Prandtl's number $= \frac{c_p \mu}{k}$

N_{Sc} = Schmidt's number $= \frac{\mu}{\rho D}$

N_{Sh} = Sherwood's number $= \frac{K_R d}{D}$

References

[1] Boye-Christensen G. and Terjesen S. G. *Chem. Engng. Sci.* 1958 **7** 222.

[2] Cullen E. J. and Davidson J. F. *Chem. Engng. Sci.* 1956 **6** 49.

[3] Dickinson R. G. and Leermakers J. A. *J. Amer. Chem. Soc.* 1932 **54** 3853.

[4] Dreger E. E., Keim G. I., Miles G. D., Shedlovsky L. and Ross J. *Industr. Engng. Chem.* 1944 **36** 610.

[5] Garner F. H. *Chem. & Ind.* 1956 **8** 141.

[6] Garner F. H. and Hale A. R. *Chem. Engng. Sci.* 1953 **2** 157.

[7] Garner F. H. and Hammerton D. *Chem. Engng. Sci.* 1954 **3** 1.

[8] Garner F. H. and Skelland A. H. P. *Industr. Engng. Chem.* 1954 **46** 1255.
[9] Garner F. H. and Skelland A. H. P. *Chem. Engng. Sci.* 1955 **4** 148.
[10] Guyer A. and Pfister X. *Helv. Chim. Acta.* 1946 **29** 1173, 1400.
[11] Heertjes P. M., Holve W. A. and Talsma H. *Chem. Engng. Sci.* 1954 **3** 122.
[12] Holm A., Lindland K. P. and Terjesen S. G. *Chem. Ber.* 8. Nordiske Kjemikermøte, Oslo, 14-17 June 1953.
[13] Hu S. and Kintner R. C. *Amer. Inst. Chem. Engrs. J.* 1955 **1** 42.
[14] Jones E. C. S. and Pyman J. *J. Chem. Soc.* 1925 **127** 2596.
[15] Kern J. W., Shriner R. L. and Adams R. *J. Amer. Chem. Soc.* 1925 **47** 1147.
[16] Lapple C. E. *Fluid and Particle Mechanics* Univ. Delaware, U.S.A. (1951).
[17] Lewis J. B. *Chem. Engng. Sci.* 1954 **3** 248 and 260.
[18] Lewis J. B. and Pratt H. R. C. *Nature, Lond.* 1953 **171** 1155.
[19] Lindland K. P. and Terjesen S. G. *Chem. Engng. Sci.* 1956 **5** 1.
[20] Maaren H. J. and Terjesen S. G. To be published.
[21] Melhus B. J. and Terjesen S. G. *Chem. Engng. Sci.* 1957 **7** 88.
[22] Nystrom R. F. and Brown W. G. *J. Amer. Chem. Soc.* 1947 **69** 2548.
[23] Plešek J. *Coll. Trav. Chim. Tchécosl.* 1956 **21** 1312.
[24] Ralston A. W. and Hoerr C. W. *J. Org. Chem.* 1944 **9** 329.
[25] Sherwood T. K. and Pigford R. L. *Absorption and Extraction*, McGraw-Hill, New York, (1952).
[26] Siemes W. *Chem. Ing. Tech.* 1954 **26** 479 and 614.
[27] Stuke B. *Naturwissenschaften* 1952 **39** 325.
[28] Timmermans J. *Physico-Chemical Constants of Organic Compounds*, Elsevier, (1940).
[29] Verkade P. E., Hartman H. and Coops J. *Rec. Trav. Chim. Pays-Bas* 1926 **45** 379.
[30] *Organic Synthesis* **17** 30.

Chemical Engineering Science, 1958, Vol. 9, pp. 242 to 249. Pergamon Press Ltd. London. Printed in Great Britain

On the rate of mass transfer from a gas to a moving liquid film

A. Acrivos

Department of Chemical Engineering, University of California, Berkeley, California

(*Received* 29 *August* 1957)

Abstract—A theoretical expression is derived for the rate of mass transfer of a substance from the gas phase to a liquid film, in which it is highly soluble, flowing down a vertical surface. It is assumed that the gas phase is in laminar motion. The problem is solved for both the special case of dilute gaseous mixtures, and the more general case of high rates of mass transfer. It is shown that when the Schmidt number is around unity, the Nusselt number is again proportional to the square root of a Reynolds number as in all laminar single phase flows, except that a new characteristic velocity has to be defined, and that the expression for the Nusselt number for mass transfer to a stationary vertical surface is also applicable for mass transfer to a falling liquid film, if this new characteristic velocity is used. The same argument holds of course for the analogous heat transfer problem, that is the transfer of heat from a surface through a moving thin liquid film into a laminar gas stream in motion.

Résumé—L'auteur déduit une expression théorique pour la vitesse du transfert massique d'un gaz à un film liquide. La solubilité du gaz dans le liquide est très grande et le liquide coule sous forme de film le long d'une surface verticale. Il suppose que la phase gazeuse est en écoulement laminaire. Ce problème est résolu d'une part pour des mélanges de gaz dilués et d'autre part pour le cas plus général des grandes vitesses de transfert de masse. Quand le nombre de Schmidt est environ égal à 1, l'indice de Nusselt est proportionnel à la racine carrée du nombre de Reynolds comme dans tout écoulement en phase laminaire. Cependant une nouvelle vitesse caractéristique doit être alors définie et l'expression de l'indice de Nusselt pour le transfert de masse à une surface verticale stationnaire est applicable au transfert de masse à unfilm liquide descendant. Le même argument est valable pour le problème analogue au transfert de chaleur d'une surface à un courant de gaz laminaire par l'intermédiaire d'un film liquide en mouvement.

Zusammenfassung—Für die Geschwindigkeit der Stoffübertragung einer Substanz aus der Gasphase in einen entlang einer senkrechten Wand strömenden Flüssigkeitsfilm, in dem diese Substanz leicht löslich ist, wird ein theoretischer Ausdruck abgeleitet. Es wird dabei angenommen, dass die Gasphase laminar strömt. Das Problem wird sowohl für den speziellen Fall der verdünnten Gasmischungen als auch für den allgemeinen Fall hoher Beträge der Stroffübertragung gelöst. Es zeigt sich, dass bei Werten der Schmidtzahl in der Nähe von 1 die Nusseltzahl proportional der Quadratwurzel einer Reynoldszahl ist wie bei allen laminaren Einphasenströmungen. Es wird hierbei allerdings eine neue charakteristische Geschwindigkeit definiert und der Ausdruck für die Nusseltzahl der Stoffübertragung an eine ruhende senkrechte Fläche ist auch anwenbar für die Stoffübertragung an einen fallenden Flüssigkeitsfilm, wenn die neue charakteristische Geschwindigkeit verwendet wird. Die gleiche Lösung gilt naturgemäss auch für das analoge Wärmeübergangsproblem, nämlich für den Wärmeübergang von einer Fläche durch einen strömenden dünnen Film an einen laminaren Gasstrom.

The need for calculating rates of mass and heat transfer to two-phase mixtures in motion arises all too frequently in the chemical engineering operations, but the complexity of the phenomena involved is such that in general *a priori* predictions in this field cannot be made with any degree of confidence. This is due primarily to the highly disorganized and often unpredictable relative spatial distributions of the two phases, that is the phase diagrams, which exist under the usual operating conditions.

Thus, it is well known that when a gas–liquid

mixture is made to flow through a tube, more or less random and non-reproducible flow configurations, loosely referred to as bubble flow, slug flow, annular flow, etc., are observed. It is not surprising therefore that no general mathematical model for predicting the behaviour of two-phase mixtures has emerged so far and that even the empirical correlations available in the literature are neither general nor very reliable.

In an attempt to arrive at a better understanding of heat and mass transfer in two-phase gas–liquid mixtures, a simple mathematical model is set up and solved in detail. As will be seen, the purpose of this study is not so much to cover as general a physical situation as possible, but to examine carefully an idealized and well defined model in the hope that the solution of a simple problem will yield results applicable to more general systems and shed some light on the behaviour of more complicated two-phase flow phenomena.

In this paper, a theoretical expression will be presented for predicting the rate of transfer of a given chemical substance from a moving gaseous phase to a flowing liquid film, in which it is highly soluble. This occurs for example in a wetted wall absorption tower and in certain other industrial operations. When the film is essentially stationary the rate of mass transfer can in many instances be easily predicted, since the problems are of course analogous to the well worked out cases of mass and heat transfer from a solid surface to a moving fluid. To date however no attempt has been made to determine how the rate of mass transfer in such operations would be affected if the liquid surface were to move with a velocity at least comparable to that of the gas stream.

The purpose of this paper, then, is to study theoretically the effect mentioned above. Such a treatment is at present possible only when the gas is in laminar motion and when the liquid film flows smoothly along a surface. Momentum and mass transfer between co-current laminar streams have been investigated in some detail by Lock [2] and by Potter [3]. The latter article also contains an extensive bibliography on the subject. The problem treated here is however both simpler and in a sense more general. Thus, on one hand the liquid stream remains essentially uninfluenced by the motion of the gas phase and it will be assumed that, for very soluble substances, the resistance to mass transfer is confined entirely to the gas stream. On the other hand, the treatment has been extended to cover the case where the rate of mass transfer is high, so that the normal component of the velocity to the surface of the liquid stream cannot be neglected.

Consider then a vertical flat plate. Gas and liquid flow co-currently, and the liquid is assumed to occupy a thin film over the surface of the plate. A substance, highly soluble in the liquid, is transferred from the gas which is in laminar motion and contains an inert. It is well known of course that unless the film is exceedingly thin it will not be laminar. But since we shall assume that the resistance to mass transfer is in the gas phase alone, the rippling which is commonly observed on the liquid surface can in this case be disregarded.

This phenomenon is described by the standard set of hydrodynamic relations – the Navier-Stokes equations, the continuity equation, and the diffusion equation. However, it is usually permissible to simplify the mathematical treatment and use instead Prandtl's well known boundary layer equations [4] which are, when applied to the gas phase,

$$u\frac{\partial u}{\partial x} + v\frac{\partial u}{\partial y} = \nu\frac{\partial^2 u}{\partial y^2} \tag{1}$$

$$\frac{\partial u}{\partial x} + \frac{\partial v}{\partial y} = 0 \tag{2}$$

$$u\frac{\partial c}{\partial x} + v\frac{\partial c}{\partial y} = D\frac{\partial^2 c}{\partial y^2} \tag{3}$$

The symbols have the following meaning:

x = the distance parallel to the liquid surface.
y = the normal distance from the liquid surface.
u, v = gas phase velocity components in the x and y direction respectively.
c = the concentration of the diffusing species in the gas phase.
D = the diffusion coefficient.
ν = the kinematic viscosity of the gas.

In addition, the solution to equations (1-3) must satisfy the boundary conditions, which for dilute mixtures are

$$\text{at } y = 0 \quad u = u_s, \; v = 0, \; c = c_s$$

$$\text{at } y = \infty \text{ and also at } x = 0, \; u = U_\infty \; c = c_\infty \quad (4)$$

where u_s = the velocity of the liquid surface, which for practical purposes is constant,

U_∞ = the velocity of the gas stream far from the surface,

c_∞ = the concentration of the diffusing substance far from the surface,

c_s = the equilibrium concentration of the diffusing substance when in contact with the liquid (for the purposes of this discussion $c_s \ll c_\infty$).

It is quite evident now that u and v must be obtained first, from the solution to equations (1) and (2), and then substituted into equation (3) before the rate of mass transfer can be predicted. Actually, equations (1) and (2) are identical with the well known boundary layer equations for a flow past a flat plate (4), the only difference being that the velocity component u is not zero at the liquid surface ($y = 0$) but is equal to a constant u_s.

Equations (1) and (2) were originally analysed by Blasius (with $u_s = 0$) who noticed that a similarity transformation could reduce them to an ordinary differential equation which be then solved numerically. Surprisingly enough, the more general problem with $u_s \neq 0$ can also be solved by the Blasius transformation. Thus, if

$$\eta = y\sqrt{\frac{U_\infty}{\nu x}} \text{ and } u = U_\infty f'(\eta) \quad (5)$$

Equations (1) and (2) reduce to the single ordinary differential equation

$$ff'' + 2f''' = 0 \quad (6)$$

with $$f = 0, \; f' = \frac{u_s}{U_\infty} \text{ at } \eta = 0$$

and $$f' = 1 \text{ at } \eta = \infty$$

Furthermore, it is easy to show that if u and v are expressed in terms of the function $f(\eta)$, then equation (3) can be transformed into

$$\frac{d^2\theta}{d\eta^2} + \frac{Sc}{2} f \frac{d\theta}{d\eta} = 0 \quad (7)$$

where $\theta \equiv \dfrac{c - c_s}{c_\infty - c_s}$ and $Sc \equiv \dfrac{\nu}{D}$

so that, at $\eta = 0$ $\theta = 0$ and at $\eta = \infty$ $\theta = 1$. The solution to equation (7) is readily shown to be

$$\theta = \frac{\int_0^\eta [f'']^{Sc} \, d\eta}{\int_0^\infty [f'']^{Sc} \, d\eta} \quad (8)$$

and therefore the rate of mass transfer at the liquid surface is

$$D\left(\frac{\partial c}{\partial y}\right)_{y=0} = D(c_\infty - c_s) \frac{[f''(0)]^{Sc}}{\int_0^\infty [f'']^{Sc} \, d\eta} \sqrt{\frac{U_\infty}{\nu x}} \quad (9)$$

Finally, the Nusselt number Nu becomes

$$Nu \equiv \frac{x}{(c_\infty - c_s)} \left(\frac{\partial c}{\partial y}\right)_{y=0} = \frac{[f''(0)]^{Sc}}{\int_0^\infty [f'']^{Sc} \, d\eta} \sqrt{\frac{U_\infty x}{\nu}} \quad (10)$$

which reduces to a particularly simple form when $Sc = 1$, in which case

$$Nu = \frac{f''(0)}{1 - (u_s/U_\infty)} \sqrt{\frac{U_\infty x}{\nu}} \quad (10a)$$

It is clear then that the Nusselt number for mass transfer can be calculated from equation (10) if the solution to equation (6) can be obtained. This can be accomplished

(1) Exactly by a numerical procedure, or

(2) Approximately, by the von Karman-Pohlhausen momentum integral method.

The integral method will be discussed first, because it leads in this case to a simple and intriguing result. This procedure has been repeatedly applied to boundary layer fluid

mechanical problems and is known to be in general quite accurate. The details can be obtained from any standard reference [4].

It is simpler in this case to start from equations (6) and (7) – although the usual procedure has been to go back to equations (1-3) – and attempt to satisfy them in the mean rather than solve them exactly. Thus, to replace the boundary layer equations one obtains the two momentum integral equations

$$-2f''(0) + \int_0^\infty ff''\,d\eta = 0 \qquad (11)$$

and

$$-2\theta'(0) + Sc\int_0^\infty f\theta'\,d\eta = 0 \qquad (12)$$

These equations do not have of course a unique solution. It is customary to satisfy them by assuming a velocity and a concentration profile, each of which contains an adjustable shape factor. Thus, two reasonable and commonly used profiles are

$$f' = \frac{u_s}{U_\infty} + \left(1 - \frac{u_s}{U_\infty}\right)\left(\frac{3\eta}{2\delta} - \frac{\eta^3}{2\delta^3}\right) \qquad (13)$$

for $\eta \leqslant \delta$, and $f' = 1$ for $\eta \geqslant \delta$

$$\theta = \frac{3\eta}{2\delta_T} - \frac{\eta^3}{2{\delta_T}^3} \text{ for } \eta \leqslant \delta_T \qquad (14)$$

and $\qquad \theta = 1$ for $\eta \geqslant \delta_T$

which satisfy the required boundary conditions and also the two differential equations (6) and (7) at $\eta = 0$. The two shape-parameters, δ and δ_T, can be determined from equations (11) and (12). It is found that

$$\delta = \frac{4{\cdot}641}{\sqrt{1 + 1{\cdot}1692\,u_1}} \text{ and that } \Delta H_1(\Delta) = \frac{1 + 1{\cdot}692\,u_1}{7{\cdot}180\,Sc} \qquad (15)$$

where $u_1 \equiv \dfrac{u_s}{U_\infty}$, $\Delta \equiv \dfrac{\delta_T}{\delta}$, and

$$\left.\begin{aligned} H_1(\Delta) &\equiv \left(\frac{3\Delta}{8} - \frac{3\Delta^2}{20} + \frac{3\Delta^4}{280}\right)u_1 \\ &\quad + \left(\frac{3\Delta^2}{20} - \frac{3\Delta^4}{280}\right) \text{ for } \Delta \leqslant 1 \\ H_1(\Delta) &\equiv \left(\frac{3}{8} - \frac{3}{20\Delta} + \frac{3}{280\Delta^3}\right)u_1 \\ &\quad + \left(\frac{3\Delta}{8} - \frac{3}{8} + \frac{3}{20\Delta} - \frac{3}{280\Delta^3}\right) \text{ for } \Delta \geqslant 1 \end{aligned}\right\} \qquad (16)$$

Therefore, if one defines as the characteristic velocity

$$U_0 \equiv U_\infty + 1{\cdot}692\,u_s \qquad (17)$$

one can readily show that the expression for the Nusselt number becomes

$$Nu = \frac{0{\cdot}323}{\Delta(0, Sc)}\left(\frac{U_0 x}{\nu}\right)^{\frac{1}{2}}\phi(u_1, Sc) \qquad (18)$$

where

$$\phi(u_1, Sc) = \frac{\Delta(0, Sc)}{\Delta(u_1, Sc)} \qquad (19)$$

It is interesting to note that the function $\phi(u_1, Sc)$, which can be evaluated from equation (15) and which is shown plotted in Fig. 1, is relatively insensitive to u_1 for most gases, that is for those with Schmidt numbers close to 1. So that the Nusselt number for such two-phase flows is again proportional to the square root of a Reynolds number, a relation which is well known to hold for single phase laminar flows, the only difference being however that the characteristic velocity of the system is a linear combination of the velocities of the gas and the liquid, as given by equation (17). According to the momentum integral approximation, therefore, the expression for the Nusselt number for mass transfer for dilute mixtures, and for $Sc \sim 1$, to a stationary vertical surface is also applicable for mass transfer to a falling liquid film if the characteristic velocity U_0 is used. The same argument holds of course for the analogous heat transfer problem, where the transfer is from a surface across a moving liquid film into a laminar gas stream and the resistance of the film is negligible.

The momentum integral method is however only approximate and before the results derived from it can be accepted they should be compared, if possible, with those of the exact solution. This

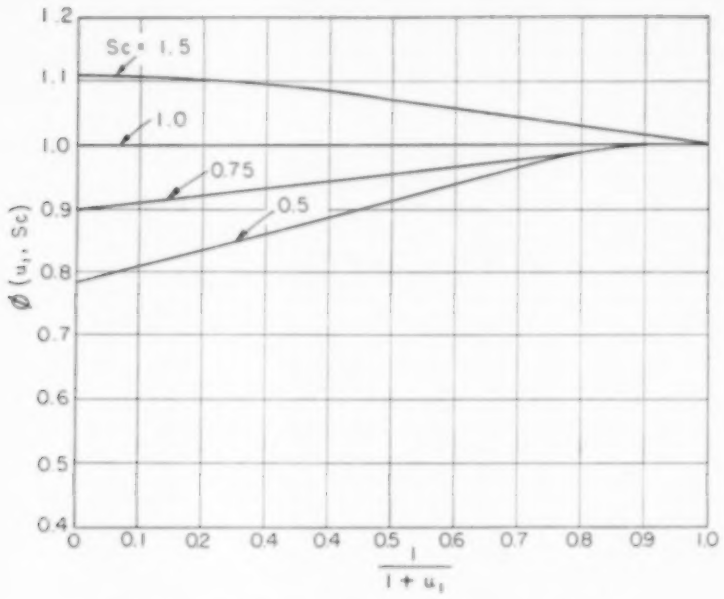

FIG 1 PLOT OF THE FUNCTION $\phi(u_1, Sc)$

can be done most readily for $Sc = 1$, for then equation (10a) can be employed which requires only the value of $f''(0)$ as a function of u_1. $f''(0)$ was obtained from a numerical solution of equation (6), and a comparison between the exact and the approximate results is shown below.

Table 1. *Values of* $Nu\sqrt{\frac{\nu}{U_x x}}$ *for* $Sc = 1$ *as a function of* u_1

u_1	*Exact*	*Approximate*	*Error*
0	0·332	0·323	2·7%
0·515	0·472	0·442	6·3%
0·764	0·531	0·489	7·9%
1	0·564	0·530	6·0%
2·030	0·724	0·682	5·8%

Moreover, as $u_1 \to \infty$ which occurs when the bulk of the gas is essentially stationary, the exact expression is

$$Nu = 0{\cdot}443\sqrt{\frac{u_s x}{\nu}}$$

whereas the approximate method predicts

$$Nu = 0{\cdot}420\sqrt{\frac{u_s x}{\nu}}$$

It is seen therefore that the von Karman-Pohlhausen method, when applied to the present problem, gives results of acceptable accuracy, especially when it is recognized that the approximate results depend somewhat, although to a slight extent it is true, on the profiles which were chosen to represent the velocity and the temperature distributions.

High Rates of Mass Transfer

Where the rate of mass transfer is high, then as was shown by Spalding [5, 6], Eckert and Schneider [1] and others, the interaction between the equations of motion and the diffusion equation cannot be neglected. Thus, even though equations (1-3) still hold, the boundary conditions given by equations (4) must be replaced by:

at $y = 0$

$$u = u_s,\ c = c_s \text{ and } (\rho - c_s)\, v = -D\frac{\partial c}{\partial y} \qquad (20)$$

at $y = \infty$ and also $x = 0$, $u = U_\infty$, $c = c_\infty$

It is interesting to note that again the Blasius transformation will reduce the problem to the solution of two ordinary differential equations

which are now coupled on account of one of the above boundary conditions. Thus, if

$$\eta \equiv y\sqrt{\frac{U_\infty}{\nu x}},\ u \equiv U_\infty f'(\eta) \text{ and } \frac{c-c_s}{c_\infty - c_s} \equiv \theta(\eta)$$

it is found that equations (6) and (7) remain unchanged, but that the boundary conditions become

$$\left.\begin{aligned} &\text{at } \eta = 0\ f' = u_1,\ f = \frac{2n_1}{Sc}\theta'(0),\ \theta = 0 \\ &\text{at } \eta = \infty\ f' = 1,\ \theta = 1 \\ &n_1 \equiv \frac{c_\infty - c_s}{\rho - c_s} \end{aligned}\right\} \quad (21)$$

This system of equations will now be solved by the momentum integral method. The assumed profiles are

$$\left.\begin{aligned} &f' = u_1 + (1-u_1)\left\{\frac{3\eta}{2\delta} - \frac{\eta^3}{2\delta^3} + b_1\frac{\eta}{\delta}\left(1-\frac{\eta}{\delta}\right)^2\right\} \text{ for } \eta \leqslant \delta \\ &\text{and } f' = 1 \text{ for } \eta \geqslant \delta \\ &\theta = \left(\frac{3\eta}{2\delta_T} - \frac{\eta}{2\delta_T{}^3}\right) + b_2\frac{\eta}{\delta_T}\left(1-\frac{\eta}{\delta_T}\right)^2 \\ &\qquad\qquad \text{for } \eta \leqslant \delta_T \\ &\theta' = 1 \text{ for } \eta \geqslant \delta_T \end{aligned}\right\} \quad (22)$$

The two constants b_1 and b_2 are chosen so that the assumed profiles will satisfy equations (6) and (7) at the liquid surface, i.e. $\eta = 0$. Thus

$$\left.\begin{aligned} b_2 &= -\frac{3}{2} + \frac{2}{n_1} - \frac{2}{n_1}\sqrt{\left(1-\frac{3n_1}{2}\right)} \text{ for } n_1 \leqslant 2/3 \\ b_1 &= -\frac{1{\cdot}5\,(1{\cdot}5 + b_2)}{(b_2 + 3/2 - 4\Delta\, Sc/n_1)}, \\ &\text{where } \Delta \equiv \frac{\delta_T}{\delta} \end{aligned}\right\} \quad (23)$$

(a) for $\Delta \leqslant 1$

$$\begin{aligned} H_1 = u_1\,\Delta\left(\frac{3}{8} - \frac{b_2}{12}\right) + (1-u_1) \\ \left\{\left(\frac{3\Delta^2}{20} - \frac{3\Delta^4}{280}\right) - b_2\left(\frac{\Delta^2}{20} - \frac{\Delta^4}{210}\right)\right. \\ + b_1\left(\frac{\Delta^2}{10} - \frac{\Delta^3}{12} + \frac{3\Delta^4}{140}\right) \\ \left. - b_1 b_2\left(\frac{\Delta^2}{30} - \frac{\Delta^3}{30} + \frac{\Delta^4}{105}\right)\right\} \end{aligned} \quad (26a)$$

(b) for $\Delta \geqslant 1$

$$\begin{aligned} H_1 = \left(\frac{3\Delta}{8} - \frac{b_2}{12}\right) \\ - (1-u_1)\left\{\left(\frac{3}{8} - \frac{3}{20\Delta} + \frac{3}{280\Delta^3}\right)\right. \\ - b_2\left(\frac{1}{10\Delta} - \frac{1}{12\Delta^2} + \frac{3}{140\Delta^3}\right) \\ - b_1\left(\frac{1}{12} - \frac{1}{20\Delta} + \frac{1}{210\Delta^3}\right) \\ \left. + b_1 b_2\left(\frac{1}{30\Delta} - \frac{1}{30\Delta^2} + \frac{1}{105\Delta^3}\right)\right\} \end{aligned} \quad (26b)$$

Therefore, before the Nusselt number can be calculated, Δ, b_1 and b_2 must be found from equations (23) and (26) as functions of the three parameters of this problem u_1, n_1 and Sc. Unfortunately, the profiles given by equation (22) cannot be used for $n_1 > 2/3$, because b_1 and b_2 become imaginary, and the profiles chosen by SPALDING [6] must be employed. This extension will however be omitted here, as it adds very little to the present development.

The problem has again a simple solution when $Sc = 1$, for then it can be shown that $\Delta = 1$ also, and that $b_1 = b_2$. Thus, when $Sc = 1$,

and therefore, from the momentum integral equations (11) and (12)

$$Nu = \left(\frac{U_\infty x}{\nu}\right)^{\frac{1}{2}} \frac{3/2 + b_2}{\Delta}\sqrt{\frac{u_1(3/8 - b_1/12) + (1-u_1)(39/280 - b_1/140 - b_1{}^2/105)}{3\,(1 - n_1/Sc\Delta + 2b_1 - 2b_2 n_1/Sc\Delta)}} \quad (24)$$

Δ is obtained from

$$Sc\,\Delta\,H_1 = \frac{(3+2b_2)(1-n_1)}{3\,(1-n_1/Sc\Delta) + 2b_1 - 2b_2 n_1/Sc\Delta}\left[u_1\left(\frac{3}{8} - \frac{b_1}{12}\right) + (1-u_1)\left(\frac{39}{280} - \frac{b_1}{140} - \frac{b_1{}^2}{105}\right)\right] \quad (25)$$

$$Nu = 0{\cdot}323\left(1 + \frac{2b_2}{3}\right)\sqrt{\frac{U_0 x}{\nu}} \qquad (27)$$

where

$$U_0 = \frac{280\,U_\infty}{39}\,\frac{u_1\left(\frac{3}{8} - \frac{b_2}{12}\right) + (1-u_1)\left(\frac{39}{280} - \frac{b_2}{140} - \frac{b_2^2}{105}\right)}{\left(1 + \frac{2b_2}{3}\right)(1-u_1)} \qquad (28)$$

According to equation (26) then, for high rates of mass transfer as well, and for $Sc \sim 1$, the Nusselt number is again proportional to the square root of a Reynolds number, and the expression for the Nu number for mass transfer to a stationary vertical surface is also applicable for mass transfer to a falling liquid film, if the characteristic velocity, U_0, given by equation (28), is used.

Finally, a few calculations were performed to check the accuracy of the momentum integral method of solution as applied to this problem. It is known that this approximate approach gives reliable results when $u_1 = 0$. On the other hand, when $u_1 = 1$, a simple exact solution can be obtained. Thus, for $Sc = 1$,

(a) From the exact solution:

$$Nu = 0{\cdot}564\sqrt{\frac{U_\infty x}{\nu}}\left[1 + 0{\cdot}6366\,n_1 + 0{\cdot}4923\,n_1^2 + \ldots\right]$$

(b) From the momentum integral method

$$Nu = 0{\cdot}530\sqrt{\frac{U_\infty x}{\nu}}\left[1 + 0{\cdot}625\,n_1 + 0{\cdot}500\,n_1^2 + \ldots\right]$$

The agreement is seen therefore to be very satisfactory.

Conclusions

An expression has been derived for the rate of mass transfer of a substance from the gas phase to a moving liquid film, in which it is highly soluble. It was assumed that the gas phase is in laminar motion. The problem was solved for both the special case of dilute gaseous mixtures and the more general case of high rates of mass transfer. It was shown that when the Schmidt number is around unity, the Nusselt number is again proportional to the square root of a Reynolds number, and that the expression for the Nusselt number for mass transfer to a stationary vertical surface is also applicable for mass transfer to a falling liquid film, if the characteristic velocity U_0 given by equation (28) is used. The same argument holds of course for the analogous heat transfer problem.

The mathematical equations were solved by the approximate von Karman-Pohlhausen momentum integral method. It was shown however, by comparing, wherever possible, with the results of exact calculations that this approximate method is of very satisfactory accuracy for the problem considered.

Acknowledgment—This research was supported in part by a grant from the National Science Foundation and a grant from the Petroleum Research Fund administered by the American Chemical Society. Grateful acknowledgment is hereby made to the donors of said fund.

Notation

U_∞ = velocity of the gas parallel to the plate and outside the boundary layer.

u, v = respectively, the vertical and horizontal velocity components divided by U_∞.

u_1 = velocity of the liquid surface u_s divided by U_∞.

x, y = position co-ordinates along the vertical surface and normal to it, respectively.

c = concentration of the solute in the gas phase, in moles per unit volume.

c_∞, c_s = respectively, the concentration of the solute outside the boundary layer, and at the liquid surface ($c_s \to 0$).

$\rho = \dfrac{c - c_s}{c_\infty - c_s}$, dimensionless concentration.

$Sc = \nu/D$, the Schmidt number, where D is the diffusion coefficient.

δ and δ_T = shape factors for the velocity and the temperature profiles respectively.

$\Delta = \dfrac{\delta_T}{\delta}$.

H_1 = defined by equations (16) and (26).

U_0 = defined by equations (17) and (27).

$\phi(u_1, Sc)$ = defined by equation (19).

$n_1 = \dfrac{c_\infty - c_s}{\rho - c_s}$.

References

[1] Eckert E. R. G. and Schneider P. J. *J. Aero. Sciences* 1956 **23** 384.

[2] Lock R. C. *Quart. J. Mech. Appl. Math.* 1951 **4** 42.

[3] Potter O. E. *Chem. Engng. Sci.* 1957 **6** 170.

[4] Schlichting H. *Boundary Layer Theory* 1955 McGraw-Hill.

[5] Spalding D. B. *Proc. Roy. Soc.* A 1953 **221** 78.

[6] Spalding D. B. *Proc. Roy. Soc.* A 1953 **221** 100.

Chemical Engineering Science, 1958, Vol. 9, pp. 250 to 262. Pergamon Press Ltd. London. Printed in Great Britain

Statistical analysis of a reactor

Linear theory

R. Aris and N. R. Amundson
University of Minnesota, Minneapolis 14, Minnesota

(*Received* 1 *March*, 1958)

Abstract—In this paper some of the statistical techniques which have become part of modern control analysis are applied to the continuous flow stirred tank reactor. Care is taken to present these methods without assuming the reader's prior knowledge, for, though they are widely used in other fields, they may as yet be unfamiliar to the chemical engineer. It is assumed that the system never departs very far from its steady state so that linearized equations are valid. One may then make a statistical design of the reactor and determine the effect of various parameters on the characteristics of the output.

Résumé—Dans cet article les auteurs appliquent au réacteur à cuve, agité à marche continue, les méthodes utilisées dans les analyses de contrôle modernes. Ces méthodes, largement utilisées dans certains domaines mais encore peu familières à l'ingénieur chimiste, sont présentées de telle sorte qu'elles ne nécessitent pas de connaissances particulières du lecteur. Les auteurs supposent que le système ne s'écarte jamais sensiblement de son état de régime, de sorte que des équations linéaires sont utilisables. Une étude statistique du réacteur est alors rendue possible, ainsi que la détermination de l'influence de divers paramètres sur les caractéristiques du produit obtenu.

Zusammenfassung—In dieser Arbeit werden einige statistische Methoden, die zur modernen Behandlung von Regelungsvorgängen gehören, auf den kontinuierlich durchströmten Reaktor von der Art des Rührkessels angewandt. Vorkenntnisse werden beim Leser nicht vorausgesetzt, da diese Methoden dem Verfahrensingenieur bisher wenig vertraut sind, obwohl sie auf anderen Gebieten als weit verbreitet gelten müssen. Es wird angenommen, dass das System nur wenig von seinem Beharrungszustand abweicht, so dass linearisierte Gleichungen gelten. Dann möge eine statistische Berechnung des Reaktors durchgeführt und die Wirkung verschiedener Parameter auf die charakteristischen Grössen am Austritt bestimmt werden.

Introduction

Of the many interesting problems connected with stirred tank reactors there is one which has recently become tractable through the development of appropriate mathematical tools. This is the problem of describing the behaviour of the reactor under the small random fluctuations which occur even under the strictest of controls. The values of input flow rate, temperature and reactant concentration are seldom steady but undergo fluctuations of a random nature because changes in ambient conditions, valve chatter and a multitude of other variations too complex to disentangle. The effect that this will have on the output may be studied by considering the input variables subject to small random fluctuations and using the techniques which have been developed by electrical engineers and mathematicians for the study of linear systems and random functions.

Since the inputs are known only statistically it is not possible to obtain more than a statistical description of the outputs. But this is of considerable value, for given thes tatistical properties of the input, including its standard deviation, one may calculate the standard deviation and other properties of the output. Such a calculation would show what limits could be tolerated in the input to achieve a product of given uniformity and show how the control parameters should be adjusted to accomplish this.

As the mathematical techniques are comparatively new and may be unfamiliar to the chemical engineer, a brief outline of the method of describ-

ing and using random functions is first given. It is shown how the random properties of the input may be obtained from strip chart data and how the properties of the output may be calculated. The method is illustrated by a numerical example.

1. The Statistical Description of Random Functions

The behaviour of a continuous flow stirred tank reactor when certain of its input variables are subject to random fluctuations is to be studied. It is therefore necessary to specify the class of random functions that will be considered and the way in which they may be described. It may be stated at the outset that the class of fluctuations is that given by a stationary, ergodic Gaussian random process with zero mean. The meaning of this will become clear from the following summary of the chief properties of a random process.

The conventional function $x = x(t)$ defined in the interval (a, b), means that for any value t_1 in the range $a < t_1 < b$ it is possible to calculate the corresponding value of x, namely $x(t_1)$. If $x(t)$ is a random function (or, more properly, a member of a random process) it is no longer possible to calculate the exact value $x(t_1)$ but only to make certain probability statements about it. Thus the probability that $x(t_1)$ is less than some prescribed constant, say x_1, may be specified by a function F_1

$$F_1(x_1, t_1) = Pr\{x(t_1) \leqslant x_1\} \tag{1.1}$$

If F_1 is differentiated partially with respect to x_1

$$f_1(x_1, t_1)\, dx_1 = Pr\{x_1 < x(t_1) \leqslant x_1 + dx_1\} \tag{1.2}$$

for very small dx_1. f_1 is a probability density. It is as if a barrier is set up at $t = t_1$ with a slit from x_1 to $x_1 + dx_1$ in it; $f_1(x_1, t_1)\, dx_1$ is then the probability that the curve $x(t)$ should pass through this slit. For a slit of finite width, extending from x_1 to x_1' say, the probability of the curve $x(t)$ passing through it is

$$Pr\{x_1 \leqslant x(t_1) \leqslant x_1'\} = \int_{x_1}^{x_1'} f_1(\xi, t_1)\, d\xi = F_1(x_1', t_1) - F_1(x_1, t_1) \tag{1.3}$$

Higher distribution functions can be set up giving the joint probability of two values $x(t_1)$ and $x(t_2)$. Thus

$$F_2(x_1, t_1; x_2, t_2) = Pr\{x(t_1) \leqslant x_1 \text{ and } x(t_2) \leqslant x_2\} \tag{1.4}$$

and if

$$f_2(x_1 t_1; x_2, t_2) = \frac{\partial^2}{\partial x_1\, \partial x_2} F_2(x_1, t_1; x_2, t_2), \tag{1.5}$$

then

$$f_2(x_1, t_1; x_2, t_2)\, dx_1\, dx_2 = Pr\{x_1 < x(t_1) \leqslant x_1 + dx_1 \text{ and } x_2 < x(t_2) \leqslant x_2 + dx_2\} \tag{1.6}$$

for very small dx_1 and dx_2. This corresponds to the setting up of two successive barriers, one at t_1 and the other at t_2 and saying that the probability of any function passing through two slits between x_1 and $x_1 + dx$, and x_2 and $x_2 + dx_2$ respectively is $f_2\, dx_1\, dx_2$. The n^{th} distribution function is defined by

$$F_n(x_1, t_1; x_2, t_2; \ldots; x_n, t_n) = Pr\{x(t_1) \leqslant x_1, x(t_2) \leqslant x_2, \ldots x(t_n) \leqslant x_n\} \tag{1.7}$$

$$f_n(x_1, t_1; x_2, t_2; \ldots; x_n, t_n) = \frac{\partial^n}{\partial x_1\, \partial x_2 \ldots \partial x_n} F_n(x_1, t_1; \ldots; x_n, t_n) \tag{1.8}$$

A formal definition of a random process may now be given. It is a set of functions $\{x(t)\}$ and a set of probability distributions $F_n(x_1, t_1; \ldots x_n, t_n)$, $n = 1, 2, 3, \ldots$ such that the relation (1.7) is true. The functions F_n are not independent, for, to be consistent, the following relations must clearly be satisfied

$$\begin{aligned} F_n(\infty, t_1;\ \infty, t_2; \ldots;\ \infty, t_n) &= 1 \\ F_n(x_1, t_1;\ \infty, t_2; \ldots;\ \infty, t_n) &= F_1(x_1, t_1) \\ F_n(x_1, t_1; x_2, t_2;\ \infty, t_3; \ldots;\ \infty, t_n) &= F_2(x_1, t_1; x_2, t_2) \\ F_n(x_1, t_1; \ldots;\ x_{n-1}, t_{n-1},\ \infty, t_n) &= F_{n-1}(x_1, t_1; \ldots; x_{n-1}, t_{n-1}). \end{aligned} \tag{1.9}$$

An important class of random processes is such that a shift of the time origin does not change its description. Such a process is called stationary, and stationary processes may reasonably be expected when the overall conditions are essentially unchanged. For a stationary process only

the differences of the t values are significant; thus

$$F_n(x_1, t_1; x_2, t_2; \ldots; x_n, t_n) = F_n(x_1, 0; x_2, t_2 - t_1; \ldots; x_n, t_n - t_1) \quad (1.10)$$

and in particular

$$F_1(x_1, t_1) = F_1(x_1, 0) \quad (1.11)$$

is independent of t_1.

Any function of x, $\phi(x)$, will have a mean or expected value

$$\overline{\phi(x)} = \int_{-\infty}^{\infty} \phi(x) f_1(x, t)\, dx \quad (1.12)$$

which is generally a function of t. If the process is stationary f_1 is independent of t and so is the mean of any function $\phi(x)$. In particular the mean of x itself

$$\bar{x} = \int_{-\infty}^{\infty} x f_1(x, t)\, dx \quad (1.13)$$

is independent of t for a stationary process. This constant may be subtracted from $x(t)$ to give the class of perturbations with zero mean.

The Gaussian term in the specification of the class of perturbations given above is less easy to justify. A stationary Gaussian process with zero mean is such that all its probability distributions f_n are normal distributions. Thus

$$f_1(x_1, t_1) = f_1(x_1) = \frac{1}{\sigma\sqrt{2\pi}} \exp\left(-\frac{x_1^2}{2\sigma^2}\right) \quad (1.14)$$

$$f_2(x_1, t_1; x_2, t_2) = f_2(x_1, 0; x_2, t_2 - t_1) \frac{1}{2\pi\sigma^2\sqrt{1-\rho^2}} \exp\left[-\frac{x_1^2 - 2\rho x_1 x_2 + x_2^2}{2\sigma^2(1-\rho^2)}\right] \quad (1.15)$$

etc., where σ is constant and ρ a function of $t_2 - t_1$ only, σ is the standard deviation of $x(t)$ i.e. the variance

$$\sigma^2 = \int_{-\infty}^{\infty} x^2 f_1(x)\, dx \quad (1.16)$$

The Gaussian random process has the very important property that it remains Gaussian after passing through a linear filter. A linear filter is the name given to a linear differential equation or equations for a function $y(t)$ when $x(t)$ occurs on the right hand side, that is, as the input. For example

$$y'(t) + \lambda y(t) = x(t)$$

is a linear filter and if the input $x(t)$ is Gaussian so is the output $y(t)$. The analysis will be limited to the Gaussian process.

The final term ergodic is of great importance. Speaking loosely it means that any particular random function from the set $\{x(t)\}$ will eventually behave like any other function from this this set. The ensemble average at a point $\int_{-\infty}^{\infty} \phi(x) f_1(x, t)\, dx$ may then be replaced by an average over a long section of any one function

$$\lim_{T\to\infty} \frac{1}{2T} \int_{-T}^{T} \phi(x(t+\tau))\, d\tau = \lim_{T\to\infty} \frac{1}{2T} \int_{-T}^{T} \phi(x(t))\, dt,$$

for in the limit when the limits of integration become infinite $t + \tau$ can be replaced by t. In particular for the functions we consider

$$\bar{x} = \lim_{T\to\infty} \frac{1}{2T} \int_{-T}^{T} x(t)\, dt = 0 \quad (1.17)$$

$$\sigma^2 = \lim_{T\to\infty} \frac{1}{2T} \int_{-T}^{T} \{x(t)\}^2\, dt \quad (1.18)$$

It is the equivalence of ensemble and time averages which permits the easy analysis of the effect of a linear filter, as in Section 3.

A most important function for the description of a random process is the auto-correlation function. For an ergodic process it is defined as

$$\phi_{xx}(\tau) = \lim_{T\to\infty} \frac{1}{2T} \int_{-T}^{T} x(t)\, x(t+\tau)\, dt \quad (1.19)$$

It is an even function of τ and if sharply peaked at the origin it implies that the value of $x(t)$ is not very strongly correlated with the value

for slightly different time $t \pm \tau$; if it is a spread-out function it means that two values are relatively strongly correlated even though at two more distant times. It may be thought of as describing in a general way the quality of the random fluctuations. From (1.18) and (1.19) it is clear that

$$\sigma^2 = \phi_{xx}(0) \tag{1.20}$$

and this variance is the most convenient measure of the variability of x.

If there are two ergodic random processes $x(t)$ and $y(t)$ the cross-correlation function

$$\phi_{xy}(\tau) = \lim_{T\to\infty} \frac{1}{2T} \int_{-T}^{T} x(t)\, y(t+\tau)\, dt \tag{1.21}$$

may be defined. For this clearly

$$\phi_{yx}(\tau) = \phi_{xy}(-\tau) \tag{1.22}$$

Finally a function of great importance is the spectral density, the Fourier transform of the correlation function.

$$G_{xx}(\omega) = \frac{1}{\pi} \int_{-\infty}^{\infty} \phi_{xx}(\tau)\, e^{-i\omega\tau}\, d\tau \tag{1.23}$$

and inversely

$$\phi_{xx}(\tau) = \tfrac{1}{2} \int_{-\infty}^{\infty} G_{xx}(\omega)\, e^{i\omega\tau}\, d\omega. \tag{1.24}$$

but since $\phi_{xx}(\tau)$ is an even function $G_{xx}(\omega)$ is real, and in fact

$$G_{xx}(\omega) = \frac{2}{\pi} \int_{0}^{\infty} \phi_{xx}(\tau) \cos\omega\tau\, d\tau \tag{1.25}$$

and

$$\phi_{xx}(\tau) = \int_{0}^{\infty} G_{xx}(\omega) \cos\omega\tau\, d\tau. \tag{1.26}$$

Similarly

$$G_{xy}(\omega) = \frac{1}{\pi} \int_{-\infty}^{\infty} \phi_{xy}(\tau)\, e^{-i\omega\tau}\, d\tau \tag{1.27}$$

$$\phi_{xy}(\tau) = \tfrac{1}{2} \int_{-\infty}^{\infty} G_{xy}(\tau)\, e^{i\omega\tau}\, d\tau \tag{1.28}$$

but $G_{xy}(\omega)$ is generally a complex valued function and

$$G_{xy}(\omega) = G^{*}_{yx}(\omega) = G_{xy}(-\omega) \tag{1.29}$$

where the asterisk denotes the complex conjugate.

These bare facts on random functions will suffice for the discussion which follows; for a full treatment the reader is referred to Laning and Battin [3].

2. The Equations of a Reactor with Random Inputs

The state of the reactor in which a single reaction is taking place may be described by two quantities, x, the concentration of one reactant and T, the temperature of the contents. Referring to the list of symbols for their meaning, the following equations, one a mass and the other a heat balance, are readily derived.

$$V\frac{dx}{dt} = q(x_0 - x) - VR(x, T) \tag{2.1}$$

$$Vh\frac{dT}{dt} = qh(T_0 - T) + (-\Delta H)\, VR(x, T) - VU^{*}(T, T_c, q_c) \tag{2.2}$$

where

V = volume of the reactor,
t = time,
q = flow rate of reactants,
q_c = flow rate of coolant,
x_0 = inlet concentration,
R = reaction rate, a function of x and T,
h = product of specific heat and density of reactant mixture,
T_0 = inlet temperature,
T_c = coolant temperature,
$-\Delta H$ = heat of reaction,
U^{*} = rate of heat removal by cooling system

The dependent variables x and T will be referred to as the output variables, the independent variable t is the time and the quantities q, x_0, T_0, T_c, q_c, which are all functions of t are called the input variables. It is these which will be regarded as subject to random fluctuations about their steady state values and their influence, severally

or together, upon the induced random fluctuations of x and T is to be studied.

Equations (2.1) and (2.2) are rendered dimensionless by the new set of variables

$$\left.\begin{aligned} \tau &= \frac{\bar{q}t}{V}, & \xi &= \frac{x}{\bar{x}_0}, \\ \eta &= \frac{Th}{(-\Delta H)\,\bar{x}_0}, & \kappa &= \frac{q}{\bar{q}} \\ P &= \frac{VR}{\bar{q}\,\bar{x}_0}, & \xi_0 &= \frac{x_0}{\bar{x}_0}, \\ \eta_0 &= \frac{T_0 h}{(-\Delta H)\,\bar{x}_0}, & \kappa_c &= \frac{q_c}{\bar{q}} \\ U &= \frac{VU^*}{(-\Delta H)\,\bar{q}\,\bar{x}_0}, \\ \eta_c &= \frac{T_c h}{(-\Delta H)\,\bar{x}_0} \end{aligned}\right\} \quad (2.3)$$

The ξ_0 and κ are quantities with mean value 1 and the mean values of η_0, η_c and κ_c are η_0, $\bar{\eta}_c$, $\bar{\kappa}_c$. The equations become

$$\frac{d\xi}{d\tau} = \kappa\,(\xi_0 - \xi) - P\,(\xi, \eta) \quad (2.4)$$

$$\frac{d\eta}{d\tau} = \kappa\,(\eta_0 - \eta) + P\,(\xi, \eta) - U\,(\eta, \eta_c, \kappa_c) \quad (2.5)$$

When the input variables are held constant at their mean values ξ and η will approach steady state values ξ_s and η_s, which satisfy

$$0 = 1 - \xi_s - P\,(\xi_s, \eta_s) \quad (2.6)$$

$$0 = \eta_0 - \eta_s + P\,(\xi_s, \eta_s) - U\,(\eta_s, \bar{\eta}_c, \bar{\kappa}_c) \quad (2.7)$$

Subtracting (2.6) from (2.4) and (2.7) from (2.5) and putting $\xi = \xi_s + z$, $\eta = \eta_s + y$ gives the full non-linear equations for the perturbations z and y, namely

$$\frac{dz}{d\tau} = -\kappa z - [P(\xi_s + z, \eta_s + y) - P(\xi_s, \eta_s)] + (\kappa\,\xi_0 - 1) + (1 - \kappa)\,\xi_s \quad (2.8)$$

$$\frac{dy}{d\tau} = -\kappa y + [P(\xi_s + z, \eta_s + y) - P(\xi_s, \eta_s)] + (\kappa\,\eta_0 - \eta_0) + (1 - \kappa)\,\eta_s - [U(\eta_s + y, \eta_c, \kappa_c) - U(\eta_s, \eta_s, \bar{\kappa}_c)] \quad (2.9)$$

It is now assumed that the departures from the steady state are small and a complete linearization is made. Introduce the following constants,

$$\alpha = (P_t)_s, \quad \beta = (U_\eta)_s, \quad \gamma = (P_\eta)_s, \quad \delta = -(U_{\eta_c})_s, \quad \epsilon = (U_{\kappa_c})_s \quad (2.10)$$

where the suffix within the bracket denotes partial differentiation and the s without that the derivative is evaluated at the steady state. Also let new random variables with zero mean value be defined by

$$\kappa = 1 + \lambda, \quad \xi_0 = 1 + \mu, \quad \eta_0 = \bar{\eta}_0 + \nu$$
$$\kappa_c = \bar{\kappa}_c + \lambda_c, \qquad \eta_c = \bar{\eta}_c + \nu_c \quad (2.11)$$

Then, neglecting all squares and products of y, z, λ, μ and ν,

$$\frac{dz}{d\tau} + (1 + \alpha)\,z + \gamma\,y = (1 - \xi_s)\,\lambda + \mu \quad (2.12)$$

$$\frac{dy}{d\tau} - \alpha z + (1 + \beta - \gamma)\,y = (\eta_0 - \eta_s)\,\lambda + \nu + \delta\nu_c - \epsilon\lambda_c \quad (2.13)$$

and the right sides of these equations are random functions of zero mean value ; they will be denoted by $e\,(t)$ and $f\,(t)$ respectively.

The problem under consideration is thus resolved into two parts. The first is to study the effect of the random inputs e and f on the solution of the equations ; the second to study the composition of e and f themselves from their component functions λ, μ etc.

3. The Solution of the Linearized Equations

The equations to be considered are

$$\frac{dz}{d\tau} + (1 + \alpha)\,z + \gamma\,y = e\,(\tau) \quad (3.1)$$

$$\frac{dy}{d\tau} + (1 + \beta - \gamma)\,y - \alpha\,z = f\,(\tau) \quad (3.2)$$

Taking the Fourier Transform of these equations and denoting the Fourier transform of a function by its capital letter the following solutions are obtained

$$Z = \frac{i\,\omega + 1 + \beta - \gamma}{\Delta(\omega)}\,E + \frac{-\gamma}{\Delta(\omega)}\,F \quad (3.3)$$

$$\text{and } Y = \frac{\alpha}{\Delta(\omega)} E + \frac{i\omega + 1 + \alpha}{\Delta(\omega)} F \qquad (3.4)$$

$$\text{where } \Delta(\omega) = -\omega^2 + i\omega(1 + \alpha + 1 + \beta - \gamma) + (1 + \alpha)(1 + \beta) - \gamma$$

$$\text{or} \quad = -\omega^2 + i\omega d_e + d_f \qquad (3.5)$$

The inverse transforms of z will take the form

$$z(\tau) = \frac{1}{\pi} \int_{-\infty}^{\infty} W_{11}(t)\, e(\tau - t)\, dt + \frac{1}{\pi} \int_{-\infty}^{\infty} W_{12}(t)\, f(\tau - t)\, dt \qquad (3.6)$$

The auto-correlation function

$$\phi_{zz}(\tau) = \lim_{T \to \infty} \frac{1}{2T} \int_{T}^{T} z(t)\, z(t + \tau)\, dt \qquad (3.7)$$

may therefore be calculated. It will involve the auto- and cross-correlation functions of e and f, i.e. ϕ_{ee}, ϕ_{ef}, ϕ_{fe} and ϕ_{ff}. Similar formula hold for $\phi_{zy}(\tau)$ and $\phi_{yy}(\tau)$. This will not be carried out in detail here as we rely for later calculations on the Fourier transforms of these relations. The derivation is given in detail in [3].

Equations (3.3) and (3.4) can be written in matrix form

$$\begin{bmatrix} Z \\ Y \end{bmatrix} = \begin{bmatrix} H_{11}(\omega) & H_{12}(\omega) \\ H_{21}(\omega) & H_{22}(\omega) \end{bmatrix} \begin{bmatrix} E \\ F \end{bmatrix} \qquad (3.8)$$

where $H_{ij}(\omega)$ is of course the transform of $W_{ij}(t)$. Using (3.6) in (3.7) and taking the Fourier transform of the resulting formula the following relation is obtained.

$$G_{zz}(\omega) = |H_{11}|^2 G_{ee} + 2\, Re\,(H_{11}^* H_{12} G_{ef}) + |H_{12}|^2 G_{ff} \qquad (3.9)$$

where G is the spectral density function, an asterisk denotes the complex conjugate and Re the real part.
Similarly

$$G_{yy}(\omega) = |H_{21}|^2 G_{ee} + 2\, Re\,(H_{21}^* H_{22} G_{ef}) + |H_{22}|^2 G_{ff} \qquad (3.10)$$

and

$$G_{zy}(\omega) = H_{11}^* H_{21} G_{ee} + H_{11}^* H_{22} G_{ef} + H_{12}^* H_{21} G_{fe} + H_{12}^* H_{22} G_{ff} \qquad (3.11)$$

From these formulae the correlation functions can be determined by the inversion formulae (1.24), (1.28) and in particular

$$\sigma_z^2 = \phi_{zz}(0) = \tfrac{1}{2} \int_{-\infty}^{\infty} G_{zz}(\omega)\, d\omega \qquad (3.12)$$

The cross correlations between the input and the output can be found by the same technique. The relations for the spectral densities are

$$\left.\begin{aligned} G_{ez}(\omega) &= H_{11}^* G_{ee} + H_{12}^* G_{ef} \\ G_{fz}(\omega) &= H_{11}^* G_{fe} + H_{12}^* G_{ff} \\ G_{ey}(\omega) &= H_{21}^* G_{ee} + H_{22}^* G_{ef} \\ G_{fy}(\omega) &= H_{21}^* G_{fe} + H_{22}^* G_{ff} \end{aligned}\right\} \qquad (3.13)$$

Before making use of these functions it is necessary to discuss the determination of spectral densities of e and f, either empirically or as compounded from the spectral densities of λ, μ etc.

4. The Analysis and Composition of the Random Inputs

On the assumption that the process is stationary and ergodic the correlation functions of actual inputs may be determined from strip chart data. Thus, suppose that in a practical case $x_0(t)$ has been observed over a long period of time, how may this record be used to estimate the auto-correlation function? This problem is treated in Laning and Battin (Section 4.3) where a full derivation is given of the following results. The function

$$V(\tau) = \frac{1}{T} \int_{0}^{T} x_0(t)\, x_0(t + \tau)\, dt \qquad (4.1)$$

where T is quite large is an estimate of the auto-correlation function. It is actually a random variable itself since it depends on the particular function $x_0(t)$ of the set $\{x_0(t)\}$ which is the record being analysed. However its mean or expected value,

$$E\left[V(\tau)\right] = \frac{1}{T}\int_0^T E\left[x_0(t)\,x_0(t+\tau)\right]dt$$

$$= \frac{1}{T}\int_0^T \phi(\tau)\,dt = \phi(\tau) \qquad (4.2)$$

is the true correlation function (the suffix $x_0 x_0$ has been omitted for simplicity).

The variance σ_v^2 of this estimate of ϕ may be estimated for a Gaussian process and it is shown in the above reference that

$$\sigma_v^2 \leqslant \frac{4}{T}\int_0^\infty \{\phi(t)\}^2\,dt \qquad (4.3)$$

this allows an estimate to be made of the length of the strip record which should be used to obtain a given accuracy.

It may also be shown that a given correlation function may be approximated by the sum of a series of functions of particularly simple type. The function $\exp(-c\,|\tau|)$ is an even function, though its derivative is not continuous at the origin. It has, moreover, a particularly simple Fourier transform, namely $2c/\pi\,(c^2+\omega^2)$. If therefore a given correlation function can be represented approximately by

$$\phi(\tau) \doteq \sum_{k=1}^{d} A_k \exp(-kc\,|\tau|) \qquad (4.4)$$

its spectral density is approximately

$$G(\omega) \doteq \frac{2}{\pi}\sum_{k=1}^{n}\frac{A_k\,kc}{k^2c^2+\omega^2} \qquad (4.5)$$

For a complete discussion of the representation of auto- and cross-correlation functions in this way the reader is referred to chapter 4 and appendix D of Laning and Battin's book. It will be assumed here that the correlation functions are approximated by the sum of functions of the type given in Table 2. The spectral densities will then be given in terms of the standard forms of this Table and be either

$$\frac{2}{\pi}\frac{P_1\,c + Q_1\,i\omega}{c^2+\omega^2} \qquad (4.6)$$

or

$$\frac{2}{\pi}\frac{Q_2\,i\omega^3 + (aP_2 - bP_3)\,\omega^2 + (a^2-b^2)\,Q_2 + 2abQ_3)\,i\omega + (a^2+b^2)\,(aP_2+bP_3)}{\omega^4 + 2(a^2-b^2)\,\omega^2 + (a^2+b^2)^2} \qquad (4.7)$$

these being the spectral densities of $P_1\psi_1 + Q_1 x_1$ and $P_2\psi_2 + Q_2 x_2 + P_2\psi_2 + Q_3 x_3$ (see Table 2).

The final enquiry of this Section must be as to how the functions e and f depend on their component parts λ, μ etc. From (2.12) and (2.13)

$$e = (1-\xi_s)\,\lambda + \mu \qquad (4.8)$$

$$f = (\eta_0 - \eta_s)\,\lambda + \nu + \delta\nu_c - \epsilon\lambda_c \qquad (4.9)$$

Suppose first that the perturbations occur severally, e.g. $\lambda = \mu = \nu = \nu_c = 0$ and only λ_c is non-zero. Then clearly $e = 0$ and $f = -\epsilon\lambda_c$ so that

$$\phi_{ee} = 0\,,\ \phi_{ef} = \phi_{fe} = 0\,,\ \phi_{ff} = \epsilon^2\phi_{\lambda_c\lambda_c} \qquad (4.10)$$

Similar formulae will hold if μ, ν, or ν_c are the only active perturbations, but if $\mu = \nu = \nu_c = \lambda_c = 0$, $\lambda \neq 0$ we have

$$\phi_{ee} = (1-\xi_s)^2\phi_{\lambda\lambda},\ \phi_{ef} = \phi_{fe} = (1-\xi_s)(\eta_0-\eta_s)\phi_{\lambda\lambda},\ \phi_{ff} = (\eta_0-\eta_s)^2\phi_{\lambda\lambda} \qquad (4.11)$$

If two or more perturbations are active at the same time their cross-correlations may be involved. The following case will show the method to be used in all cases.

Let $\nu_c = \lambda_c = 0$

$$\phi_{ee}(\tau) = \lim_{T\to\infty}\frac{1}{2T}\int_{-T}^{T}\left\{(1-\xi_s)\,\lambda(t) + \mu(t)\right\}\left\{(1-\xi_s)\,\lambda(t+\tau) + \mu(t+\tau)\right\}dt$$
$$= (1-\xi_s)^2\phi_{\lambda\lambda}(\tau) + (1-\xi_s)\left\{\phi_{\lambda\mu}(\tau) + \phi_{\mu\lambda}(\tau)\right\} + \phi_{\mu\mu}(\tau) \qquad (4.12)$$

$$\phi_{ef}(\tau) = (1-\xi_s)(\eta_0-\eta_s)\phi_{\lambda\lambda}(\tau) + (1-\xi_s)\,\phi_{\lambda\nu}(\tau) + (\eta_0-\eta_s)\,\phi_{\mu\lambda}(\tau) + \phi_{\mu\nu}(\tau) \qquad (4.13)$$

Since the spectral densities, G, are linear transforms of the correlation functions, ϕ, the same relations also hold between the spectral densities $G_{ee}(\omega)$, $G_{ef}(\omega)$, $G_{ff}(\omega)$ and their components $G_{\lambda\lambda}(\omega)$ etc. It follows from the approximation technique outlined above that all the spectral densities may be approximated by expressions of the form (4.6) and (4.7).

5. The Correlation Functions of the Outputs

It is now possible to show how the formulae of Section 3 may be used systematically to determine the correlation functions of the outputs. The quantities involved in the formulae (3.9)–(3.11) are of the form $|H_{11}(\omega)|^2$. Comparing (3.8) with (3.3) it is easy to see that

$$|H_{11}(\omega)|^2 = \left|\frac{1+\beta-\nu+i\omega}{(d_f-\omega^2)+i\omega d_e}\right|^2 = \frac{(1+\beta-\gamma)^2+\omega^2}{\omega^4+\omega^2(d_e^2-2d_f)+d_f^2} \qquad (5.1)$$

In general the coefficients in (3.9)–(3.11) may be written

$$\frac{A\,\omega^2 + Bi\,\omega + C}{\omega^4 + {}^2\,\omega\,(d_e^2 - 2d_f) + d_f^2}$$

Table 1 gives values of A, B and C for the other functions which occur in (3.9)–3.11).

In each case one of these functions is multiplied by a spectral density, G_{ee}, G_{ef} or G_{ff}, and these, following the result of the previous section are presumed to be approximated by the sum of rational functions of ω. These approximations are substituted in formulae (3.9)–(3.11) and the

Table 1

	A	B	C		A	B	C
$\lvert H_{11}(\omega)\rvert^2$	1	0	$(1+\beta-\gamma)^2$	$H^*_{11}H_{21}$	0	$-\alpha$	$\alpha(1+\beta-\gamma)$
$\lvert H_{12}(\omega)\rvert^2$	0	0	γ^2	$H^*_{11}H_{22}$	1	$\beta-\alpha-\gamma$	$(1+\alpha)(1+\beta-\gamma)$
$\lvert H_{21}(\omega)\rvert^2$	0	0	α^2	$H^*_{12}H_{21}$	0	0	$-\alpha\gamma$
$\lvert H_{22}(\omega)\rvert^2$	1	0	$(1+\alpha)^2$	$H^*_{12}H_{22}$	0	$-\gamma$	$-\gamma(1+\alpha)$
$H^*_{11}(\omega)H_{12}(\omega)$	0	γ	$-\gamma(1+\beta-\gamma)$	$H^*_{21}H_{22}$	0	α	$\alpha(1+\alpha)$

Table 2. Standard correlation functions and spectral densities

Correlation function	*Parity*	*Spectral density*	*Assoc. Coeff.*
$\phi_1(\tau) = e^{-c\lvert\tau\rvert}$	even	$\bar{\phi}_1(\omega) = \frac{2}{\pi}\frac{c}{c^2+\omega^2}$	P_1
$x_1(\tau) = \begin{cases} e^{-c\tau}, & \tau = 0 \\ -e^{-c\tau}, & \tau > 0 \end{cases}$	odd	$\bar{x}_1(\omega) = \frac{2}{\pi}\frac{i\omega}{c^2+\omega^2}$	Q_1
$D(\omega^2) = \omega^4 + 2(a^2-b^2)\omega^2 + (a^2+b^2)^2$			
$\phi_2(\tau) = e^{-a\lvert\tau\rvert}\cos b\tau,\ a>0$	even	$\bar{\phi}_2(\omega) = \frac{2}{\pi}\frac{a(a^2+b^2+\omega^2)}{D(\omega^2)}$	P_2
$x_2(\tau) = \begin{cases} e^{a\tau}\cos b\tau, & \tau < 0 \\ & a>0 \\ -e^{-a\tau}\cos b\tau, & \tau > 0 \end{cases}$	odd	$\bar{x}_2(\omega) = \frac{2}{\pi}\frac{i\omega^3+(a^2-b^2)i\omega}{D(\omega^2)}$	Q_2
$\phi_3(\tau) = e^{-a\lvert\tau\rvert}\sin b\lvert\tau\rvert,\ a>0$	even	$\bar{\phi}_3(\omega) = \frac{2}{\pi}\frac{b(a^2+b^2-\omega^2)}{D(\omega^2)}$	P_3
$x_3(\tau) = e^{-a\lvert\tau\rvert}\sin b\tau,\ a>0$	odd	$\bar{x}_3(\omega) = \frac{2}{\pi}\frac{2abi\omega}{D(\omega^2)}$	Q_3

resulting formulae split into partial fractions. Four cases arise in doing this according as the roots of $|\Delta(\omega)|^2 = 0$ are (I) real or (II) complex and the spectral densities G_{ee} etc., (*a*) involve only ψ_1 and x_1 or (*b*) involve the functions $\psi_2, \ldots, x_3$. Tables may be prepared which will simplify this process of splitting into partial fractions and allow a direct calculation of the coefficients $P_1, \ldots, Q_2$. In any event, the spectral densities of the output are reduced by this means to sums of terms like (4.6) and (4.7) and by Table 2 these may be immediately inverted to give the corresponding correlation functions.

The variances are obtained from the auto-correlation functions immediately by setting $\tau = 0$. An auto-correlation function is even and so must always be of the form

$$\Sigma_i \left[P_{1i}\, \psi_{1i}(\tau) + P_{2i}\, \psi_{2i}(\tau) + P_{3i}\, \psi_{2i}(\tau) \right]$$

where the i denotes that the constants in the function take on particular values. The corresponding variance is thus $\Sigma \left[P_{1i} + P_{2i} \right]$, and one obvious check on the correctness of numerical work is that this should be positive.

6. An Example

As an example a second order irreversible reaction, $2A \rightarrow$ products, taking place in a stirred tank of volume $V = 100\ \text{ft}^3$ may be considered. If the other physical quantities are as follows: $q = 0{\cdot}3\ \text{ft}^3/\text{sec}$, $\bar{x}_0 = 1\ \text{lb mole/ft}^3$, $T_0 = 650\ ^\circ\text{K}$, $-\Delta H = 20{,}000\ \text{But/lb mole}$, $h = 60\ \text{Btu/ft}^1\ ^\circ\text{K}$, $R(x, T) = x^2 k_1 \exp(-E/RT)$ where $k_1 = 2{\cdot}7 \times 10^{11}$, $E = 44{,}700\ \text{Btu/lb mole}$, $R = 1{\cdot}987\ \text{Btu/lb mole}\ ^\circ\text{K}$. Under these conditions and with a cooling coil of 500 ft^2 (heat transfer coefficient 100 Btu/hr ft^2 °K) carrying cooling water with $\bar{T}_c = 520\ ^\circ\text{K}$, $q_c = 0{\cdot}138\ \text{ft}^3/\text{sec}$, the reactor will run stably at $\bar{T}_s = 824{\cdot}9\ ^\circ\text{K}$ with a concentration $\bar{x}_s = 0{\cdot}0843\ \text{lb mole/ft}^3$ i.e. producing 989 lb moles/hr of product.

In the dimensionless variables introduced in Section 2 $\eta_0 = 1{\cdot}95$, $\eta_c = 1{\cdot}56$, $\bar{\kappa}_c = 0{\cdot}460$, $\eta_s = 2{\cdot}475$, $\xi_s = 0{\cdot}0843$, and the parameters are $\alpha = 21{\cdot}730$, $\beta = 0{\cdot}428$, $\gamma = 10{\cdot}091$, $\delta = 0{\cdot}428$, $\epsilon = 1{\cdot}052 \times 10^{-4}$. With these values the denominator of all the functions H_{ij} is $(\omega^2 + \omega_1^2)(\omega^2 + \omega_2^2)$ where $\omega_1 = 17{\cdot}309$, $\omega_2 = 2{\cdot}584$.

Two series of results will be presented using this example. In the first the effect of "white noise" in each of the input variables will be considered to show (a) the type of auto-correlation function which results for the output and (b) how the standard deviation of the output is sensitive to the different inputs. In the second the variation of the auto-correlation function of the output with increasing spread of correlation of the perturbed inlet concentration is shown.

The term "white noise" used above refers to an idealized random process in which there is no correlation between the values of $x(t)$ at different instants, i.e. $\phi_{xx}(\tau) = 0$, $\tau < 0$. Since $\int_{-\infty}^{\infty} \phi_{xx}(\tau)\, d\tau$ is finite in all cases, ϕ_{xx} must be infinite for $\tau = 0$ and it is proportional to the so-called Dirac delta function. Naturally this process cannot be realized in practice but it is the limit of the situation in which the perturbations are due to infinitely many infinitesimal, uncorrelated impulses. It has the virtue that its spectral density is a constant and so it is very valuable for comparing the effect of different inputs. Accordingly, the following cases will be considered:

(1) Inlet concentration alone is perturbed, $G_{\mu\mu} = 1/\pi$

(2) Inlet temperature alone is perturbed, $G_{\nu\nu} = 1/\pi$

(3) Flow rate alone is perturbed, $G_{\lambda\lambda} = 1/\pi$

The results for unit perturbation of this kind in coolant temperature and flow rate may be obtained immediately from those for inlet temperature by multiplying the correlation functions by δ^2 and ϵ^2 respectively. In all cases the correlation function can be written

$$\phi(\tau) = \begin{cases} C_1^- e^{\omega_1 \tau} + C_2^- e^{\omega_2 \tau}, & \tau < 0, \\ C, & \tau = 0, \\ C_1^+ e^{-\omega_1 \tau} + C_2^+ e^{-\omega_2 \tau}, & \tau > 0, \end{cases} \qquad (6.1)$$

the values of the constants C, being given in Table 3 together with the standard deviation $\sigma = \sqrt{C}$ for the autocorrelations.

Plots of $\phi(\tau)$ are shown in Figure 1.

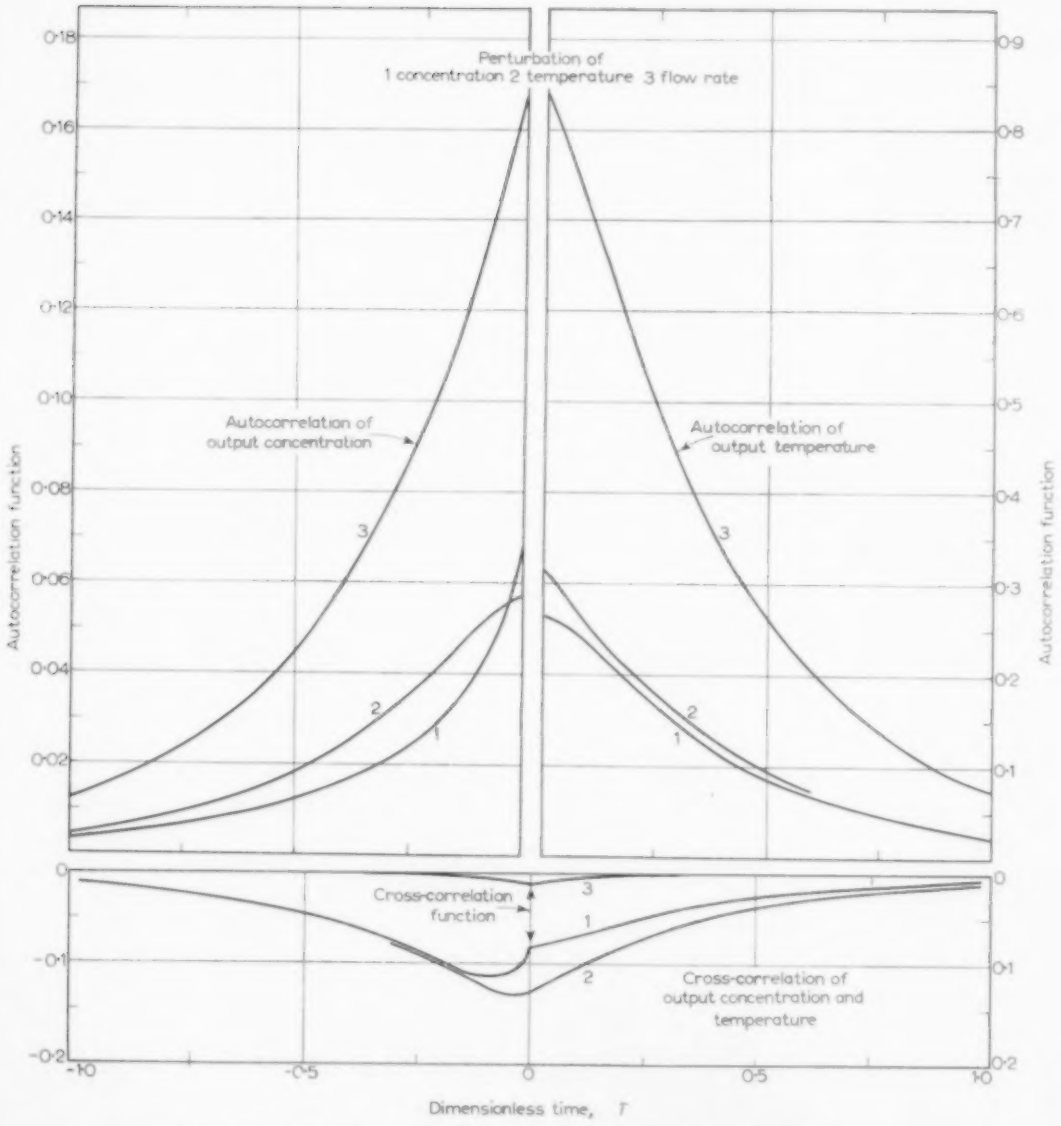

FIG. 1. Plots of auto- and cross-correlation functions for agitated reactor.

Table 3

Correlation function	*Perturbation*	C_1^-	C_2^-	C	C_1^+	C_2^+	σ
Auto-correlation of concentration	Conc.	0·022	0·045	0·067	0·022	0·045	0·259
	Temp.	− 0·010	0·067	0·057	− 0·010	0·067	0·239
	Flow	− 0·001	0·168	0·167	− 0·001	0·168	0·409
Auto-correlation of temperature	Conc.	− 0·047	0·312	0·265	− 0·047	0·312	0·515
	Temp.	− 0·021	0·337	0·316	− 0·021	0·337	0·562
	Flow	− 0·109	0·947	0·838	− 0·109	0·947	0·915
Cross-correlation of temperature and concentration	Conc.	0·085	− 0·166	− 0·081	0·011	− 0·092	—
	Temp.	− 0·040	− 0·169	− 0·129	0·005	− 0·134	—
	Flow	− 0·004	− 0·005	− 0·009	− 0·001	− 0·008	—

Finally let the inlet concentration be perturbed by a Gaussian random disturbance having a correlation function

$$\phi_{\mu\mu} = \tfrac{1}{2}\, c\, e^{-c|\tau|} \quad c > 0 \qquad (6.2)$$

of which the spectral density is

$$G_{\mu\mu} = \frac{1}{\pi}\,\frac{c^2}{\omega^2 + c^2}$$

The case of white noise is the limit as $c \to \infty$. Figure 2 show the results of these calculations, the bearing of which will now be discussed.

7. Discussion

The standard deviations given in the last column of Table 3 show that variations in flow rate cause the greatest variations in the output concentration and temperature. In both cases the effect of perturbance of the inlet temperature and of the inlet concentration are very much the same, but the effect of perturbations in flow rate is some 60-70 per cent greater. This is confirmed in Fig. 1 where the auto-correlation functions are shown; since these are even functions only half of each need be shown, but the difference of scales should be noted. Here again the curves corresponding to perturbations of inlet temperature and concentration follow one another closely. Those corresponding to perturbations of flow rate lie well above the others, but fall off at much the same rate. This rate may be judged by saying that when $\tau = 1$ (i.e., after one holding time of the reactor) $\phi(\tau)$ has dropped to less than 9 per cent of its value at $\tau = 0$, namely the variance.

The cross-correlation of output temperature and concentration is also shown in Fig. 1. As would be expected this is negative, meaning that increases of temperature are generally accompanied by decreases in concentration. Also the greatest correlation is for τ in the region of 0 to − 0·1. This cross-correlation is

$$\phi_{zy}(\tau) = \lim_{T\to\infty} \frac{1}{2T} \int_{-T}^{T} z(t)\, y(t+\tau)\, d\tau$$

and the fact that it is greatest when τ is small and negative (say $\tau = -0{\cdot}05$ as in curve 2) implies that the products $z(t)\, y(t - 0{\cdot}05)$ are greatest. This means that deviation in y due to some perturbation comes about rather rapidly than deviation in z. Thus $\phi(-0{\cdot}01)$ will be smaller than $\phi(-0{\cdot}05)$ because the deviation in z is still small although that in y has grown, and on the other hand $\phi(-0{\cdot}1)$ is smaller than $\phi(-0{\cdot}05)$ because the deviation in y has begun to decay although that in z is fully developed. Thus the response of concentration lags behind that of temperature by some small multiple of the value of τ for which $|\phi_{zy}(\tau)|$ is greatest. In the case of curve 1, corresponding to perturbations of inlet concentration the lag is slightly greater. This is because a sudden slight increase in inlet concentration will increase the reaction rate and hence the temperature; but the fall of concentration which accompanies a rise in

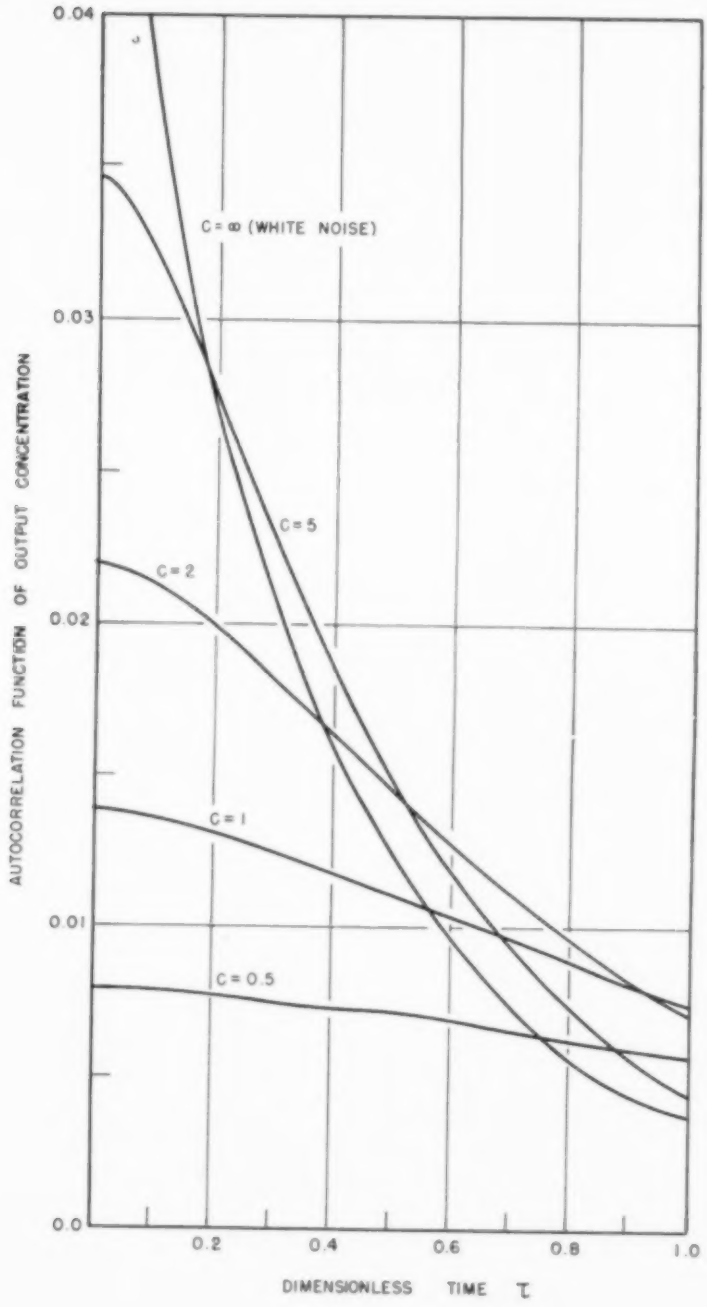

FIG. 2. Plots of auto-correlation function of output concentration for correlated input concentration perturbations.

temperature is inhibited by the initial rise in concentration and so is greatest at slightly later time. Curve 3 corresponding to flow rate fluctuations shows that cross-correlation of output temperature and concentration is very distinctly smaller than in the previous cases. This may be explained as follows: an increase in flow rate reduces the holding time and so the extent of the reaction. But it also tends to increase the temperature in that the cooling coils remove less heat and this increases the extent of the reaction. It appears that these two effects to a large degree balance one another and keep the product of the concentration and temperature deviations relatively small.

In Fig. 2 the output auto-correlation function of concentration is shown for various correlated inputs. The greater spread of the input auto-correlation (i.e., the smaller value of c) is reflected in that of the output auto-correlation function. As a measure of this the values of $\phi(1)/\sigma^2$, the ratio of the auto-correlation function at $\tau = 1$ to its value at $\tau = 0$, are given below.

c	∞	3	2	1	0·5
$\phi(1)/\phi(0)$ input	0	0·007	0·13	0·38	0·61
$\phi(1)/\phi(0)$ output	0·055	0·13	0·32	0·55	0·79

They clearly show that the process tends to prolong the range of the correlation of the output variables and this is naturally most marked when the input concentration is least correlated.

Acknowledgements—The authors are indebted to Mr. J. Coste who carried out the calculations from which the figures were drawn. Fruitful discussions were also carried out with Mr. John W. Tierney of Remington Rand Univac, St. Paul. The referee has also made some valuable comments which have been used to improve the presentation.

Notation

a, b, c = constants
$d_e = 2 + \alpha + \beta - \gamma$
$d_f = (1 + \alpha)(1 + \beta) - \gamma$
e = random input $= (1 - \xi_s)\lambda + \mu$
E = Fourier transform of e
f = random input $= (\eta_0 - \eta_s)\lambda + \nu + \delta\nu_c - \epsilon\lambda_c$
f_i = ith probability density function
F = Fourier transform of f
F_i = probability function
G_{xx} = spectral density of x
G_{xy} = cross-spectral density of x and y
H_{ij} = Fourier transform of W_{ij}, transform function
h = product of specific heat and density of reactants
P = dimensionless reaction rate
q = flow rate
R = reaction rate function
t = time
T = temperature
U = heat transfer function, dimensionless
U^* = heat transfer function
V = volume of reactor
$V(\tau)$ = estimate of auto-correlation function (§4)
W_{ij} = impulse response
x = concentration
y = perturbation on dimensionless temperature
Y = Fourier transform of y
z = perturbation on dimensionless concentration
Z = Fourier transform of z
$\alpha = (P_\xi)_s$
$\beta = (U_\eta)_s$
$\gamma = (P_\eta)_s$
$\delta = -(U_{\eta_c})_s$
ΔH = heat of reaction
$\epsilon = (U_{\kappa_c})_s$
η = dimensionless temperature
κ = dimensionless flow rate
λ = perturbation on κ
μ = perturbation on ξ_0
ν = perturbation on η_0
ξ = dimensionless concentration
ϕ_{xx} = autocovariance on x
ϕ_{xy} = cross-correlation on x and y
ω = Fourier transform variable
subscript zero ~ influent values
subscript c ~ coolant
bar over letter ~ mean value
subscript s ~ steady state
other subscripts refer to partial derivatives

References

[1] Aris, Rutherford and N. R. Amundson *Chem. Engng. Sci.* 1958 **7** 121-155.

[2] Bilous O. and N. R. Amundson *Amer. Inst. Chem. Engrs. J.* 1955 **1** 513-521; *ibid.* 1956 **2** 117-126.

[3] Laning J. H. and R. H. Battin *Random Processes in Automatic Control*, McGraw Hill, (1956).

Letters to the Editors

Discussion of the paper "Correlation of scraped film heat transfer in the votator" (A. H. Skelland*)

THE purpose of this discussion is twofold. Part 1 relates directly to the reference article, and presents a comparison of SKELLAND's votator heat transfer correlations and data with theoretical predictions based on a simple unsteady-state heat penetration model as it applies to scraped-wall heat transfer. Part 2 presents a similar model as it generally applies to a moving impeller, all or part of which may be made into effective heat transfer surface by coring and circulating a heat transfer fluid through it. Although this part is not directly related to the article, its inclusion here seems appropriate since it does provide a way of increasing the heat transfer capability of equipment similar in principle to the votator. The resulting heat transfer gain may sometimes be substantial, e.g., in equipment where it may be impractical to actually scrape the wall.

PART 1. SCRAPED-FILM HEAT TRANSFER

Ideally, i.e. under conditions which permit a simple and exact theoretical representation, material at a uniform bulk temperature continually moves down the rear surfaces of the scraper blades to the cylindrical heat transfer surface where it either heats or cools by molecular conduction until the following blade scrapes it up and thoroughly mixes it with the bulk fluid. Since the depth of conductive heat penetration per pass is small in the range of r.p.m's. where votators usually operate†, the small variation in peripheral fluid velocities within the thin heat transfer layer may be neglected. It is also assumed that the entrance and longitudinal flow effects are rendered unimportant by the intensity of the cross-sectional mixing. Under these ideal conditions, the heat transfer mechanism is identical to molecular conduction into a semi-infinite solid, where the contact time is the time between successive blade passes. Using the surface temperature gradient equation in [1], the average rate of heat influx for a given contact time may be readily calculated and expressed in terms of an effective scraped-film coefficient, h_s‡ :

$$h_s = 2\left(\frac{k\,\rho\,c_p}{\pi\,\theta}\right)^{1/2} \qquad (1)$$

where k = thermal conductivity
ρ = density
c_p = heat capacity
θ = contact time = $1/N_b\,n$
N_b = number of blades
n = revolutions/hour

For the votator $N_b = 2$, and the final result is

$$h_s = 1{\cdot}6\,(k\,\rho\,c_p\,n)^{1/2} \qquad (2)$$

Equation 2 represents the idealized situation as described above, and deviations would be expected to occur in practice. At low Reynolds numbers, for example, the bulk mixing intensity would be low and temperature gradients would penetrate deeper into the bulk fluid. Measured effective film coefficients ought to be less than predicted from equation (2). At high Reynolds numbers, on the other hand, the turbulence intensity would be high and eddy penetration of the theoretical heat transfer layer ought to give higher film coefficients than predicted. Nevertheless, because of the simplicity and theoretical aspects of equation (2), it would be interesting and perhaps informative to compare it with the empirical correlations and data of SKELLAND, whose paper also includes earlier data of HOULTON [3].

Grouping terms in SKELLAND's correlation (which is based on data mainly in the transition region) yields

$$h_s \propto (D_t^{\cdot11}\,v^{\cdot40}/\mu^{\cdot10}L^{\cdot37})\,(k^{\cdot53}\,\rho^{\cdot57}\,c_p^{\cdot47}\,n^{\cdot17}) \qquad (3)$$

$$\simeq (v^{\cdot40}/L^{\cdot37})\,(k\,\rho\,c_p)^{1/2}\,n^{\cdot17}$$

It is seen that k, ρ and c_p appear approximately to the $\frac{1}{2}$ power as in equation (2), but exponent n is quite different. Also, D_t and μ are relatively unimportant which is in agreement with equation (2) v and L, however, were found to be quite important. This may be attributed to entrance and axial flow effects which were neglected in the theoretical treatment.

If, however, the water data of HOULTON (turbulent range) are used to establish the coefficients, grouping terms then yields

---

Chem. Engng. Sci. 1958 **7** 166.

†Even for water, a fluid of relatively high thermal diffusivity, the calculated maximum depth of molecular heat penetration is only about 0·007 in. at 500 r.p.m. in a 2-bladed votator.

‡JEPSON [5] used this same model in connexion with extruder heat transfer studies. He calculated scraped-film coefficients using a graphical integration of the temperature-distance profiles for various contact times.

$$h_s \propto \frac{D_t^{.44}\, v^{.07}}{L^{.37}\, \mu^{.10}} (k^{.53}\, \rho^{.57}\, c_p^{.47}\, n^{.50}) \qquad (4)$$

$$\simeq \left(\frac{D_t}{L}\right)^{.4} (k\, \rho\, c_p\, n)^{1/2}$$

Functionally, equation (4) is in very good agreement with equation (2) except for the (D_t/L) term which may be attributed to entrance effects.

In Figure 1, Skelland's and Houlton's experimental scraped-film heat transfer coefficients are compared with theoretical values based on the simplified heat transfer model (equation 2). Points on the 45° line would indicate perfect agreement. Average fluid properties were used to calculate the theoretical h_s's according to equation (2).

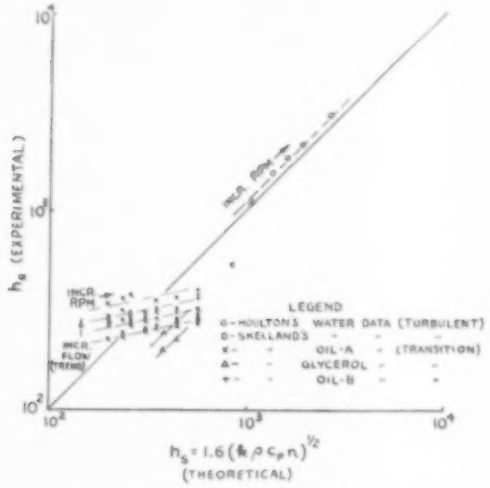

Fig. 1. Comparison of votator data (ordinate) with equation 2 (abscissa).

Houlton's water data are in substantial agreement with theory and average about 15 per cent higher than predicted. Since these data are in the turbulent region, experimental values would be expected to be higher because of turbulent eddy penetration into the heat transfer layer. (Various aspects of the film-penetration theory have been expounded by a number of writers [2, 6, 8, 9], just to mention a few.) As r.p.m's. increase, one might at first expect the divergence between experimental and theoretical coefficients to increase because of greater turbulence. But at higher r.p.m's. the theoretical heat transfer layer is also thinner and eddy penetration is more difficult. These two effects apparently compensate, and the divergence remains constant.

In the transition range (oil data of Skelland there seems to be very little correlation. The fact that the experimental film coefficients increase with respect to theoretical values as r.p.m's. decrease is particularly difficult to rationalize. If it may be assumed that the data are substantially correct and that the votator operates completely full at all times (i.e., without boundary separation behind the blades), then about the only conclusion that I can draw is that the heat transfer mechanism, together with entrance and longitudinal flow effects, in the transition region is very complex indeed, and cannot even be approximated by the heat transfer mechanism described above.

Part 2. Impeller Heat Transfer

The votator will be used for illustration, although the following argument applies equally well for various heat transfer apparatus. As the impeller turns, fluid flow is induced past its surface by drag and pressure forces (see Figure 2). The problem is basically that of heat penetration from the surface into this moving film. This problem has already been solved for a specific set of boundary conditions by Esler [3], and its mass transfer

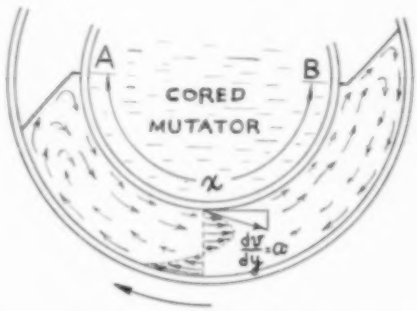

Fig. 2. Cross-sectional flow pattern in the votator. (Mutator assumed stationary with cylinder rotating.)

analogue by Kramers and Kreyger [7]. In order that their solution be applicable to the problem at hand, it is necessary to assume that: (1) the cross-sectional mixing is sufficiently intense so that the fluid is at a uniform bulk temperature as it starts flowing along the impeller surface at point A, (2) the boundary layer is laminar, and (3) the speed of rotation is sufficiently high so that the depth of heat penetration during the fluid travel from A to B is small, thus permitting the use of a linear velocity gradient. Under these conditions, the film coefficient, h_i, is given by

$$h_i = 0{\cdot}808 \left(\frac{a\, \rho\, c_p\, k^2}{x}\right)^{1/3} \qquad (5)$$

where x = path length in the direction of flow over the heat transfer surface.

$a = dv/dy$ = velocity gradient at the surface, which may be an effective or average velocity gradient if point values vary.

ρ, c_p, k as defined in Part 1.

In geometrically similar equipment under similar operating conditions we may write

$$x \propto D_t = \gamma D_t$$

$$a = dv/dy_x \frac{nD_t}{D_t} = \phi n$$

Equation (5) then becomes

$$h_i = 0{\cdot}808 \left(\frac{(\phi/\gamma)\, n\, c\rho_{\,p}\, k^2}{D_t}\right)^{1/3} \qquad (6)$$

$$= \text{Constant} \cdot \left(\frac{n\, \rho\, c_p\, k^2}{D_t}\right)^{1/3}$$

It is sometimes possible to estimate a and x with fair accuracy and obtain some idea of the relative heat transfer gain which may be obtained by coring the impeller. As in the case of scraped-film heat transfer, similar deviations (depending primarily on Reynolds number) would be expected in practice.

Comparison with Dimensional Analysis

Dimensional analysis, neglecting entrance and axial flow effects, would yield equations of the form

$$\frac{hD_t}{k} = \text{constant} \cdot \left(\frac{n\, D_t^2 \rho}{\mu}\right)^m \left(\frac{c_p\, \mu}{k}\right)^n \qquad (7)$$

Equations (2) and (6), respectively, may be written in similar form

$$\frac{h_s D_t}{k} = 1{\cdot}6 \left(\frac{n\, D_t^2\, \rho}{\mu}\right)^{1/2} \left(\frac{c_p\, \mu}{k}\right)^{1/2} \qquad (2')$$

$$\frac{h_i D_t}{k} = 0{\cdot}808 \left(\frac{\phi}{\gamma}\right)^{1/3} \cdot \left(\frac{nD_t^2 \rho}{\mu}\right)^{1/3} \cdot \left(\frac{c_p\, \mu}{k}\right)^{1/3} \qquad (6')$$

where $(nD_t^2\rho/\mu)$ is the "mixing vessel" Reynolds number since the impeller and tube diameters are the same.

Equations (2′) and (6′) would have to be modified in order to take into account departures from the idealized flow models assumed in the derivations. A Reynolds number correction would account for differences in the character of the fluid motion near the heat transfer surfaces. The effect of Reynolds number, in turn, would be influenced by the thickness of the theoretical heat transfer layer. This thickness depends partly on the same variables which determine the Reynolds number and partly on the thermal diffusivity of the fluid, and may be characterized by the Peclet number. These corrections, respectively, would be of the form

$$\text{constant} \cdot \left(\frac{nD_t^2\, \rho}{\mu}\right)^{\alpha}$$

and,

$$\text{constant} \cdot \left(\frac{nD_t^2\, \rho\, c_p}{k}\right)^{\beta} = \text{constant} \left(\frac{nD_t^2\, \rho}{\mu}\right)^{\beta} \left(\frac{c_p\, \mu}{k}\right)^{\beta}$$

Equations (2′) and (6′) then became

$$\frac{h_s D_t}{k} = \text{constant}_1 \cdot \left(\frac{nD_t^2\, \rho}{\mu}\right)^{1/2 + \alpha_1 + \beta_1} \left(\frac{cp\, \mu}{k}\right)^{1/2 + \beta_1} \qquad (2'')$$

$$\frac{h_i D_t}{k} = \text{constant}_2 \cdot \left(\frac{nD_t^2\, \rho}{\mu}\right)^{1/3 + \alpha_2 + \beta_2} \left(\frac{cp\, \mu}{k}\right)^{1/3 + \beta_2} \qquad (6'')$$

Equations (2″) and (6″) are identical to equation (7) except that the coefficients m and n are expressed in terms of components which characterize the reference states (as assumed in the derivations) and deviations therefrom. Admittedly, this type of analysis may not be generally useful because of the interactions between α and β, but it may, in some situations, allow a somewhat better appraisal of the heat transfer mechanism.

Research Department G. A. Latinen
Monsanto Chemical Company
Springfield, Massachusetts

Notation

D_t = internal diameter of votator tube — ft
N_b = number of votator blades
L = length of votator tube — ft
h_s = scraped film heat transfer coefficient — BTU/hr ft^{2}F
h_i = impeller surface heat transfer coefficient — BTU/hr ft^{2}F
n = mutator shaft speed — rev/hr
$\theta = 1/N_b\, n$ = contact time of a fluid element with cylinder heat transfer surface — hr
k = thermal conductivity — BTU/hr ft^{2}F/ft
ρ = fluid density — lb/ft^3
c_p = fluid heat capacity — BTU/lb °F
v = average axial flow velocity of fluid through votator — ft/hr
μ = absolute fluid viscosity — lb/ft hr
$a = dv/dy$ = average surface velocity gradient along impeller heat transfer surface — ft/hr
x = path length in direction of flow past heat transfer surface — ft
γ = constant $= x/D_t$
ϕ = constant $= a/n$
m, n, α, β = exponents (see text)

REFERENCES

[1] CARSLAW H. S. and JAEGER J. C. *Conduction of Heat in Solids*, p. 41, Oxford University Press, London 1947.
[2] DANCKWERTS P. V. *Industr. Engng. Chem.* 1951 **43** 1460.
[3] ELSER K. *Schic. Arch.* 1949 **15** 359.
[4] HOULTON H. G. *Industr. Engng. Chem.* 1944 **36** 522.
[5] JEPSON C. H. *Industr. Engng. Chem.* 1953 **45** 902.
[6] JOHNSON A. I. and CHEN HUANG, *Amer. Inst. Chem. Engrs. J.* 1956 **2** 412.
[7] KRAMERS H. and KREYGER P. J. *Chem. Engng. Sci.* 1956 **6** 42.
[8] RUCKENSTEIN E. *Chem. Engng. Sci.* 1958 **7** 265.
[9] TOOR H. L. and MARCHELLO J. M. *Amer. Inst. Chem. Engrs. J.* 1958 **4** 97.

Notes on the diffusion-type model for longitudinal mixing in flow (Lievenspiel, Smith and Van der Laan)

THE value of LIEVENSPIEL and SMITH'S recent paper [1] on diffusion models of mixing has been greatly enhanced by VAN DER LAAN'S letter [2]. May I ask the courtesy of your columns to add two points which may be of practical interest.

It is in principle impossible to inject a delta function of tracer into the flowing system, though in practice the time of injection may be very short indeed. However no great effort need be expended on devizing an injection system if the concentration, as a function of time, is measured at two points in the bed. In this case it is the difference of means which is nearly proportional to the distance between the points and the difference of variance which gives the effective diffusion coefficient.

Consider the equations (1) of Van der Laan's letter but without the injection term on the right hand side of (1b). Suppose, instead of injection at z_0 and measurement at z_m, that both z_0 and z_m are points at which the concentration-time function is measured and injection takes place upstream of the point z_0. The form of the concentration function injected does not matter, it suffices to know that at $z = z_0$ the measured concentration function is $R_0(\vartheta)$ say. It is now only necessary to solve Van der Laan's equations (1b) (with right hand side zero) and (1c) subject to the conditions (3b), (3d) and (3f) $R(z_0, \vartheta) = R_0(\vartheta)$, $R(z, 0) = 0$, $z > z_0$. This solution is readily obtained by the Laplace transformation and at $z = z_m$ gives

$$\overline{R}_m(p) = \overline{R}(z_m, p) = \overline{R}_0(p) \left[\frac{(1+q-q_b)\,e^{-(q-\frac{1}{2})Pe\,\zeta} - (1-q-q_b)\,e^{-(q+\frac{1}{2})Pe\,\zeta}}{(1+q-q_b)\,e^{-(q-\frac{1}{2})Pe(\zeta+1)} - (1-q-q_b)\,e^{-(q+\frac{1}{2})Pe(\zeta+1)}}\right]$$

where $\zeta = z_1 - z_m$ and the other symbols are as given in Van der Laan's letter. If this expression is expanded in powers of p the coefficients give the moments as Van der Laan shows in equations (5) and (6); the conditions under which this may be done I have recently examined in more detail elsewhere [3]. We find that the expression in the square brackets may be written $1 - \mu p + \frac{1}{2}(\sigma^2 + \mu^2)\,p^2 \ldots$

where $\mu = 1 + Pe^{-1}\,e^{-Pe\,\zeta}(1 - e^{-Pe})(1 + \beta)$

$$\sigma^2 = 2Pe^{-1} + 4\,Pe^{-2}\,e^{-Pe\,\zeta}\left[(1 - Pe\,(1+\beta)\,\zeta) - e^{-Pe}\left(1 - Pe\,(1+\beta)\,(\zeta+1)\right)\right] - Pe^{-2}\,e^{-2Pe\,\zeta}(1 - e^{-2Pe})(1+\beta)^2.$$

Now if $\overline{R}_0(p) = 1 - \mu_0 p + \frac{1}{2}(\sigma_0^2 + \mu_0^2)\,p^2 \ldots$ so that μ_0 and σ^2 are the mean and variance of the concentration-time curve at the measuring point z_0 then

$$\overline{R}_m(p) = 1 - (\mu_0 + \mu)\,p + \tfrac{1}{2}(\sigma_0^2 + \sigma^2 + \overline{\mu_0 + \mu^2})\,p^2 - \cdots = 1 - \mu_m p + \tfrac{1}{2}(\sigma_m^2 + \mu_m^2)\,p^2 - \cdots$$

Thus the difference in means is $\mu_m - \mu_0 = \mu$ and the difference in variances $\sigma_m^2 - \sigma_0^2 = \sigma^2$. Two remarks may be made concerning μ and σ. Firstly they are independent of the conditions at $z = 0$; all we require is that the injection of tracer should take place up stream of $z = z_0$. Secondly by taking the second point of measurement sufficiently far from the end $z = z_1$ the terms introduced by the conditions at this end may be made negligible. The terms are in any case so small that an iterative refinement of the approximate value $Pe = 2/\sigma^2$ can easily be made.

The second point concerns the calculation of σ_0^2 and σ_m^2 from the observed concentration time curves. Firstly, it is clearly best to calculate σ^2 as $\int_0^\infty (\vartheta - \mu)^2\,R(\vartheta)\,d\vartheta$ rather than as $\int_0^\infty \vartheta^2\,R(\vartheta)\,d\vartheta - \mu^2$, since the latter may lead to a small difference of large quantities. Secondly, in practical evaluation of these integrals it will be necessary to stop the integration at some finite ϑ, and it would be useful to estimate the error involved in this. The normal distribution will provide a suitable, though rough, estimate;

it may be shown that for very long columns the normal distribution is approached [3].

The normal distribution with zero mean and variance σ^2 is

$$N(t) = \frac{1}{\sqrt{2\pi}\,\sigma} \exp - \frac{t^2}{2\sigma^2}$$

$$\text{and} \int_{-\infty}^{T} t^2 N(t)\,dt = \sigma^2 \left\{ 1 - \frac{1}{\sqrt{2\pi}} \frac{T}{\sigma} \exp - \frac{T^2}{2\sigma^2} - \int_{0}^{\infty} N(t)\,dt \right\}$$
$$= \sigma'^2$$

which clearly tends to σ^2 quite rapidly as $T \to \infty$. If $T = \sigma\,\tau = \sigma'\,\tau'$

$$\frac{\tau^2}{\tau'^2} = \frac{\sigma'^2}{\sigma^2} = 1 - \left\{ \frac{\tau}{\sqrt{2\pi}} e^{-\frac{1}{2}\tau^2} + \frac{1}{\sqrt{2\pi}} \int_{\tau}^{\infty} e^{-\frac{1}{2}t^2}\,dt \right\}$$

Suppose then that σ'^2 has been calculated by integration up to time Θ so that T corresponds to $\Theta - \bar{\vartheta}$ and $\tau' = (\Theta - \bar{\vartheta})/\sigma'$ then τ can be obtained from the following Table:

Table 1

τ'	τ	σ^2/σ'^2
2·5	2·423	1·064
3·0	2·976	1·008
3·5	3·494	1·003
4·0	3·999	1·0005

Thus 1% accuracy is attained if τ' is approximately 3.

R. Aris

University of Minnesota
Minneapolis 14, *Minn.*

References

[1] Lievenspiel O. and Smith W. K., *Chem. Engng. Sci.* 1957 **6** 227.

[2] Van der Laan E. Th., *Chem. Engng. Sci.* 1958 **7** 187.

[3] Aris R., *Proc. Roy. Soc.* 1958 **A245** 268.

Mass transfer to growing drops

In recent years there have been some investigations of the mechanism of diffusion into a drop growing at a nozzle. Coulson and Skinner [1] have extracted organic acids from water with benzene droplets, which were formed at a constant rate and then pushed back into the nozzle at the same rate before they could break away. The absorption of pure sulphur dioxide by growing water drops has been measured by Groothuis and Kramers [2].

The results of these workers may be compared with an equation proposed by Ilkovic [3] and fully derived by MacGillavry and Rideal [4]. The equation was used to estimate the diffusion-controlled current in a dropping-mercury cathode. The model for the derivation is a sphere expanding at a constant volume rate, with short range diffusion of a solute towards its surface, where the concentration is zero. The mass of solute that has diffused in time t after the appearance of the sphere is given by

$$m = 3{\cdot}57\,c\,D^{\frac{1}{2}}\,V^{\frac{3}{4}}\,t^{\frac{1}{2}} \qquad (1)$$

Since the derivation assumes that the penetration depth is small compared with the sphere radius, the equation is valid for diffusion in either phase, so long as the resistance to transfer lies in one phase only.

A representative selection of experimental results [1, 2] is plotted on Fig. 1, in comparison with equation (1). Coulson and Skinner's results were modified to allow for extraction during the contraction of the droplet. A consideration of the theory indicated that 70·6 per cent of the extraction took place during drop growth, i.e. in half the "drop time," so the values of m and t were altered accordingly. In view of the partition coefficients it was assumed that the transfer of the propionic acid was

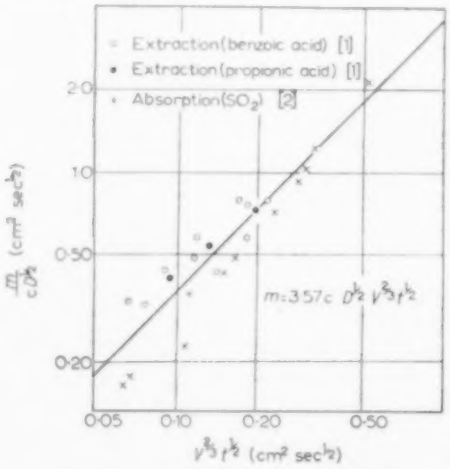

Fig. 1. Comparison of equation (1) with published data.

controlled by diffusion in the benezene phase and the transfer of the benzoic acid was controlled by diffusion in the water phase. In the case of the sulphur dioxide absorption [2], the driving-force concentration was taken as the solubility of the gas.

The points plotted in Fig. 1 show a mean deviation from equation (1) of $\pm$ 18 per cent. This may be due to heat effects (in the sulphur dioxide absorption), circulation, or the non-spherical shape of the drops. Nevertheless, the equation provides an approximate method of predicting mass transfer rates to growing drops.

It has been pointed out [5] that mass transfer during the "formation" of a drop may be largely due to its vibration just after it breaks off. This is confirmed by the fact that recently found rates of gas absorption [6] and extraction [7] by forming drops are several times those predicted by equation (1).

Department of Chemical Engineering M. H. I. Baird
Tennis Court Road
Cambridge

Notation

c = solute concentration in bulk of continuous phase, referred to $c = 0$ at interface
D = diffusion coefficient of solute
m = mass of solute transferred during drop growth
t = time of drop growth
V = volume of drop after time t.

References

[1] Coulson J. M. and Skinner S. J. *Chem. Engng. Sci.* 1952 **1** 197.
[2] Grootheus H. and Kramers H. *Chem. Engng. Sci.* 1955 **4** 17.
[3] Ilkovic D. *Coll. Czech. Chem. Commun.* 1934 **6** 498.
[4] MacGillavry D. and Rideal E. K. *Rec. trav. chim.* 1937 **56** 1013.
[5] Licht W. and Pansing W. F. *Industr. Engng. Chem.* 1953 **45** 1885.
[6] Yano T. and Kawai K. *Chem. Engng.* (*Japan*) 1957 **21** 413.
[7] Ueyama K. and Kida H. *Chem. Engng.* (*Japan*) 1957 **21** 188.

Book Reviews

A. Grumbt : **Gleichgewichtsgase der Verbrennung und Vergasung. Wärmetechnische Berechnung.** Springer, Berlin, 1958. 148 Seiten mit 88 Abbildungen.

In diesem Buch hat der Verfasser nicht nur die bisher schon vorliegenden Erkenntnisse aus zahlreichen verstreuten Schrifttumsquellen in willkommener Weise zusammengefasst, sondern er zeigt darüber hinaus die Möglichkeit gemeinsamer Berechnungsverfahren für feste, flüssige und gasförmige Brennstoffe. Als Grundlage dienen allgemeingültige Gesetze, nach denen Verbrennungs-und Vergasungsvorgänge ablaufen. Es werden eine grosse Zahl von Diagrammen gebracht, die zum Teil bisher noch nicht veröffentlicht waren. Sie gestatten, mit tragbarem Aufwand auch in schwierigere Probleme Einblick zu gewinnen.

Der Stoff ist in einen umfangreichen Hauptabschnitt über die Verbrennung und einen zweiten von geringerem Umfang über die Vergasung eingeteilt. An den ersten Teil schliesst sich ein Anhang an, der vorzugsweise die in den Text vielfach eingestreuten Beispiele übersichtlich ordnet. Auf dem einfachsten Fall einer vollkommenen Verbrennung mit Luftüberschuss ohne Dissoziation aufbauend, wenden sich die Betrachtungen der Verbrennung unter Luftmangel sowie der Verbrennung bei Luftüberschuss mit CO_2-und H_2O-Dissoziation zu und führen in den folgenden Abschnitten auf die bei der Dissoziation im Spiel befindlichen Teilgase sowie auf die simultanen Gleichungssysteme zur Berechnung der Teildrücke mit den Gleichgewichtskonstanten. Über die Enthalpien und Entropien der beteiligten Gasmischungen geben It.-, Ix- und IS-Diagramme Aufschluss, die sich u.a. an die bekannten Begriffe von Mollier anlehnen. Mit andern namhaften Fachleuten, wie Bošnjaković hat der Verfasser bei der Bearbeitung in Verbindung gestanden und so sein geschlossenes Bild des wissenschaftlichen Standes der Dinge geschaffen. Schliesslich geht er auf die technischen Arbeitsfähigkeiten der Verbrennungsvorgänge, auf die Umsetzung eines Wärmegefälles in Ausströmgeschwindigkeit mit Hilfe von Düsen und auf die Thermodynamik chemischer Prozesse ein und leitet so zu wichtigen Anwendungsfragen und dem zweiten Hauptabschnitt über, der im wesentlichen zwischen Kohlenstoffvergasung und Brennstoffvergasung unterscheidet und ebenfalls reichhaltig mit Zustandsdiagrammen ausgestattet ist. Ausklingend kommt die Brennstoffvergasung mit und ohne Berücksichtigung einer Methanbildung zur Sprache. Für die Ermittlung der bei den Vorgängen mitwirkenden Teilgasmengen ist die Grenztemperatur massgebend. Das Ermittlungsverfahren und die Beziehungen, denen die Grenztemperatur unterliegt, werden angegeben.

H. Pichler

Electrostatics in the Petroleum Industry. Edited by A. Klinkenberg and J. L. Van der Minne. Elsevier, 1958 191 pp. $7.00.

This most interesting book is concerned with the hazard of explosion and fire, arising during the handling of inflammable liquids, by reason of the generation and discharge of static electricity. Its particular purpose is to present the results of certain research and development work by the Shell group of companies against a background of general knowledge and experience in this field.

The main material is in fact presented three times over ; first, very briefly in an introductory chapter (4 pages) ; second, in a somewhat qualitative manner, but with due regard to the sort of quantities that practical people need to know, in three succeeding chapters (32 pages) ; and the third, with extensive theoretical background, in the space of five more chapters (84 pages). The first two presentations make up Part I of the book ; and the second occupies a considerable proportion of Part II. The former will appeal more to the practical man concerned with storage and handling problems, and the latter to the research worker or student desirous of acquiring a deeper understanding of the subject than is perhaps necessary for day-to-day applications. Whether either would be quite happy about having to pay for that part of the book in which he is less interested is uncertain.

Both interests are however combined in the later chapters of Part II. One of these deals with practical methods of measuring the relevant electrical properties of liquids (charging tendency and conductivity) and the electrification of liquids in actual equipment (charging current and resultant field strength). Two other chapters, in still more readable vein, describe field experiments on the generation and discharge of hazardous amounts of static electricity in storage tanks and fuelling equipment.

The theoretical chapters of Part II are documented fairly fully. There is also, at the end of the volume, a short bibliography which claims to cover general surveys on static electricity. Some of the references included at this point are however of rather specialized significance, and they, having already been given at the end of the appropriate chapter, might well have been omitted here. On the other hand, surveys should perhaps have been included which extend the discussion to static hazards in the related fields of textiles, explosives and powdered materials generally, for these naturally receive little or no attention in the main text.

The principal thesis of the book can be briefly stated. It is that the solution to the problem of static electricity in inflammable liquids is to be found along two lines which must be regarded as complementary. They are :

(1) The complete bonding and earthing of plant and equipment.

(2) The improvement of the electrical conductivity of the liquid, where necessary by the incorporation of effective additives.

The latter have recently been the subject of extensive research and highly effective additive mixtures are announced. It is argued, quite cogently, that by increasing the conductivity of a product in this way immediately after manufacture, all subsequent processes are safeguarded, provided that earthed equipment is employed. This being so, pumping speeds, for example, need no longer be restricted.

Although the book is concerned almost exclusively with the petroleum industry so far as application is concerned, the principles are relevant to other industries, especially the chemical. Indeed, all who are concerned with handling low-flash-point, low-conductivity liquids on any appreciable scale should consider the implications of what it has to say.

J. H. Burgoyne

E. Sauer: **Tierische Leime und Gelatine** Springer Verlag, Berlin, 1958. VII + 335 pp. DM 40·50.

Der rasche Fortschritt von Wissenchaft und Tecknik in den letzten 10 Jahren erfordert die Herausgabe von Monographien, da es selbst dem Fachmann schwerfällt, dem Laien aber unmöglich ist, alle Neuerscheinungen in den verschiedensten Zeitschriften zu lesen. Das vorliegende Buch will einen Überblick über den heutigen Stand der Technologie von Leim und Gelatine geben.

Die Einteilung des Buches ist übersichtlich geordnet. Nach einem kurzen geschichtlichen Abriss folgt ein Kapitel über die Struktur des Kollagens und Glutins und den Vorgang der Umwandlung der beiden Substanzen ineinander. Weiterhin finden sich viele Angaben über die physikalischen Eigenschaften von Glutin, wie z.B. Viskosität, Oberflächenspannung, Quellung und optische Eigenschaften usw.

Für die verschiedenen Verwendungsarten des Glutins sind kurze spezielle Beschreibungen vorhanden: die Theorie des Klebevorgangs, Gelatine für photographische Zwecke, Speisegelatine und technische Gelatine.

Sehr ausführlich mit vielen Skizzen von Maschinen und Anlagen ist das Kapitel über die technische Herstellung von Glutin ausgestaltet, wobei noch besonders die Prüf— und Analysenmethoden zu erwähnen wären.

Neben den Haut—und Knochenleimen wird speziell noch Fischleim und Kasein ausführlich behandelt.

Als Nachteil wird beim Studium des Buches empfunden, dass an vielen Stellen wie z.B. bei der Beschreibung der Quellung, Gelbildung, Gerbung usw. nicht mehr an neuerer Literatur berücksichtigt wurde.

Trotzdem kann gesagt werden, dass es dem Praktiker in der Glutinherstellung mit den vielen Tabellen und Schaubildern manchen Hinweis geben kann, jeder aber, der sich über Gelatine und Leime unformieren will, erhält einen umfassenden Überlick.

F. Moll

SELECTION OF CURRENT SOVIET PAPERS OF INTEREST TO CHEMICAL ENGINEERS*

M. I. KUAIDZHE: Sorption and catalytic properties of some natural substances. *Zh. prikl. Khim.* 1958 **31** 1001-1006.

M. E. POZIN, B. A. KOPILEV and N. A. PETROVA: Absorption of ammonia by ammoniacal copper solution in a foam apparatus. *Ibid.* 1958 **31** 1007-1013.

L. A. MOCHALOVA and M. KH. KISHINEVSKI: On mass transfer during absorption by bubbling method. *Ibid.* 1958 **31** 1013-1018. Determination of mass transfer coefficients for bubbling and chain-bubbling through continuous liquid media.

G. N. GASYUK, A. G. BOLSHAKOV, A. V. KORTNEV and P. YA. KRAINY: Coefficients of mass transfer in liquid phase. *Ibid.* 1958 **13** 1019-1025. Desorption of CO_2 in an apparatus operating on air lift principle.

N. I. GELPERIN, N. G. KROKHIN and E. N. KISELEVA: Extraction from solution by condensing solvents. *Ibid.* 1958 **31** 1026-1036. General correlation of mass transfer coefficients in liquid-liquid extraction with extract solvent introduced in vapour form.

V. M. VLASENKO, G. K. BORESKOV and G. E. BRAUDE: Catalytic purification of nitrogen-hydrogen mixture from CO. *Khim. Prom.* 1958 200-205.

Z. S. VANYUSHINA, M. S. VILESOVA and G. A. CHISTYAKOVA: Synthesis of hexamethylenediamine by continuous catalytic hydrogenation of adipic nitrile. *Ibid.* 1958 205-208.

P. V. ZIMAKOV and L. M. KOGAN: Influence of temperature on the process of hypochlorination of ethylene. *Ibid.* 1958 210-213.

I. I. STRIZHEVSKI: Properties of liquid and solid acetylene. *Ibid.* 1958 221-227.

I. E. NEYMARK: Manufacture of mineral technical adsorbents of different porous structure. *Ibid.* 1958 227-234.

L. D. RATOBILSKAYA: Problems of flotation of minerals of higher solubility. *Ibid.* 1958 234-239.

E. M. GOLDIN: On the theory of clarifying centrifuges with continuous feed. *Ibid.* 1958 247-249.

I. I. CHERNOBILSKI and Z. V. SEMILET: Investigation of the coefficient of heat transfer on the irrigated side in an irrigation heat exchanger. *Ibid.* 1958 249-252.

A. N. KIRGINTSEV: On dependence of the coefficient of equilibrium crystallisation on crystal size. *Zh. neorg. Khim.* 1958 **3** 533-538.

V. V. FOMIN and E. P. MAYUROVA: Extraction of nitric acid by a molar solution of tributylphosphate in benzene. *Ibid.* 1958 **3** 540-541.

A. V. KISELEV, V. V. KHOPINA and YU. A. ELTEKOV: Adsorption of toluene and *n*-heptane mixtures on silica gels and carbon black. *Izv. Akad. Nauk SSSR*, Otd. khim. Nauk. 1958 664-672.

V. M. TATEVSKI and V. A. BENDERSKI: New relationships in physico-chemical properties of hydrocarbons. *Zh. obshch. Khim.* 1958 **28** 1733-1737.

S. T. BOWDEN: Heats of vaporisation, surface tension and orthobaric densities of vapour-liquid systems. *Zh. fiz. Khim.* 1958 **32** 1265-1268.

D. S. TSIKLIS: Phase equilibria in the system acetaldehyde-water-methane at high pressures. *Ibid.* 1958 **32** 1367-1371.

D. S. TSIKLIS and G. M. SVETLOVA: Solubility of gases in *cyclo*hexane. *Ibid.* 1958 **32** 1476-1480.

S. I. KRICHMAR: On the problem of natural convection at a vertical plate. *Ibid.* 1958 **32** 1580-1585. Diffusional flow to a vertical electrode in presence of natural convection.

B. S. PETUKHOV and E. A. KRASNOSHCHEKOV: Hydraulic resistance during viscous non-isothermal flow of a liquid in tubes. *Zh. tekh. Fiz.* 1958 **28** 1207-1214.

V. A. RACHKO: Investigation of the process of condensation of pure steam on tube banks. *Ibid.* 1958 **28** 1237-1250.

V. A. RACHKO: Investigation of the influence of steam parameters and depth of tube bank on the process of condensation of pure steam. *Ibid.* 1958 **28** 1251-1260.

V. M. BROLYANSKI and I. P. ISHKIN: Thermodynamic analysis of irreversible processes in refrigeration machines. *Izv. Akad. Nauk SSSR, Otd. tekh. Nauk* 1958 No. 5 40-45.

*Translations or photostats of the article can be supplied on request by the Pergamon Institute (a non-profit making foundation) at a nominal charge.

L. N. Zhdanovich and P. I. Kanavets: Granulation of fine coal from Irkutsk district for manufacture of coke. *Ibid.* 1958 No. 5 131-136

E. F. Kurgaev: Investigations of sedimentation of solid particles at low Reynolds numbers. *Ibid.* 1958 No. 5 137-141.

A. G. Estafev, D. D. Zhikov and N. M. Karavaev: Relative influence of some factors on the process of mass transfer in plate columns. *Ibid.* 1958 No. 6 77-83. Theoretical consideration of effects of plate efficiencies and reflux ratio on variation of composition along the column.

V. V. Bakakin, I. N. Plaksin and E. M. Chapligina: Influence of oxygen and nitrogen on separation by selective flotation of minerals of titanium and zirconium and the effect of their crystalline structure. *Ibid.* 1958 No. 6 84-90.

D. S. Rasskazov and A. E. Sheindlin: Experimental investigation of the specific heat of steam and water at high parameters. *Dokl. Akad. Nauk SSSR* 1958 **120** 771-774.

M. A. Styrikovich and L. E. Faktorovich: Influence of tube length on the value of critical heat flows in forced motion of steam-water mixtures. *Ibid.* 1958 **120** 1018-1020.

D. A. Efros: Displacement of a two-component mixture with low viscosity of one component. *Ibid.* 1958 **121** 59-62. Displacement of a system of two immiscible liquids, one having low viscosity, from a porous medium by a third liquid.

I. N. Plaksin and R. Sh. Shafeev: Influence of electrochemical heterogeneity of surface of sulphide minerals on xanthate distribution in flotation. *Ibid.* 1958 **121** 145-148.

A. S. Kovbasyuk: Aerodynamics of flow in a cone-type cyclone chamber. *Teploenergetika* 1958 No. 6 30-35.

V. E. Maslov and Yu. L. Marshak: Investigation into separation of suspended solid particles by a liquid film during vortex motion. *Ibid.* 1958 No. 6 64-70.

S. I. Kosterin and B. I. Sheinin: Fractional resistance to flow of steam-water mixtures in a straight horizontal pipe. *Ibid.* 1958 No. 6 71-76.

L. D. Volyak: Equations for calculation of surface tension of liquids. *Ibid.* 1958 No. 7 33-37.

L. I. Chernyeva: Experimental investigation into the thermodynamic properties of freon 142. *Ibid.* 1958 No. 7 38-43.

N. M. Zinger: Investigation of water-air ejector. *Ibid.* 1958 No. 8 26-31.

N. V. Pavlovich and D. L. Timrot: Experimental investigation of the viscosity of methane. *Ibid.* 1958 No. 8 61-65.

L. D. Berman and S. N. Fuks: Mass transfer in horizontal condensers during presence of air in steam. *Ibid.* 1958 No. 8 66-73.

V. G. Fastovski and R. I. Artim: Experimental investigation of critical heat flux in boiling of binary mixtures. *Ibid.* 1958 No. 8 74-77.

A. V. Yanishevski and I. S. Pavlushenko: Determination of interfacial area of emulsions. *Zh. Prikl. Khim.* 1958 **31** 1215-1220.

G. A. Gazyev, Ya. D. Zelvenski and U. A. Shalygin: Vapour-liquid equilibrium data of binary systems ethanol-*iso*propanol and carbon disulphide-methyl iodide. *Ibid.* 1958 **31** 1220-1227.

Ya. R. Katsobashvili and N. V. Tsiborova: Coke formation in the process of catalytic hydrogenation of petroleum and petroleum residues. *Ibid.* 1958 **31** 1252-1258.

V. A. Kargin, R. P. Lastovski and T. A. Matveeva: Analysis and purification of substances by new methods of electrodialysis. *Khim. Prom.* 1958 261-267.

K. P. Grinevich and V. A. Zaytsev: New method of synthesis of oxides of mesitylene and methyl-*iso*butyl-ketone. *Ibid.* 1958 276-279.

A. I. Gelbshtein, A. A. Zansokhova and G. G. Shcheglova: Vapour-phase alkylation of benzene by ethylene using phosphoro-diatomaceous catalyst. *Ibid.* 1958 284-287.

F. P. Zaostrovski and P. K. Kovtun: Condensation of ammonia from nitrogen-hydrogen mixtures. *Ibid.* 1958 292-295.

N. N. Umnik and N. M. Zhavoronkov: Investigation and calculation of multistage columns for molecular distillation. *Ibid.* 1958 296-302.

A. T. Davidov and P. F. Skoblionok: Effect of medium on ion exchange adsorption. Dependence of exchange constant on dielectric constant of the solvent. *Zh. fiz. Khim.* 1958 **32** 1703-1710.

M. Kh. Karapetyans: On approximate calculation of temperature dependence of heat capacity. *Ibid.* 1958 **32** 1763-1773.

V. V. Udovenko and L. P. Aleksandrova: Solubility in the system formic acid – 1, 2-dichloroethane – water. *Ibid.* 1958 **32** 1889-1892.

Yu. I. Shimanski: Temperature dependence of heat of vaporisation of pure liquids. *Ibid.* 1958 **32** 1893-1899.

S. I. Sklyarenko, B. I. Markin and L. B. Belyaeva: Determination of saturated vapour pressure of low volatile substances. *Ibid.* 1958 **32** 1916-1921.

L. S. Sterman: On the theory of vapour separation. *Zh. tekh. Fiz.* 1958 **28** 1562-1574. Theoretical consideration of entrainment of liquid drops by vapours.

G. V. Filippov: On turbulent flow in entry sections of tubes with circular cross-section. *Ibid.* 1958 **28** 1823-1828.

V. P. Frontasev: New data on thermal conductivity of water in the range of 10 to 60 C. *Ibid.* 1958 **28** 1839-1844.

L. Kh. Freydlin, A. A. Balandin, N. V. Borunova and A. E. Agronomov: On connection between activity and stability of nickel-alumina catalysts and macrostructure of the carrier. *Izv. Akad. Nauk SSSR, Otd. khim. Nauk* 1958 923-928.

V. A. Glembotski and A. E. Kolchemanova: Interaction between collector and galenite and its flotation in the presence of ions of heavy metals. *Izv. Akad. Nauk SSSR, Otd. tekh. Nauk* 1958 No. 7 76-81.

G. A. Tirski: On unsteady state heat transfer in a system of disc rotating in viscous liquids. *Ibid.* 1958 No. 7 106-107.

G. I. Maykapar: On laminar flow of liquids of varying viscosities. *Ibid.* 1958 No. 7 108-114. Theoretical considerations of flow between parallel plates and through a tube with and without heat transfer.

I. N. Plaksin, V. I. Tyurnikova and O. V. Tretiakov: Distribution of xanthogenates on the surface of sulphide minerals as a function of the length of hydrocarbon radicals. *Ibid.* 1958 No. 7 148-149.

B. A. Fidman: On energy balance in sudden turbulent motion. *Ibid.* 1958 No. 8 139-142.

E. M. Chaplygina: On use of high-speed photography in laboratory investigation of the process of flotation. *Ibid.* 1958 No. 149-150.

N. D. Tomashev, R. M. Altovski and A. G. Arakelov: Anodic protection of titanium in sulphuric acid. *Dokl. Akad. Nauk SSSR* 1958 **121** 885-888.

M. V. Polikovski and G. G. Shklover: Experimental investigation of steam-jet ejectors. *Teploenergetika* 1958 No. 9 46-50.

B. V. Dzadzikin and V. L. Leichuk: Heat transfer at high temperatures between pipe wall and air in turbulent flow, and calculation of wall temperature. *Teploenergetika* 1958 No. 9 74-79.

A. I. Golub: Vapour-phase catalytic oxidation of naphthalene and naphthalene fractions. *Koks i Khim* 1958 No. 7 44-47.

Yu. I. Dytnerski and C. U. Umanov: New apparatus for the intensification of the processes of heat and mass transfer. *Ibid.* 1958 No. 9 43-44. Vertical column with packing consisting of 9 mm tubes arranged vertically. Correlation for flooding rate given.

A. Z. Bikkulov and N. I. Chernozhukov: Use of furfural for refining of lubricants from Eastern crude. *Khim. Tekhnol. Topl. Masel.* 1958 No. 6 52-57.

P. I. Lukyanov: Rational design of reactor plant for pyrolysis of petroleum raw material to ethylene. *Ibid.* 1958 No. 6 58-64.

A. N. Bashkirov, S. M. Loktev qne G. B. Sabirova: Hydrogenation of aldehydes and ketones in mixtures with other organic compounds. *Ibid.* 1958 No. 7 39-44.

B. K. Marushkin, M. F. Bondarenko, V. L. Tsalik and F. G. Baydavletova: Effect of recycle on sharpness of separation during purification with selective solvents. *Ibid.* 1958 No. 8 21-24.

N. B. Zhadanovski: Experience in operating a plant for production of hydrogen by catalytic conversion of hydrocarbon gas with steam. *Ibid.* 1958 No. 8 38-44.

V. S. Alyev, N. P. Kasimova and N. B. Altman: Effect of water vapour on high temperature cracking of gas oil. *Ibid.* 1958 No. 8 44-49.

N. I. Gelperin, I. G. Matveev and K. V. Wilshaw: Absorption of SO_2 and CS_2 by some hydrocarbons of diphenylmethane type. *Zh. prikl. Khim.* 1958 **31** 1323-1332.

M. E. Pozin and E. Ya. Tarat: Kinetics of absorption of water vapour by sulphuric acid in turbulent (foam) regime. *Ibid.* 1958 **31** 1332-1341.

I. P. Mukhlenov: Kinetics of heat and mass transfer in a foam layer. *Ibid.* 1958 **31** 1342-1348.

I. S. Pavlushenko and A. V. Yanishevski: On stirring speed in mixing of two immiscible liquids. *Ibid.* 1958 **31** 1348-1354. Determination of minimum effective stirring speed as a function of type of impeller, its position, size of vessel, presence of baffles and physical properties of liquids studied.

Sh. L. Leichuk and V. I. Sedlis: Influence of effectiveness of plasticisers on viscosity of polyvinylchloride. *Ibid.* 1958 **31** 1397-1402.

I. M. Dolgopolski, A. L. Klebanski and D. M. Krasinskaya: Polymerisation of divinylacetylene. *Ibid.* 1958 **31** 1403-1408.

M. F. Skalozubov and V. I. Matsokin: Radiometric determination of surface area of dispersions and porous substances. *Ibid.* 1958 **31** 1429-1431.

V. V. Ipatev, V. I. Tikhomirov and N. F. Soboleeva: Investigation of rate of absorption of hydrogen sulphide by arsenic-soda solutions. *Ibid.* 1958 **31** 1472-1477.

M. I. Gerber, V. P. Teodorovich and A. D. Shusharina: Investigation of rate of absorption of hydrogen sulphide by arsenic-soda solutions. *Ibid.* 1958 **31** 1478-1483.

R. P. Kirsanova and S. Sh. Bik: Vapour-liquid equilibrium data for the system acetaldehyde-methanol at atmospheric pressure. *Ibid.* 1958 **31** 1610-1612.

V. I. Shestakov and D. F. Terentev: Determination of optimum temperature regime of contact plants in oxidation of sulphur dioxide. *Khim. Prom.* 1958 350-354.

N. I. Gelperin, V. Ya. Kruglikov and V. G. Einstein: Heat transfer between fluidised bed and the surface of a single tube in transverse and longitudinal flow of gas. *Ibid.* 1958 358-363.

G. P. Piterskikh and A. I. Angelov: Principles of separation of minerals in heavy suspensions using hydrocyclones. *Ibid.* 1958 364-370.

P. G. Romankov, Bao Tchi-Tsuan and M. I. Kurochkina: Some problems in theory and practice of extraction from solid materials. *Khim. Nauka i Prom.* 1958 **3** 506-511. Graphical representation of Piret's equation, discussion of its application to practical cases and results of experiments on extraction of soya-bean oil.

V. V. Streltsov and A. A. Komarovski: Mass transfer from a stationary granular bed to a moving liquid. *Ibid* 1958 **3** 511-514.

G. K. Gontcharenko and A. P. Gotlinskaya: One mechanism of mass transfer in extraction from solutions. *Ibid.* 1958 **3** 515-517. Critical consideration of results obtained by other workers indicates the presence of interfacial resistance to transfer.

A. A. Noskov and V. N. Sokolov: On calculation of hydraulic resistance of irrigated sieve plates. *Ibid.* 1958 **3** 518-520.

Yu. V. Gurikov: Some problems relating to construction of two-phase vapour-liquid equilibrium diagrams of ternary homogeneous solutions. *Zh. fiz. Khim.* 1958 **32** 1980-1996.

I. R. Krichevski and G. A. Sorina: Phase and volume relations in liquid-gas systems under high pressure VI. System *cyclo*hexane-hydrogen. *Ibid.* 1958 **32** 2080-2086.

E. I. Akhumov and B. Ya. Rosen: On correlations for adsorption of bromine and iodine by mineral adsorbents in presence of chlorides and sulphates of sodium and potassium. *Ibid.* 1958 **32** 2094-2096.

N. N. Verigin: Diffusion at the surface of a solid immersed in liquid. *Ibid.* 1958 **32** 2097-2106. Theoretical treatment of two limiting cases of unidimensional dissolution of a non-homogeneous solid: free diffusion and convection at very high rates.

A. E. Lutski and A. N. Panova: Heat capacity of liquid nitrobenzene. *Ibid.* 1958 **32** 2183-2187.

S. G. Entelis, M. A. Tsikulin, L. V. Volkov and N. M. Chirkov: Determination of specific areas of porous substances and of powders by gaseous flow under low pressure. *Ibid.* 1958 **32** 2187-2191.

S. I. Kosterin, B. I. Sheinin and A. K. Katarzhis: Experimental investigation of actual steam content in steam-water flow through inclined pipelines. *Teploenergetika* 1958 No. 10 55-61.

N. V. Tsiderberg and V. N. Popov: Experimental investigation of heat conduction of Helium. *Ibid.* 1958 No. 10 61-65.

S. V. Donskov: Heat loss from a cylinder in transverse flow of a loose body (sand). *Ibid.* 1958 No. 10 65-72.

S. M. Pavlov: Investigation into mass transfer between the main flow and the circulation zone behind a body, and the degree of mixing in this zone. *Ibid.* 1958 No. 10 72-76.

A. D. Altshul: About velocity profile and resistance at turbulent flow in engineering pipelines. *Ibid.* 1958 No. 10 76-78.

END